Department of Mathematics and Statistics

Mathematical Analysis of Microflows Under Electroosmotic Forces

Qian Sun

This thesis is presented for the Degree of
Doctor of Philosophy
of
Curtin University

November 2013

Declaration

To the best of my knowledge and belief, this thesis contains no material previously published by any other person except where due acknowledgment has been made.

This thesis contains no material which has been accepted for the award of any other degree or diploma in any university.

.....
Qian Sun
November 2013

Abstract

Microdevices have been used widely in modern science and technology applications such as drug delivery systems and Lab-on-a-chip diagnostic devices. Study of fluid flows in microchannels and microtubes is essential for the optimal design of microdevices and optimization of the system performance. This project thus focuses on the study of two microflow problems, namely the time periodic electroosmotic flow in two-dimensional straight channels taking into account microslip on boundary, and the flow of a Newtonian fluid in circular microtubes with boundary slip under the combined effect of electric driving force and pressure driving force.

For the time period electroosmotic flows in microchannels with boundary slip, based on the principles of continuum mechanics and making some simplifying assumptions, the underlying boundary value problem is established which consists of a second order partial differential equation with a time periodic wave-form driving force and a set of boundary conditions. The boundary value problem is then solved to yield the exact solution by using a complex variable approach combined with the method of separation of variables. A subsequent numerical analysis, based on the mathematical model and the solutions derived, is then carried out to investigate the influence of the model parameters on the flow behavior. The investigation shows that the model parameter κ and the slip length l have significant influence on the flow dynamics. By varying the parameter κ, the flow pattern may change from plug flow to uniform flow, and the magnitude of velocity may be controlled through the slip length.

For the slip flow of fluids driven by the combined effect of electric force and pressure gradient, the underlying boundary value problem is established and solved to yield the exact solution for the velocity field through use of Fourier series expansion in time and Bessel functions in space. Based on the analytical expression of the velocity field, the transient flow rate and stress field in the fluid are also determined. The exact solutions and subsequent numerical investigations show that the slip length and electric field parameters have significant effects on the velocity profile. By varying these system parameters, one can achieve smooth

velocity profiles or wave-form profiles with different wave amplitude and frequency. This opens the way for optimizing the flow by choosing the slip length, the electrical field and electrolyte solutions.

List of publications during PhD candidature

- Q. SUN, Y. H. Wu, L. S. liu and B. Wiwatanapataphee, "Solution of time periodic Electroosmotic flow with slip boundary," *Abstract and Applied Analysis*, Volume 2014, Article ID 789147, In press.
- Q. SUN, Y. H. Wu, and L. S. liu, B. Wiwatanapataphee, "Study of a Newtonian fluid through circular channels with slip boundary taking into account electrokinetic effect," *Abstract and Applied Analysis*, Volume 2013, Article ID 718603.

Acknowledgements

The research reported in this thesis was carried out from October 2010 to November 2013. During this period, I was a PhD student in the Department of Mathematics and Statistics, Curtin University.

I wish to acknowledge the financial support of the China Scholarship Council and Curtin University for my PhD study through a joint CSC-Curtin Scholarship.

I would like to express my thanks to my supervisor, Prof. Yonghong Wu, for his encouragement and supervision throughout the past three years with remarkable patience and enthusiasm.

I would like to thank my co-supervisors, Prof. Lishan Liu of Qufu Normal University and Dr. Qun Lin of Curtin University, for their continuing encouragement and advice during my PhD study.

I also wish to acknowledge the help from Prof. B. Wiwatanapataphee of Mohidol University while she worked at Curtin University. I also would like to thank Prof. Kok Lay Teo, for his kindness and help during my PhD study.

I would like to give thanks to all my friends and classmates for their support and friendship particularly, Dr. Changjun Yu, Dr. Qinqin Chai, Dr. Bin Li, Dr. Jingyang Zhou, Yujing Wang, N. Khajohnsaksumeth, Dr. Honglei Xu, Yufei Sun, Yan Zhang, Mingliang Xue, Yanli Zhou, Dr. Changhua Jiang, A/Prof Chuanjiang Li, A/Prof. Tieqiao Tang, Dr. Xuegang Hu, A/Prof. Lingling Xu, and A/Prof. Xiangyu Gao.

I thank all of the staff in the Department of Mathematics and Statistics for contributing to a friendly working environment. The administrative staff, Joyce Yang, Shuie Liu, Lisa Holling, Jeannie Darmageo, Cheryl Cheng and Carey Ryken Rapp, deserve special thanks for providing kind and professional help on numerous occasions.

Finally, on a more personal note, I sincerely thank everyone in my family, especially my parents, for their love, understanding and support during my entire period of my PhD candidature in Australia.

Contents

1 Introduction **1**

1.1 Background 1

1.2 Objectives of the thesis 2

1.3 Outline of the thesis 3

2 Literature review **4**

2.1 General 4

2.2 Micro-systems and devices with fluid flows 5

2.2.1 Micro-Electro-Mechanical-Systems (MEMS) 5

2.2.2 Lab-on-a-chip (LOC) devices 6

2.3 Governing equations for fluid flows under electric fields 7

2.3.1 Equations for Electric double layer (EDL) 8

2.3.2 Equations for fluid flows 14

2.3.3 Boundary conditions 20

2.4 Methods for the solutions of boundary value problems 25

2.5 Existing results 26

2.5.1 Electrokinetic flows 27

2.5.2 Pressure driven flows 34

2.5.3 Time period electroosmotic flows 36

2.6 Concluding remarks 39

3 Solution of time periodic electroosmosis flow with slip boundary **40**

3.1 General 40

3.2 Problem description and mathematical formation 41

3.3 Solution of the boundary value problem 44

3.4 Numerical investigation 48

3.5 Concluding Remarks 55

4 Solution of Newtonian fluid flows through circular microchannels with slip boundary and electrokinetic phenomena **56**

4.1 General 56

4.2 Mathematical model and formulation 57
4.3 Exact solution for the transient velocity field 61
4.4 Solutions for the flow rate and stresses 67
4.5 Numerical investigation 69
4.6 Concluding Remarks 82

5 Summary and future research directions **83**
5.1 Summary 83
5.2 Future research directions 85

Bibliography **86**

CHAPTER 1

Introduction

1.1 Background

Over the last couple of decades, one of the most important worldwide scientific research focuses has been on the study of materials at micro and nano-scales. The continuing research development in theories and technologies in this field led to the invention of many microdevices and microsystems for application in engineering, biology and modern medicine. Most of these devices and systems involve fluid flows through micro-channels or micro-tubes, which are known as microflows [1–4]. Typical examples include drug delivery systems [5], micropumps, nano-particle mixers, biological sensing and energy conversion devices [6].

To a large degree, the performance of microsystems depends on the flow behavior of fluid in micro channels. Hence, the study of microflows has attracted more and more attention from the science and engineering research community for developing better models and deriving a better understanding of the dynamics of microflows. Many research projects have been carried out to study microflows from various aspects, particularly the interaction between fluid and solid surface at micro-scale, the flow behavior under different driving mechanism such as pulsatile pressure field and electromagnetic field, the interaction between fluid and inserted micro or nano-particles, and the influence of system parameters on the dynamics of microflows.

For the interaction between fluids and the solid surface, traditionally the no slip boundary condition is used, namely the velocity of fluid relative to the solid surface is zero. Although many experiments support this assumption particularly at micro-scale, it has been found through experiments that micro-slip occurs between fluids and the solid surface at micro-scale [7–11]. The so-called Navier slip boundary condition, namely the velocity of fluid relative to the solid surface is proportional to the shear stress on the surface, has thus been used by many

researchers for the study of fluid flows in microchannels [9,12,13]. Other nonlinear boundary slip models have also been proposed [14]. Also, various attempts have been made to use nanotechnologies for surface treatment to achieve large slip so as to maximize the transport efficiency of fluids through micro-channels.

Many investigations have been carried out to study various flow problems of Newtonian and non-Newtonian fluids in micro-channels. Exact and numerical solutions to many flow problems under the no-slip condition have been obtained [7, 8, 14, 15]. However, so far only very few exact solutions for the slip models have been established. Recently, steady slip solutions have been obtained for microflows through channels, circular tubes and annulus, as well as rectangular and elliptical ducts [10, 11, 14, 16–18]. More recently, exact solutions of velocity and stress fields have been obtained for transient flows of fluids in microtubes under constant and pulsatile pressure gradient [10, 16].

1.2 Objectives of the thesis

A great deal of work in the study of fluid flow in microchannels and microtubes has been done, but many issues and problems still require further investigation.

This project focuses on the study of two types of transient flows in microchannels taking into account microslip on the boundary. The main objective of the research is to establish exact solutions for the problems, investigate the dynamics of microflows under different types of driving forces, and consequently explore methods for controlling the fluid flow behavior and flow pattern in microchannels. The specific objectives are as follows

(1) Construct the boundary value problem governing the time periodic electroosmosis flow between two parallel plates taking into account micro-slip on the boundary. This includes formulation for the electric driving force and construction of the governing field equation and the slip boundary condition.

(2) Derive the exact solution for the electroosmosis flow in microchannels with boundary slip.

(3) Investigate the behavior of electroosmosis flows in microchannels under different conditions and the influence of boundary slip, and explore methods for controlling the flow pattern.

(4) Formulate the governing equations for transient slip flows in circular microtubes driven by the combined effect of electric force and pressure gradient.

(5) Derive analytical solutions for the transient slip flows in micro-channels of circular cross-section governed by the boundary value problem established in (4).

(6) Explore methods for controlling the velocity profile and flow pattern for flows in circular micro-tubes driven by both electric force and pressure gradient through varying the model parameters and external controllable factors.

1.3 Outline of the thesis

This thesis develops various analytical and numerical results for transient slip flows of Newtonian fluids through micro-channels and micro-tubes driven by electrical and pressure fields. The thesis is divided into five chapters.

Chapter 1 introduces the background of research and highlights the objectives of the research.

Chapter 2 gives a review of previous work and results relevant to this study, which include review of fundamental equations, boundary conditions, methods of solutions and some existing solutions.

Chapter 3 derives exact solutions for the time periodic electroosmosis flows. The flow behavior under different conditions and the influence of boundary slip are also investigated.

Chapter 4 develops the analytical solutions for the transient microflows in circular tubes driven by the combined effect of pressure and electric fields, including the exact solutions for the velocity field, the flow rate and the stress field. The flow dynamics under different conditions and the influence of the electric field and the microslip on boundary are also investigated.

Chapter 5 summarizes the main results of the thesis and discusses some problems for further research.

CHAPTER 2

Literature review

2.1 General

Miniaturization has been one of the swiftest revolution in the past decades. The term "microfluidics" was invented about 40 years ago when microfabicated fluid system was developed at Stanford (gas chromatography) and at IBM (inkjet printer nozzles, which use piezoelectrics or thermal bubble ejection to deposit ink on paper). Since then, many microscale or even nanometer scale devices have been developed. Nowadays, microscale and nanometer scale devices have been used widely in engineering, industry, biomedicine, and scientific research. Typing examples of applications are drug delivery, DNA analysis/sequencing systems, and biological/chemical agent detection sensors on microchips. As most of the microdevices and micro-systems involve microflows, namely the flow of fluids in micrometer scale channels/tubes, it is important to understand the flow behaviour of fluids at microscales. In order to achieve precise control of the systems for optimal performance, over the last couple of decades, a great deal of research has been carried out to study microflows for various different applications. In this chapter, we will give a review of work in various areas relevant to the proposed research.

Section 2.2 will introduce some microsystems which involve microflows, including the micro-electro-mechanical-systems (MEMS) and the lab-on-a-chip (LOC) devices. Section 2.3 will briefly review the fundamental equations governing fluid flows under electric field and pressure gradients. Section 2.4 will review the main methods for the solution of the underlying boundary value problems. Section 2.5 will briefly review some previous work in electrokinetic flows, pressure driven flows and time period electroosmotic flows. Section 2.6 will give some concluding remarks.

2.2 Micro-systems and devices with fluid flows

In the past decades, micromachining technology that emerged in the late 1980s has drawn more and more attention. Micromachines have a great effect on many areas, such as biology, optics and electrical engineering. Micro-system-technology can provide micro-mechanical elements to fabricate micro-size sensor and actuators. These micro-mechanical parts can be integrated with signal conditioning and processing circuitry to form Micro-electro-mechanical systems (MEMS). Many systems involve fluid flows [1, 3, 4], such as micropumps, heatsinks, heatexchangers and drug delivery systems. A subset of MEMS devices is called Lab-on-a-chip, which is also called "Micro Total Analysis Systems" (μTAS) and becomes popular for its several advantages. The main advantage is that we can use it to simplify the laboratory procedure, as it can transfer the labor intensive, time consuming and high cost laboratory procedures to a chip. In the rest of this section, we will give a more detailed review of the Micro-electro-mechanical systems (MEMS) and the Lab-on-a-chip (LOC) devices.

2.2.1 Micro-Electro-Mechanical-Systems (MEMS)

Micro-electro-mechanical systems (MEMS) involve the technology of very small devices. It was officially adapted at a meeting in Salt Lake City in 1989 [19]. MEMS are also referred to as micromachines, or micro systems technology MST. MEMS is the integration of mechanical elements, sensors, actuators, and electronics on a commom sillicon substrate through microfabrication technology. The advance in MEMS has lead to the development of smaller devices. Micro-electromechanical systems (MEMS) inherit the previous research achievements to develop laboratory-based biochips and complex DNA sequence of the amino acid sequence of the protein synthesis (synthesis) process.

In recent years, many important research directions are toward the biomedical laboratory instrumentation and automation in order to achieve the highly integrated Lab-on-a-chip systems. The systems drew such attention because they can control the movement of liquid quickly and automatically. With the development of MEMS technology, many papers on new microfluidic systems and microfluidic devices have been published with focus on how they are to operate effectively in control of microfluidics. Because of modern technology, cost and reliability of components, microfluidic components must be used to facilitate relatively simple device structure for future products. In these mechanism, the surface tension (surface tension) plays an important role on the flow in micro channels. Many

teams studied how to apply the surface tension in microfluidic systems.

In [20], Yang and Chen used dielectric to produce electricity wet Lab-on-a-chip systems, in order to achieve DNA / protein synthesis and other micro and small automatic biochemical analyzer response. They also produced a digital microfluidic system chips which have many advantages over the traditional continuous microfluidic system, such as control of the individual reagent separately, fully control of the complex biological detection reaction process, the flexibility of the reaction process step design, and the immediately known synthesis effects on combining with micro-optical detection system. In addition, component-based DNA/ protein synthesizers have many advantages, such as reducing the required sample size, low cost, and combination of personal digital assistant (PDA) to achieve programmable.

2.2.2 Lab-on-a-chip (LOC) devices

Lab-on-a-chip fluid technology has received more and more attentions since its name was first used. A lab-on-a-chip (LOC) is a device that integrates one or several laboratory functions on a single chip of only millimeters to a few square centimeters in size. Lab-on-a-chip systems use chip-based micromachining techniques to reduce the scale of fluid controlling systems and enhance biological and chemical analysis [21]. The term "Lab-on-a-Chip" was introduced later on when it turned out that μTAS technologies were more widely applicable than only for analysis purposes. Micro and nanofluidic channels are the most fundamental structures in lab-on-a-chip devices. They can transfer the analysis of the existing laboratory function to portable equipment such as a chips.

The application of Lab-on-a-chips has significant role for biological medicine, medicine diagnosis, food hygiene environment monitoring and the development of molecular biology. In [22], Wu and Yue reported a simple, programmable controlling discrete droplet control chip. It overcomes the limitations of the traditional continuous flow transmission by controlling the voltage pulse sequence on the micro electrode array, to achieve transmission of discrete droplet and mix rapidly. Under the 30 V driving voltage, about $0.9\mu L$ deionized water droplet transmission speed can be up to 24mm/s. Under the 40V driving voltage, $0.8\mu L$ deionized water droplet and $1.4\mu L$ 0.0001 mol/L Rhodamine droplet can mix in $\frac{7}{30}$ second. For pure diffusion, these deionized water droplet mix will cost approximately 10 minutes.

In the earliest experiments, the pioneering groups of Austin and Craighead observed unusual transport characters of DNA [23,24]. They found a new technique

for fabricating two-dimensional artificial gels for DNA electrophoresis, which differs from previous approaches in that the entire device is fabricated as a monolithic unit using exclusively planar processing techniques adapted from semiconductor electronics fabrication.

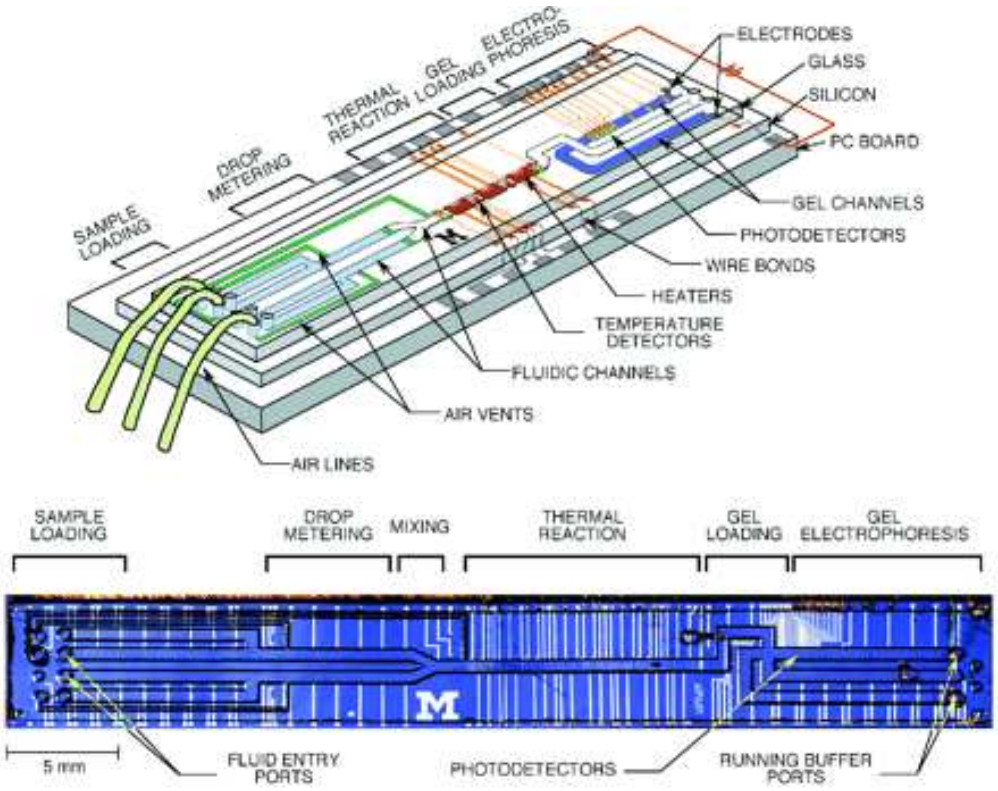

Figure 2.1: A device that uses microfabricated fluidic channels, heaters, temperature sensors, and fluorescence detectors to analyze nanoliter-size DNA samples [25]. (Top) Schematic of integrated device with two liquid samples and electrophoresis gel present. (Bottom) Optical micrograph of the device from above. http://lsi.epfl.ch/page-13122-en.html

2.3 Governing equations for fluid flows under electric fields

The flow of fluids under electric field in microsystems is governed by the fundamental equations of fluid dynamics, including the equations of motions, the continuity equation, the constitutive equations and boundary conditions. The driving forces include pressure gradient driving force and electric driving force. In this section, we will review methods and equations for the determination of

the electric driving force, then give the fundamental equations for determination of the velocity field and then describe different types of boundary conditions.

2.3.1 Equations for Electric double layer (EDL)

In this section, we discuss the properties of channel surface to understand the formation of the electric double layer (EDL), which leads to the formation of electric driving force. There are four factors affecting the formation of EDL, including the density of surface charges, roughness of the surface, the distribution pattern of surface charges and the chemical material consisted of the channel surface. Here, we limit our discussion only to silicon channels and the reason is that most micro and nanochannels being used are silicon channels. There are several reasons for using silicon channels. Firstly, silicon and its compound such as silica have remarkable electric and mechanical features, for instance, the adequate dielectric properties. Secondly, silicon and its compound have inherent advantages for some devices, because of the high-index contrast between the silica cladding and silicon core. Thirdly, many properties of silicon have been studied in the progression of semiconductor industry. Another reason is that silicon materials are cheap compared with other materials [26].

Electrokinetic phenomena are present due to electric double layer (EDL), which forms as a result of the interaction of ionized solution with static charges on dielectric surface [27]. For a lot of solid materials, when they are in contact with polarity solutions or electrolyte solutions, electric charges are produced on the solid surface due to the complex ionization, ion adsorption and ionic solvation. The surface charges will affect the polarity solution distribution of ions and formation of the electric double layer (EDL). The electric double layer in fact consists of several layers including the Stern layer, the Stern plane and a diffuse layer from the solid material to the solution center. There exists a plane near the Stern plane called shear plane which has significant effect on electroosmotic (EOF).

For instance, when silica (SiO_2) is put into water (H_2O) or in contact with an aqueous solution, its surface hydrolyzes and forms silanol group, which will react with water. There will be positive charge groups (H_3O^+, $SiOH^+$), negative charge groups (SiO^-) or neutral groups ($SiOH$), depending on the pH value of the electrolyte solution. The pH value of pure water is 7, and the pH value of most physiological fluids, for instance the saline and the blood serum, is 7.4 to 7.5. In this situation, the channel surface always negatively charged.

The surface charge density ρ is a measure of electric charge present at an

interface per unit volume of space. The unit volume here refers to unit length, unit surface area or unit volume in 1D, 2D and 3D respectively. In the solution materials, the total charges consist of free charges and bound charges,namely

$$\rho = \rho_f + \rho_b, \tag{2.1}$$

where ρ_f denotes the density of free charges and ρ_b is the density of bound charges. Free charges are the overage charges and they can move into electrostatic equilibrium, where electrostatic equilibrium means the charges are stable and the resultant electric field is not affected by constitute electric currents and time [28].

The applied electric field E makes the bound charges to build electric dipoles. The bound charges are the whole net accumulation of charges from the orientation of the dipoles. They are called bound as they are stable. In the dielectric material the charges are the electrons bound to the nuclei [29].

The surface charge density ρ is affected by the cleaning situation and deposition of the solution during micro fabrication. Experimentally, Israelachvili investigated the surface charge density [30], and found that when the pH value of the solution is higher than 4, in a 2D channel, the surface charge density of the silicon surface is $0.2C/m^2$ for an aqueous solution.

From the above discussion, we know that the density of the surface charge affects the EDL property. Usually, it is assumed that the channel wall is ideally smooth and the surface charges are distributed uniformly on all the channel wall surface. This assumption is reasonable for actual channels because, in comparison with the height of the channel, the channel surfaces are smooth enough.

If the channel surface is negatively charged, the positive ions are attracted toward the surface, which forms the Stern layer as shown in Figure 2.2. The typical thickness of the Stern layer is one ionic diameter. The ions within the Stern layer are attracted to the wall with a very strong electrostatic force; hence they are immobilized near the charged surface [31]. Then after the Stern layer there forms the diffuse layer, where the ion density variation obeys the Boltzmann distribution, consistent with the derivation based on the EDL consisting of two distinct zones: Stern and diffuse layers [32]. The extend of the EDL, namely the distance from the wall, can be approximately predicted by the Debye length (λ). The Debye length depends on the molar concentration of the ionized fluid, and can be estimated using the Debye-Huckel parameter (ω) by,

$$\omega = \frac{1}{\lambda} = \sqrt{\frac{e^2 \sum_i n_i z_i^2}{\epsilon \epsilon_0 k_B T}}, \tag{2.2}$$

where n is the concentration of the electrolyte, k_B is the Boltzmann constant, e is the electron charge, z is the valence, T is the absolute temperature in kelvins, ϵ_0 is the dielectric permittivity of vacuum, and ϵ is the dielectric constant of the solvent. The subscript i indicates the ith specy.

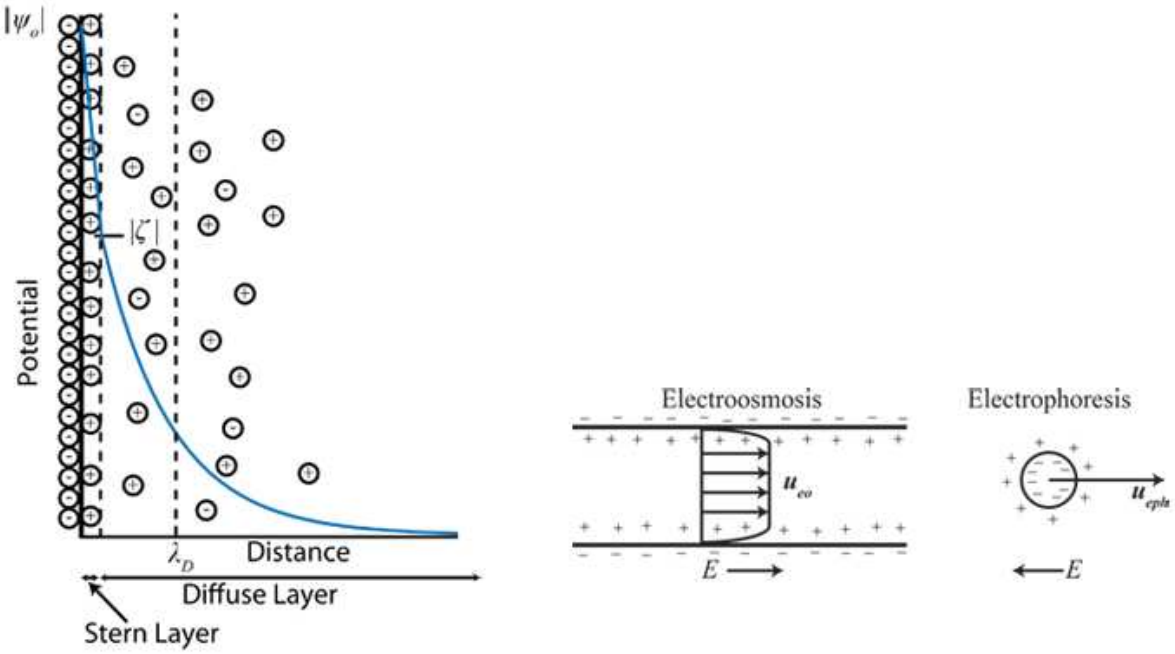

Figure 2.2: Schematic diagram showing the electric double layer (EDL) next to a negative charged solid surface and the resulting electrokinetic phenomena of electrophoresis. Stern assumed that it is possible that some of the ions are specifically adsorbed by the surface in the plane, and this layer has become known as the Stern Layer, after the Stern Layer there form the diffuse layer. The Debye length are shown by λ_D. $http://web.mit.edu/lemi/rsc_electrokinetics.html$

The EDL can be characterized, thus ion distribution can apply an electrokinetic potential ψ. Since the oppositely charged ions in the Stern layer shield some of the electric charges on the surface, the electrokinetic potential drops rapidly across the Stern layer. The value of ψ at the edge of the Stern layer is known as zeta potential (ζ). For most practical cases, we can employ the zeta potential to describe electrokinetic flows rather than the wall potential ψ_0. In

electrochemical equilibrium, the density of electrolyte complies with the Boltzmann distribution [33]:

$$\rho_i(r) = \rho_i^0 e^{\frac{-z_i e\phi^*(r)}{kT}}, \tag{2.3}$$

where $r(x, y, z)$ is the vector of location in Cartesian coordinates, ρ_i^0 is the density of ion specy i at the location where $\phi^* = 0$, z_i is the valence of ion specy i, e is the elementary charge, ϕ^* is the electrical potential in Volts, k is the Boltamann constant and T is the absolute temperature in Kelvins. The charge density difference $\rho_1 - \rho_2$ is affected by the surface charge density on the wall. If the surface charges on the wall are zero, which means the solution is electrically neutral, $\rho_1 - \rho_2 = 0$. As the surface charge density increases, more counter-ions will be adsorbed to the wall, and thus $\rho_1 - \rho_2$ increases. Because the solution is electrically neutral in the core, $z_i\rho_i^0 = 0$. Binary electrolytic solutions refer to electrolytes which contain one cation species and one anion species after ionization, such as $NaCL$, KCl, K_2SO_4 which are common electrolytes. If a solution is a binary electrolyte solution, then $z_1 + z_2 = 0$, and $\rho^0 = \rho_1^0 = \rho_2^0$ [34]. Based on the theory of electricity [33], the electrical potential satisfies the Poisson's equation,

$$\begin{aligned}\nabla^2\phi^*(r^*) &= -\frac{1}{\varepsilon_d\varepsilon_0}\rho_e(r^*) \\ &= -\frac{1}{\varepsilon_d\varepsilon_0}e\sum_i z_i\rho_i(r^*),\end{aligned} \tag{2.4}$$

where ε_d denotes the dielectric constant of the substance, ρ_e is the total charge density in the solution, and ε_0 denotes the free space permittivity. Substituting equation (2.3) into equation (2.4), we have

$$\begin{aligned}\nabla^2\phi^*(r^*) &= -\frac{1}{\varepsilon_d\varepsilon_0}\rho_e(r^*) \\ &= -\frac{1}{\varepsilon_d\varepsilon_0}e\sum_i z_i\rho_i^0 e^{\frac{-z_i e\phi^*(r^*)}{kT}},\end{aligned} \tag{2.5}$$

For binary electrolytes, $z_1 = -z_2 = z^0$, $\rho_1^0 = \rho_2^0 = \rho^0$, and thus the Poisson-Boltzanmm equation (2.5) becomes

$$\nabla^2\phi^*(r^*) = \frac{2e\rho^0 z^0}{\varepsilon_d\varepsilon_0}\sinh(\frac{z^0 e\phi^*(r^*)}{kT}), \tag{2.6}$$

For low surface potential, $\frac{z^0 e\phi^*}{kT} << 1$, and we have

$$\sinh(\frac{z^0 e\phi^*(r^*)}{kT}) \approx \frac{z^0 e\phi^*(r^*)}{kT} \tag{2.7}$$

and so equation (2.6) becomes

$$\nabla^2\phi^*(r^*) = \kappa^2\phi, \tag{2.8}$$

where $\kappa = (\frac{2z^{02}e^2\rho^0}{\varepsilon_d\varepsilon_0 kT})^{1/2}$. Equation (2.8) can be used to describe electrostatic interactions between molecules in ionic solutions [30, 35].

By introducing the normalized variables and parameters

$$\begin{aligned}
&\phi_0 = \frac{kT}{e},\\
&\phi(r(x,y,z)) = \frac{\phi^*(r^*(x,y,z))}{\phi_0},\\
&x = \frac{x^*}{L},\\
&y = \frac{y^*}{h},\\
&z = \frac{z^*}{w}
\end{aligned} \tag{2.9}$$

equation (2.8) becomes

$$\varepsilon_1^2\frac{\partial^2\phi}{\partial x^2} + \frac{\partial^2\phi}{\partial y^2} + \varepsilon_2^2\frac{\partial^2\phi}{\partial z^2} = h^2\kappa^2\phi, \tag{2.10}$$

where $\varepsilon_1 = \frac{h}{L}, \varepsilon_2 = \frac{h}{w}$.

We can also transform the Poisson equation (2.5) by mole fractions of ion species and Faraday's constant as follows [33]

$$\begin{aligned}\nabla^2\phi^*(r^*) &= \frac{1}{\varepsilon_d\varepsilon_0} e\sum_i z_i\rho_i(r^*) \\ &= \frac{1}{\varepsilon_d\varepsilon_0} eN_A\sum_i z_i n_i(r^*) \\ &= \frac{1}{\varepsilon_d\varepsilon_0} Fn_t\sum_i z_i Z_i(r^*),\end{aligned} \tag{2.11}$$

where n_t is the total molar concentration of all ions, $n_t = \sum_i n_i$, N_A is the Avogadro number, Z_i is the mole fraction of ion species i, $Z_i = \frac{n_i}{n_t}$, and the total mole fractions of all ions and solvent is 1, i.e. $\sum_i Z_i = 1$. Then with (2.9), equation (2.11) can be written as

$$\nabla^2\phi = -\frac{Fn_t h^2}{\varepsilon_e\phi_0}\sum_i z_i Z_i, \tag{2.12}$$

where $\phi_0 = kT/e = Rt/F$, $\varepsilon_e = \varepsilon_d\varepsilon_0, \varepsilon_1 = h/w, \varepsilon_2 H = h/L$. Equation (2.12) is the Poisson equation for electroosmotic flow in a channel.

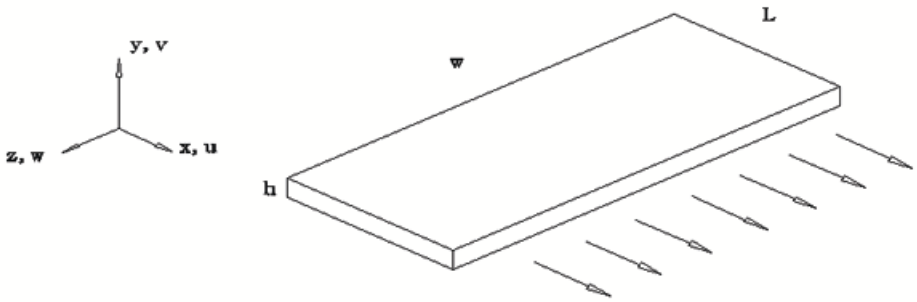

Figure 2.3: Geometry of one dimension channel. w is the width of the channel, L is the length of the channel, u, v, w are the fluid velocities in the x, y, z direction. $w >> h, l >> h$

For a one dimensional channel as shown in Figure 2.3, if the channel is wide and long, namely $\varepsilon_1 = \frac{h}{L} << 1$ and $\varepsilon_2 = \frac{h}{w} << 1$, equation (2.10) becomes

$$\varepsilon_a^2\frac{\partial\phi^2}{\partial y^2} = \phi. \tag{2.13}$$

where $\varepsilon_a = \frac{1}{h^2\kappa^2}$

For binary electrolytes, the Poisson-Boltzanmm equation (2.6) becomes

$$\frac{\partial \phi^*}{\partial y^{*2}} = \frac{2e\rho^0 z^0}{\varepsilon_d \varepsilon_0} \sinh(\frac{z^0 e\phi^*(r^*)}{kT}). \tag{2.14}$$

2.3.2 Equations for fluid flows

The basic variables for fluid flows include velocity vector, pressure, stress tensor, deformation rate and fluid density. By assuming fluid as a continuum, the flow of fluids must satisfy the fundamental equations of continuum mechanics including the stress equations of motion, the continuity equation, the geometric equations and the constitutive equations. By manipulating these equations, the so-called Navier-Stokes equations can be derived which together with the continuity equation, constitute four governing field equation for the determination of the three velocity components and the fluid pressure for the three dimensional flows of incompressible fluids. The rest of this section is organized as follows. Firstly, the fundamental equations for continuum mechanics are presented together with the principles and assumptions behind the equations. Then, the Navier-Stokes equations are derived with some comments on their applicability and limitations.

Stress Equations of Motion

Stress is a fundamental component of continuum mechanics. We use it to measure the internal force intensity developed within a body in response to external forces. Determination of stress plays an important role in the study of many problems.

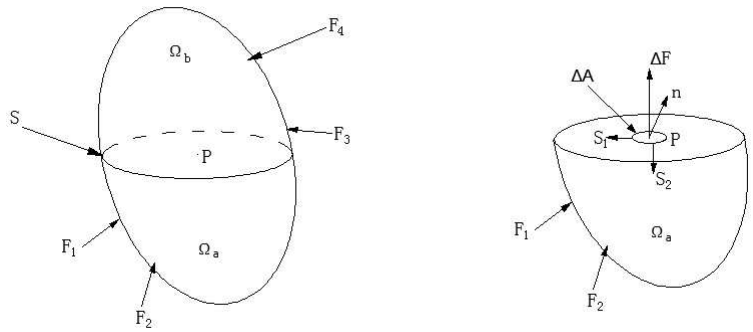

Figure 2.4: Sketch for showing the concept of stress vector.

In order to get the stress equations of motion, we review the concepts of normal stress and shear stress first. Consider an arbitrary body of material Ω, subject to gravity and surface force as shown in Figure 2.4. S is a cross section

which passes through an arbitrary interior point P and separates the body Ω into two parts Ω_a and Ω_b. If we separate Ω_a from Ω_b and only consider the force acting on Ω_a, then there will be a resultant force $\triangle F$, which acts on a small area $\triangle A$ around the point P. The quantity $\frac{\triangle \mathbf{F}}{\triangle A}$ is the average force acting on the unit area $\triangle A$, and the limit of this quantity is defined as the stress vector acting at point P on the plane S, namely

$$\sigma = \lim_{\triangle A \to 0} \frac{\triangle F}{\triangle A}$$

Thus, the stress vector means the intensity of force acting at the interior material point.

In general, the force $\triangle F$ will not be normal to the surface $\triangle A$, and can be resolved into three orthogonal components $\triangle F_n$, $\triangle F_{s1}$, $\triangle F_{s2}$, where $\triangle F_n$ is normal to the area $\triangle A$, and $\triangle F_{s1}$ and $\triangle F_{s2}$ are parallel to the area $\triangle A$ but orthogonal to each other. Thus it results

$$\sigma = \lim_{\triangle A \to 0} \Big(\frac{\triangle F_n}{\triangle A}, \frac{\triangle F_{s1}}{\triangle A}, \frac{\triangle F_{s2}}{\triangle A} \Big). \tag{2.15}$$

The component

$$\sigma_n = \lim_{\triangle A \to 0} \frac{\triangle F_n}{\triangle A}$$

is in the normal direction and is thus called normal stress, while the components

$$\sigma_{s1} = \lim_{\triangle A \to 0} \frac{\triangle F_{s1}}{\triangle A} \tag{2.16}$$

and

$$\sigma_{s2} = \lim_{\triangle A \to 0} \frac{\triangle F_{s2}}{\triangle A} \tag{2.17}$$

are parallel to the plane on which the force are acting, and are called shear stresses.

Therefore, the stress vector on any plane passing through an arbitrary point in a body can be readily characterised by a normal stress and two shear stresses. From the definition, the normal stress may cause tension or compression in material, while the shear stress may cause changes in shape of the object.

To easily identify the stress component σ, double subscript notation is used. The first subscript denotes normal direction of the plane on which the stress acts,

and the second subscript denotes direction of the stress. For example, σ_{xy} denotes the shear stress acting on the x-plane and alone the y-direction. In continuum mechanics, a stress component is positive if it acts on a positive plane and points to the positive coordinate direction or it acts on a negative plane and points to the negative coordinate direction. Except for these two cases, all other cases give a negative stress component.

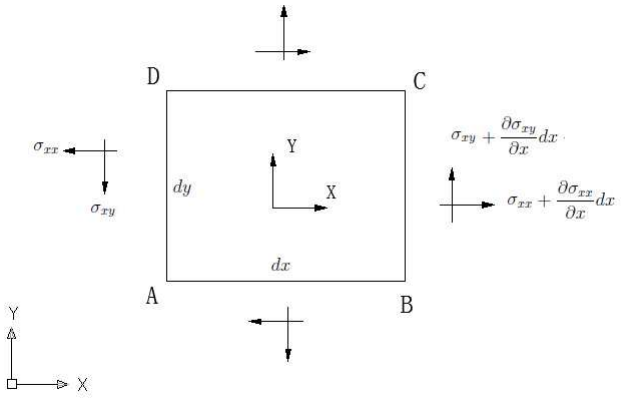

Figure 2.5: Free body diagram showing the forces acting on a differential element.

The stress components must satisfy a set of equations, namely the stress equations of motion which can be derived from Newton's second law. To derive the stress equations of motion, consider the free body diagram of a differential element in 2-D as shown in Figure 2.5. Assume that there are stresses σ_{xx} and σ_{xy} acting on plane AD, then based on the assumption of stress continuity, the stresses on the plane CB are

$$\sigma_{xx}(x + dx, y) = \sigma_{xx}(x, y) + \frac{\partial \sigma_{xx}}{\partial x} dx + O[(dx)^2] \tag{2.18}$$

$$\sigma_{xy}(x + dx, y) = \sigma_{xy}(x, y) + \frac{\partial \sigma_{xy}}{\partial x} dx + O[(dx)^2]. \tag{2.19}$$

Similarly, we can obtain the stresses on the plane CD as

$$\sigma_{yy}(x, y + dy) = \sigma_{yy}(x, y) + \frac{\partial \sigma_{yy}}{\partial y} dy + O[(dy)^2] \tag{2.20}$$

$$\sigma_{yx}(x, y + dy) = \sigma_{yx}(x, y) + \frac{\partial \sigma_{yx}}{\partial y} dy + O[(dy)^2]. \tag{2.21}$$

Denoting the body force (force per unit mass) as (X, Y) and acceleration as (a_x, a_y), Then from the Newton's second law in the x direction, we have

$$\sum F_x = ma_x \tag{2.22}$$

which is

$$-\sigma_{xx}dy + (\sigma_{xx} + \frac{\partial \sigma_{xx}}{\partial x}dx)dy + (\sigma_{yx} + \frac{\partial \sigma_{yx}}{\partial y}dy)dx - \sigma_{yx}dx + \rho X dxdy = \rho dxdy a_x \tag{2.23}$$

which yields

$$\frac{\partial \sigma_{xx}}{\partial x} + \frac{\partial \sigma_{yx}}{\partial y} + \rho X = \rho a_x \tag{2.24}$$

Similarly, in the y direction, by applying Newton's second law to the differential element, we get

$$\frac{\partial \sigma_{yy}}{\partial y} + \frac{\partial \sigma_{xy}}{\partial x} + \rho Y = \rho a_y \tag{2.25}$$

Further, by assuming no rotation and consequently setting the force moment to zero, namely $\sum M_0 = 0$, we have

$$\sigma_{xy} = \sigma_{yx}$$

which indicates that the stress tensor is a second order symmetric tensor. Using the index notation, the equations of motion can be written as

$$\frac{\partial \sigma_{ji}}{\partial x_j} + \rho X_i = \rho a_i \tag{2.26}$$

where i, $j = 1$ and 2 for two dimensional problems; while for three dimensional problems, $i, j = 1, 2$ and 3.

Equation of Continuity

Let ρ be the density of fluid and v is the velocity vector, and consider a closed surface S, fixed in space, enclosing a fixed volume (Ω) of fluid. Based on the principle of mass conservation, namely mass cannot be created or destroyed unless

there is nuclear reaction, the mass efflux out of Ω through S is equal to the decrease of mass within Ω due to the change in density, that is

$$\iint_S \rho v \cdot n dS = -\iiint_\Omega \frac{\partial \rho}{\partial t} d\Omega \tag{2.27}$$

By using the divergence theory, equation (2.27) becomes

$$\iiint_\Omega [\frac{\partial \rho}{\partial t} + div(\rho v)] d\Omega = 0. \tag{2.28}$$

Due to the arbitrarity of Ω, (2.28) gives

$$\frac{\partial \rho}{\partial t} + div(\rho v) = 0, \tag{2.29}$$

which is known as the continuity equation. For incompressible fluid, ρ is a constant and thus the continuity equation becomes

$$div(v) = \frac{\partial v_j}{\partial x_j} = 0. \tag{2.30}$$

Geometric Equations

Another set of fundamental equations is the so-called geometric equations, which relate the velocity vector to the deformation rate of the fluid. Deformation includes normal deformation and shear deformation respectively for measuring the change in size and shape of an object. For three dimensional problems, the deformation rate is a tensor as follows

$$d = \begin{pmatrix} d_{xx} & d_{xy} & d_{xz} \\ d_{yx} & d_{yy} & d_{yz} \\ d_{zx} & d_{zy} & d_{zz} \end{pmatrix}$$

where d_{xx}, d_{yy} and d_{zz} are normal deformation rate in x, y and z directions for measuring the rate of change is size in x, y and z directions respectively; other components of d are shear deformation rates measuring the change in shape on different coordinate planes.

By assuming that the velocity field is continuous in fluid, a set of equations can be derived to relate the velocity vector with the deformation rate tensor as follows

$$d = \frac{1}{2}(\nabla \mathbf{v} + \nabla \mathbf{v}^T) \tag{2.31}$$

or in index natation

$$d_{ij} = \frac{1}{2}(\frac{\partial v_i}{\partial x_j} + \frac{\partial v_j}{\partial x_i}), \tag{2.32}$$

which is the so-called geometric equations.

Constitutive Equations

Different models have been proposed to describe the relationship between deformation rate and stress in fluids. These models can be classified as Newtonian models and no-Newtonian models. Here in this work, we focus on isotropic Newtonian fluids for which the shear stress is assumed to be linearly proportional to the rate of deformation. The stress-deformation rate relation is as follows

$$\sigma_{ij} = -p\sigma_{ij} + \lambda d_{kk}\delta_{ij} + 2\mu d_{ij}, \tag{2.33}$$

where μ is the coefficient of viscosity and p is the fluid pressure. For incompressible fluids, $d_{kk} = 0$ and thus

$$\sigma_{ij} = -p\delta_{ij} + 2\mu d_{ij}, \tag{2.34}$$

which are the so-called constitutive equations for isotropic incompressible Newtonian fluids.

Navier-Stokes Equations

The above equations are all field equations which must be satisfied at all points within a continuum. To solve the above equations, substituting (2.34) into the equation of motion with external applied electric field E, one obtains

$$\rho\frac{Dv_i}{Dt} = \rho X_i - \frac{\partial p}{\partial x_j}\delta_{ij} + \mu(\frac{\partial^2 v_i}{\partial x_j \partial x_j} + \frac{\partial^2 v_j}{\partial x_i \partial x_j}) + \rho_e E, \tag{2.35}$$

where

$$\frac{Dv_i}{Dt} = \frac{\partial v_i}{\partial t} + v_j\frac{\partial v_i}{\partial x_j}, \tag{2.36}$$

Using the continuity equation (2.30) yields

$$\frac{\partial^2 v_j}{\partial x_i \partial x_j} = \frac{\partial}{\partial x_i}(\frac{\partial v_j}{\partial x_j}) = 0, \tag{2.37}$$

and thus equation (2.35) becomes

$$\frac{Dv_i}{Dt} = X_i - \frac{1}{\rho}\frac{\partial p}{\partial x_i} + \frac{\mu}{\rho}\frac{\partial^2 v_i}{\partial x_j \partial x_j} + \frac{\rho_e}{\rho}E \tag{2.38}$$

which are the so called Navier-Stokes equations for incompressible Newtonian fluids. The Navier-Stokes equations, written out in unbridged form, are

$$\begin{aligned}
\frac{Du}{Dt} &= X - \frac{1}{\rho} + \frac{\partial p}{\partial x} + \frac{\mu}{\rho}\nabla^2 u + \frac{\rho_e}{\rho}E, \\
\frac{Dv}{Dt} &= Y - \frac{1}{\rho} + \frac{\partial p}{\partial y} + \frac{\mu}{\rho}\nabla^2 v + \frac{\rho_e}{\rho}E, \\
\frac{Dw}{Dt} &= Z - \frac{1}{\rho} + \frac{\partial p}{\partial z} + \frac{\mu}{\rho}\nabla^2 w + \frac{\rho_e}{\rho}E.
\end{aligned} \tag{2.39}$$

The Navier-Stokes equations for other kinds of fluids can be derived using the same process but different constitutive equations. The Navier-Stokes equations (2.38) together with the continuity equation (2.30) constitute a system of four partial differential equations for four unknown variables u, v, w and p and thus are solvable in principle. These four partial differential equations define all possible motions of an incompressible Newtonian fluid. The feature which distinguishes one flow situation from another is the nature of the boundary conditions satisfied by the velocity field v and p.

2.3.3 Boundary conditions

The Navier-Stokes equations and continuity equation constitute four equations in terms of four unknown variables, namely three velocity components plus the fluid pressure. These equations must be supplemented by boundary conditions in order to completely determine the velocity and pressure fields. In this subsection, various types of boundary conditions on fluid-solid interfaces are discussed.

Non-slip and slip boundary conditions

The so called no-slip boundary condition assumes that the fluid velocity relative to the solid is zero on the fluid-solid interface (Figure 2.6). However the no-slip condition is a hypothesis rather than a condition deduced from any principle. Evidences of slip of a fluid on solid surface were reported by many researchers [36, 37]. The electroosmoic force has an effective thickness of order of 1nm to 100nm. On the other hand, the micro and nano tubes for the laboratory- on-a

chip applications and micro-electromechanical systems only have a typical height from 1 nm to 100 μm. This magnitude disparity in the electric double layer and the tubes and channels height is a great challenge in numerical simulation of electroosmotically driven microflows. Therefore it is necessary to develop a unified slip boundary condition taking into account the electric double layer effects by specifying a proper velocity slip boundary condition on the wall.

For nanoscale or microscale channels of high precision such as flow sensor, velocity slip affects the fluid flow in different extent. Yang [38] investigated the micro pipe liquid flow velocity slip phenomenon in theoretical analysis, and established the criterion for near wall flow velocity slip layer and calculation of velocity slip.

The viscosity of liquid is mainly caused by the cohesion and adhesion between the molecules. Viscosity can make the liquid adhesive on the solid wall. Due to the role of the inter molecular force, liquid intermolecular forces always exist. Due to the high randomness of fluid molecular movement, the force between the liquid and solid cannot be measured by calculating molecules force between liquid and solid surface.

Zhang [39] established the method for calculating the acting force between the solid and liquid molecular groups based on the three Hamaker material hypotheses. The slip boundary has a significant effect on liquid flow and heat transfer of the liquid. The channel wall characters and shear stress have direct influence on the velocity slip. Zhang and his co-workers assumed uniform distribution of liquid molecules inside the pipes and neglected the impact of random motion of molecules. They used numerical integration to calculate the force between liquid molecules and the solid wall. When the wall provides a large enough force to resist the shear stress from the liquid, the near wall micelles can maintain stationary state. The liquid and solid molecular potential parameters as well as the shear stress of the liquid will affect the velocity slip. Velocity slip wall micelles suffer from the wall frictional force. As the fraction increases, the velocity of the micelles in flow increases. They use friction coefficients to calculate the wall fraction then determine the velocity of the liquid group. The investigation reveals that, in a micron pipe, a small velocity slip may occur when the flow pressure gradient is relatively large, and will cause errors in the pipe flow calculation.

Liquid slip boundary means the velocity of liquid molecules at the channel wall is nonzero. While no slip represents a situation where the liquid in the first molecular layer is stagnant and all the other molecules are sheared past the first molecular layer. The liquid molecules flow though the first molecular layer is

subject to strong friction on the wall. The lower the friction with the wall is, the less force is needed for a given flow velocity. Therefore, slip is very important in nanofluidics since it dramatically reduces the required pressure in pressure-driven flows. Low fraction flows in carbon tubes and pipes and several functional device architectures are described and discussed in [40]. In most experiments which are probing slip, the slip length can be inferred from measuring [41].

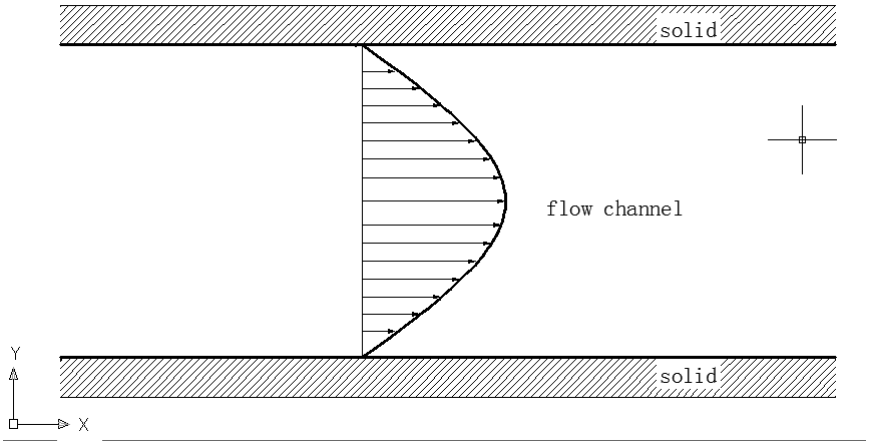

Figure 2.6: Typical velocity profile subject to no slip at the solid walls.

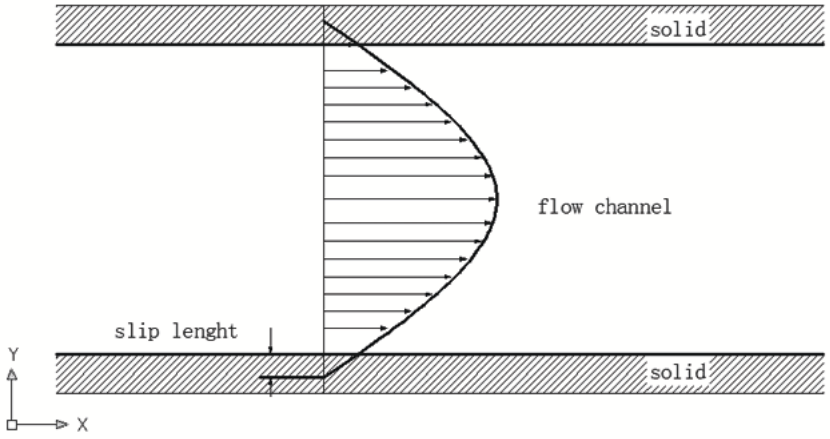

Figure 2.7: A schematic illustrating the slip length.

A definition of a slip length or a slip coefficient b on a rigid surface, with unit normal vector $\mathbf{n}$ directed into the fluid, linearly relates the velocity at the wall to the wall shear strain rate

$$v_{||} = b\mathbf{n} \cdot [(\bigtriangledown \mathbf{v}) + (\bigtriangledown \mathbf{v})^T] \cdot (\mathbf{I\text{-}nn}) \tag{2.40}$$

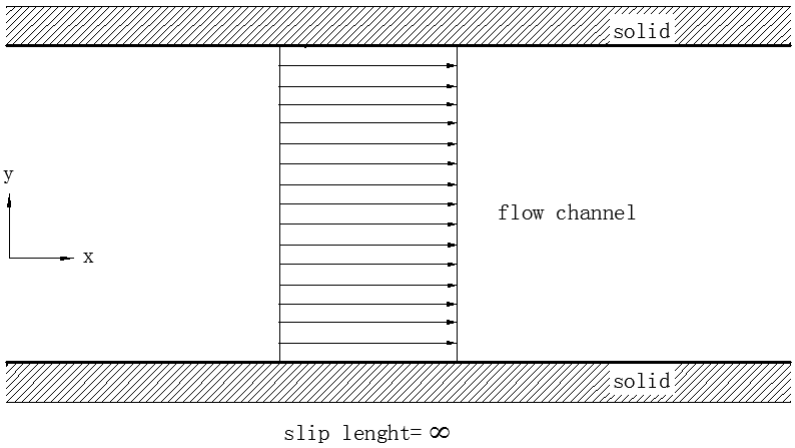

Figure 2.8: Typical velocity profile subject to perfect slip boundary condition and the slip length $l = \infty$

where $v_{||}$ is the component of fluid velocity tangent to a solid surface, $\mathbf{v}$ is the velocity field for a Newtonian fluid. This relation was first proposed by Navier [42]. As we can see in Figure 2.7, the slip length is the local equivalent distance below the solid surface while the no-slip boundary condition would be satisfied if the flow field were extended linearly outside of the physical domain. Figure 2.8 represents a situation where the liquid does not experience any friction with the wall. Recently, it is found that slip length in nanochannels is influenced by the surface roughness and hydrophobicity [43, 44]. Over the last few years, various investigations have been made to study various flow problems of Newtonian and non-Newtonian fluids with slip boundary conditions.

Microfluids flow through a straight channel is one of the simplest but most popular configurations in micro fluidic systems. Hang-Bob Lee and Wook Yeo studied the water flow between two infinite parallel plates and slip on NAPL-wetted surfaces [45], and the Navier-Stokes equation for the case was shown to be

$$\mu \frac{d^2 u_x(y)}{dy^2} = \rho g(\frac{dh}{dx}). \tag{2.41}$$

The boundary conditions for the velocity component is $u = u_s$, on $y = 0$ (on the solid surface). After integrating equation (2.41) twice with respect to y, and using the boundary condition, the following velocity was obtained

$$u = \frac{\rho g}{2\mu}(-\frac{dh}{dx})(-y^2 + ye) + u_s, \tag{2.42}$$

where ρ is the liquid viscosity, g denotes acceleration due to gravity, e is the aperture size, μ is the viscosity, $\frac{dh}{dx}$ is the hydraulic gradient and u_s represents the slip velocity. From Navier's hypothesis, the velocity on the surface is proportional to the shear stress $u = \beta\frac{du}{dy}$, where β is the slip length. Saidi investigated the solutions of the 3-dimension non-Newtonian fluid flow with slip condition of Coulomb's type imposed on a part of the boundary [46]. In that paper, existence and uniqueness results for the weak solution are proved by using Tichonov's fixed point theory. Donghyun You and Parviz Moin [47] investigated effects of hydrophobic surfaces on the drag and lift of a circular cylinder at Reynolds numbers of 300 and 3900. A cylinder of which the entire surface is hydrophobic, and cylinders with alternating circumferential bands of slip and no-slip conditions are considered.The effect of a hydrophobic surface can be modeled using slip boundary conditions,

$$u_s = L_x\frac{\partial u}{\partial y}, v_s = v_{wall} = 0, w_s = L_z\frac{\partial w}{\partial y} \tag{2.43}$$

where u, v, and w are the streamwise, vertical, and spanwise velocity components, u_s, v_s and w_s are the corresponding velocity components at the hydrophobic wall, and L_x and L_z denote slip lengths in x and z directions, respectively.

Impulsive boundary condition

The impulsive boundary condition has been addressed in relatively few publications. For instance, Stewartson [48] considered the flow with the motion in the boundary layer associated with a semi-infinite plate, which starts to move impulsively along its length with constant velocity U in a fluid at rest at infinity. The x-axis is along the plate length and y-axis is perpendicular to the plate. u and v are the components of fluid velocity along and perpendicular to the plate respectively. The motion begins at $t = 0$, and the field equation for the fluid boundary-layer are

$$\frac{\partial u}{\partial x} + \frac{\partial v}{\partial y} = 0. \tag{2.44}$$

and

$$u\frac{\partial u}{\partial x} + v\frac{\partial u}{\partial y} = -\frac{1}{\rho}\frac{\partial p_1}{\partial x} + v\frac{\partial^2 u}{\partial y^2}. \tag{2.45}$$

The velocity in the main stream is constant and equal to U relative to the channel and the boundary conditions are

$$\begin{aligned} &u = v = 0, \quad \text{when} \quad y = 0, x > 0, t > 0; \\ &u = U, \quad \text{when} \quad y > 0, \quad \text{and} \quad \text{either} \quad t \geq 0, x = 0, \quad \text{or} \quad x > 0, t = 0; \\ &u \to U, \quad \text{when} \quad y \to \infty, x \geq 0, t \geq 0 \end{aligned} \tag{2.46}$$

Dose used Rayleigh's method and the momentum integral to get two approximate solutions of this problem. Eric and coworkers reported numerical solutions for impulsively started electroosmotic flow. The lumen space is divided into N_{aq} concentric annuli each of thickness $\triangle r$, so the boundary conditions include condition for $V(t = 0; i)$ and $V(t, N_{aq} + 1)$ [49].

Kai and his colleagues [50] used the finite differential method to analyze the diffusion of an impulse KCL sample solution in the rectangular section of straight pipes driven by electroosmosis.

2.4 Methods for the solutions of boundary value problems

Various methods have been used to solve fluid flow problems through channels and pipes. These methods include analytical methods and numerical methods. Major analytical methods for channel or pipe flows include separation of variables for steady state problems, expansion of solution in time by Fourier series and in apace by Bessel functions for time dependent problems, complex variable methods and etc.

In [51], the authors consider the flow of time dependent laminar electrokinetic slip flow. The governing equation is

$$\frac{1}{\mu}\frac{\partial p}{\partial z} + (\frac{\partial^2 v}{\partial x^2} + \frac{\partial^2 v}{\partial y^2}) + \frac{1}{\mu}\rho E = \frac{1}{v}\frac{\partial v}{\partial t} \tag{2.47}$$

The boundary conditions for the velocity field are

$$
\begin{aligned}
&v(x,y,0)=0,\\
&v(w,y,t)=b_1\frac{\partial v}{\partial x}(w,y,t),\\
&v(x,h,t)=b_2\frac{\partial v}{\partial y}(x,h,t),\\
&\frac{\partial v(0,y,t)}{\partial x}=0,\\
&\frac{\partial v(x,0,t)}{\partial y}=0.
\end{aligned}
\tag{2.48}
$$

The authors obtained the general expression for the time dependent solution of the problem by using Green's function method. The authors also obtained an oscillating solution by using a complex variable approach together with the separation of variables method.

Typical numerical methods for channel and pipe flows include finite difference methods [52, 53] and finite element methods [54, 55]. In [56], the authors use the finite element method for the study of a low Reynolds number flow. In [57], the authors used the finite element method to solve the following boundary value problem for unsteady incompressible flows:

$$
\begin{aligned}
&\rho(\partial_t u+u\cdot\nabla u)-\nabla\cdot\sigma=f \qquad &&\text{in } \Omega\times[0,T]\\
&\bigtriangledown\cdot u=0 &&\text{in } \Omega\times[0,T],
\end{aligned}
\tag{2.49}
$$

subject to the essential and natural boundary conditions

$$u=g \qquad \text{on } \Gamma_g\times[0,T] \tag{2.50}$$

$$n\cdot\sigma=h \qquad \text{on } \Gamma_h\times[0,T]. \tag{2.51}$$

2.5 Existing results

Over the past decades, a great deal of results for flow of fluids in microsystems have been obtained. In this section, we review some previous work, including electrokinetic flows, pressure driven flows, time period electroosmotic flows.

2.5.1 Electrokinetic flows

The rapid development of microfabrication technologies have enabled a variety of microfluidic systems. These applications can be utilized on medical, environmental monitoring, and defense, such as drug deliver systems, DNA analysis/sequencing systems, and biological /chemical agent detection sensors on microchips. These systems require seamless integration of sample connection, separation and chemical detection units with fluid pumping, valves and necessary electronics on a single microchip. In this section, we review and report ideas of microflow control elements using electrokinetic flow control schemes. The electrokinetic phenomena is consisted of electroosmosis, electrophoresis, streaming potential and sedimentation potential. Electrokinetic effects are significant in the flow of the micron and nanometer scale devices.

Electroosmosis is the motion of ionized liquid relative to the stationary charged surface by the effect of electrical force. Electroosmosis started to be utilized for chemistry and biology applications in 1930s. The use of electroosmosis driven flow makes the micro fluid in pipe flow very common and draws more and more attention these days. At present, the electroosmosis driven flow in microfluidic systems has been widely used in biological and electrophoresis chips, which is one of the most successful control methods of flow in the micro and nanometer channels or tubes.

In the micro and nano scale devices, electroosmosis driven flow has two main advantages over the pressure driven flows: firstly, the fluid velocity of seepage field in most situation cannot be affected by the cross section of pipes or tubes, which makes us easy to drive and control micro scale fluid. While in the pressure driven flow, the pressure gradient needs to be inversely proportional to the square of the pipe or tank hydraulic radius to guarantee a certain velocity. Secondly, apart from near wall part, the rest of the velocity is almost the same. In this kind of uniform flow, the biological samples or chemical reagent concentration diffusion is slow, which is good for the sample or the reagent transfer though electroosmosis and separation.

Phenomenons of these have been found, but the practical application of electroosmosis driving is until recently. Sarah and Li in [58] studied the electroosmosis effect for the flow in rectangle channels. Harrison and Fluri [59] investigated several flow designs which are used for electrophoretic sample loading and separation on microchip devices for capillary electrophoresis. Jacobson later applied these to the analysis system of micro samples of transmission and control [60]. Wang [61] used numerical simulation to study the influence of the variable elec-

tric potential in capillary on electroosmosis effect in connect areas, and find that the electric potential changes will greatly affect the speed of the flow field and pressure distribution. Electroosmosis driving control method is simple and all the parts are fixed, which can be applied easily in microchannels. However, in the practise experiment the tubes are usually bent. The lengths of the bent channel wall inside and outside are different and the influence of the centrifugal effect, electroosmosis flow through bend point tend to cause uneven velocity distribution. Velocity gradient will aggravate the spread of the sample.

In fluid mechanics, the Reynolds number (Re) is a dimensionless quantity that is used to help predict similar flow patterns in different fluid flow situations, which is affected by different fluids, fluid velocities, and dimensions of the object in which the fluid is flowing past. The Reynolds number expresses the ratio of inertial force to the shear stress. The concept was introduced by George Gabriel Stokes in 1851 [62]. For flow in a pipe or a tube, the Reynolds number is defined as

$$Re = \frac{\rho v D_H}{\mu}, \tag{2.52}$$

where D_H is the hydraulic diameter of the pipe, its characteristic traveled length, v is the mean velocity of the fluid (units: m/s), μ is the dynamic viscosity of the fluid (Pas or Ns/m or kg/(ms)), ρ is the density of the fluid (kg/m^3). It is clear from equation (2.52) that a small Reynolds number signals a predominant shear effect and a large Reynolds number signals a predominant inertial effect.

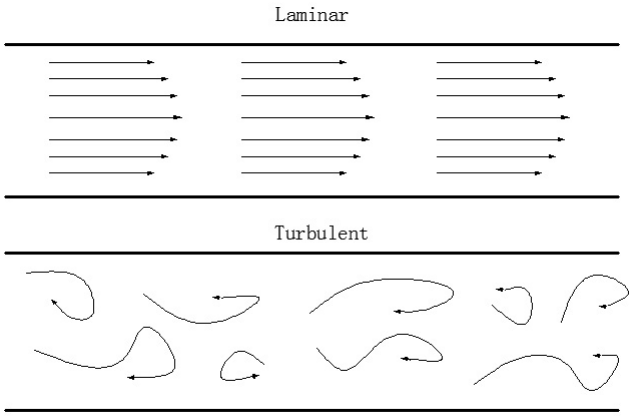

Figure 2.9: Laminar and Turbulent flows

Numerous experiments have been performed to check the validity of the solution to Poiseuille flow. At a sufficient large distance from the entrance, the

solution is valid and the individual fluid particles follow smooth paths parallel to the axis of the tube. In that case, the flow is said to be a laminar flow. However, if the channel is too large or the velocity is too high, the solution is invalid. The paths of individual particles are no longer smooth and parallel to the tube axis but are tortuous and randomly oriented. This kind of flow is said to be turbulent, as shown in Figure 2.9.

For example, if the channel height is 15nm, the mean velocity of the flow is 2mm/s, the solution is a dilute aqueous solution which has the similar density and viscosity as water. The Reynolds number is

$$\begin{aligned} Re =& \frac{\rho v D_H}{\mu} \\ =& \frac{(1.0 * 10^3 km/m^3)(20^{-3} m/s)(15^{-8} m)}{10^{-3} kg/m/s} \\ =& 0.00003. \end{aligned} \tag{2.53}$$

When Reynolds number is around 2000 or higher, then turbulent flow usually occur. Therefore the electroosmotic flow in a 15nm high tube is essentially a laminal flow.

It is believed that the solution of the time-dependent 3-D Navier-Stokes equations can describe turbulent flows completely. However we can not use today's supercomputer to solve these equations directly for the required range of length and time scale, even for simple problems. Hence turbulent motion is usually described in terms of time averaged quantities rather than instantaneous ones. As a matter of practice, we usually classify various flows as steady /unsteady laminar flows and steady /unsteady turbulent flows.

Zhang [39] studied of the characteristics of liquid flow through a rectangular microchannel with electrokinetic effects. In the paper, Zhang used numerical algorithms to calculate the connection between the pressure gradient and the Reynolds number of three different sizes of flow channels, for three different solutions (concentration of $10^{-2}M, 10^{-4}M$ of KCl solution and deionized water). A finite control volume method was applied to solve the governing equations and studied the connection between the pressure gradient and the Reynolds number. As the Reynolds number increases, the pressure gradient also increases.

Ming and Zhou [63] studied the rational design of pipe bending shape to decrease the bend effect. They considered a straight channel and a radius 180 degree turn with the precious results. Because the shape of the inner wall in the turn part was changed when the channel is bent. They decreased the bend effect

through the study of the rational design of pipe bending shape. The method is as follows: before modification, the pipe channel's the center is $x = 0, y = 0$, radius of the circular part is 1.6. Modified change for the center of the circle to $x = 0, y = 0.6$, and radius of the circular part changes to 1.8 (Figure 2.10). After changing the shape of the inner wall, the electric field intensity on the inner wall is less than that on the outer wall, i.e. the velocity of the outer wall is faster than the inner wall surface. So that the speed of inner wall and outer wall get certain balance, which makes the flow velocity uniform. This is particularly important on the microchip electrophoresis separation process. One usually induces bent channel to increase the separation length. However, the difference of the inner wall and outer wall affects the resolution rate. Therefore, appropriately changing bend channels shape improves electrophoresis separation efficiency to some extent. As for how to make the arc length as close as possible to inner and outer wall and not affect the normal fluid in a channel, has yet to be further studied.

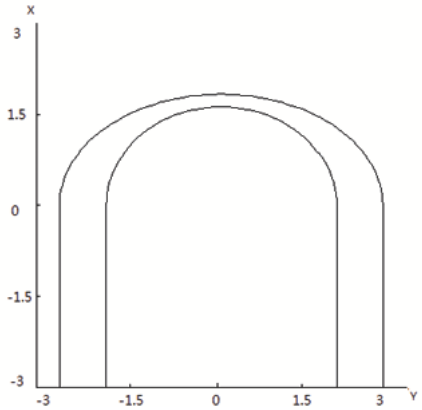

Figure 2.10: Schematic of the modified 180^o curve pipe, drawn after Ming and Zhou [63].

Electrophoresis is the motion of the charged surfaces and macromolecules relative to the stationary liquid by an applied electric field [64]. Capillary electrophoresis (CE) is developing quickly in recent years, which is a new separation technology and has been applied widely for separation of large and small molecules, such as the organic molecular protein, separation of different metals anions and inorganic anions.

Capillary electrophoresis (CE) has several different modes, which mainly include capillary zone electrophoresis (CZE), micellar electrokinetic chromatography (MEKC), capillary isoelectric focusing (IEF) etc. All of them need a high voltage (0-30kV) to achieve highly efficient separations. In [65], the electrokinetic

velocity v_{EK} of one ion species in the capillary system is

$$v_{EK} = v_{EOF} + v_{EP}, \tag{2.54}$$

where v_{EP} and v_{EOF} are the electrophoretic migration velocity of this ion species and the electroosmotic flow velocity. The electrokinetic mobility of the ion species is

$$u_{EK} = u_{EOF} + u_{EP}, \tag{2.55}$$

where $u_{EOF} = \frac{v_{EOF}}{E}$ is the electroosmotic mobility of the solution, E is the field strength. $u_{EP} = \frac{v_{EP}}{E}$ is the electrophoretic mobility of the ion species, and $u_{EK} = \frac{v_{EK}}{E}$ is the electrokinetic movement rate of ion species. Equation (2.47) is for an ion species while for different ion species the electrophoretic mobilities u_{EP} will be different. From equation (2.55) and $u_{EK} = \frac{v_{EK}}{E}$, the electrokinetic velocity v_{EK} for different ion species are different. When the electrolyte is put into the inlet, the electrokinetic will separate different ion species, which include ions, protein and some charged macromolecules (DNA).

Capillary zone electrophoresis (CZE) method is the most popular and easiest form of capillary electrophoresis (CE) these days. In this mold, the sample can be applied to a narrow band (area), which is surrounded by buffer reservoirs. Then a high voltage power supply will be applied on. The electric field can make every components in this sample migrates based on their apparent mobility. In ideal condition, all components in the sample will finally separate from each other and form their own area of pure material except for the neutral molecules.

CE has several advantages, such as high resolution and high speed. The theoretical plate number is thousands per meter of millions or even millions of per meter. Usually the analysis of ion time will be controlled in 10 minutes. And CE can also separate different forms of elements with similar electrophoretic mobility at the same time.

Due to the above advantages, capillary electrophoresis (CE) is a new type of separation technology in the element speciation analysis. Although the capillary electrophoresis (CE) analysis is still at the beginning of the development, there are still some aspects requiring apparent attention. (i) In capillary electrophoresis (CE), the solutions apparent mobilities can control the time which required for injecting them to get the detector. This is different from high performance liquid chromatography (HPLC). The time resistant in the detector is the same as all solutions, which is only controlled by the flow rate of the carrier liquid. (ii) Most

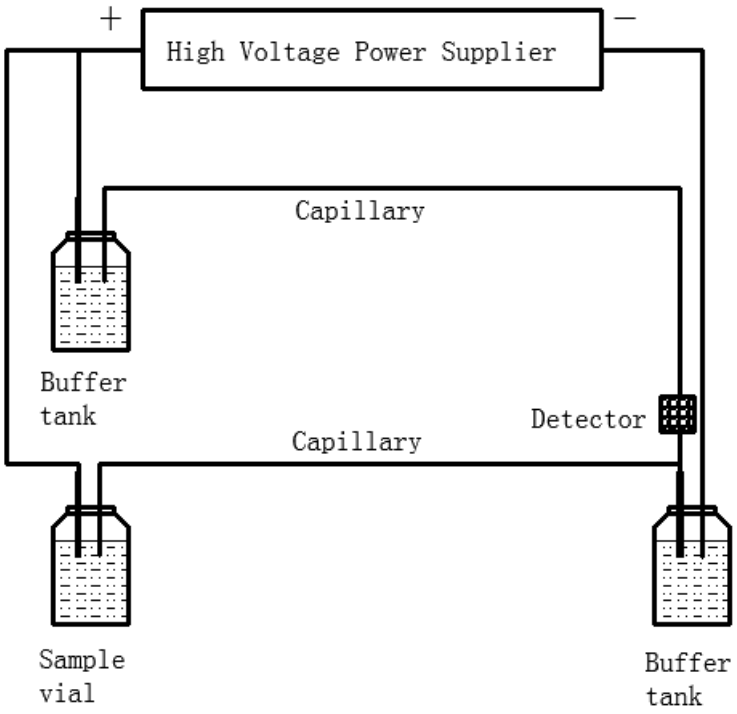

Figure 2.11: The basic instrumental set-up capillary electrophoresis (CE) system. It consists of a high voltage power supply, a fused silica (SiO_2) capillary, two buffer tanks and one director. Sample injection is completed by temporarily replacing one of the buffer tanks with a sample vial, drawn after Xu [66].

capillary electrophoresis (CE) application do not need sample preparation besides a possible dilution while other applications, such as analysis of biological sample, need some treatment before injection.

Streaming potential is the electric field created by the motion of charges particles relative to a stationary liquid [64]. The superposition of two pieces with charged membrane together form a channel in the middle which can be seen as a capillary. We take the single capillary as an example. Because the membrana surface contains stable positive charge, when the electrolyte solution goes into the channel, the anion will move to the back end when we apply pressure on the front due to the adsorption of negative charge. And at the same time, the anion at the front will accelerated. Then there will be a potential between the front and the back, which is the streaming potential under the membrane. There are three different potential differences in charged membrane, which are surface potential ψ^0, stern potential ψ^d and Zeta potential ξ. All of these potential equals to zero potential at the membrane surface infinity. Stern layer is the contact surface ions, which is near the surface charge of the stabilizing ion layer (Stern layer) and the

current portion of the electric double layer.

Stern potential actually affects the behavior of each layer charge, and the charge can be characterized by membrane electrical properties. But the Stern potential can not be measured directly, we need the Zeta potential ξ to represent. Zeta potential is widely used for calculating of the magnitude of the electrical charge on the EDL. It is not equal to the Stern potential or electric surface potential in the double layer. We use the Zeta potential to show the Stern layer potential. And use this to reflect the membrane charge performance. We can measure streaming potential, and then calculate the Zeta potential (ξ) values. That is why the measurement of streaming potential is very important.

For a long time, streaming potential is of interest in areas of biological, physical, chemical and earth sciences. Streaming can be used to measure the microchannel surface Zeta potential and conductivity. At present, there are reports about streaming potential [67,68]. While the stern potential cannot be measured directly, we will consider the zeta (electrokinetic) potential as a replacement. The zeta potential is the potential at the plane of shear between the surface and solution where there is relative motion between them. The relationship between the measurable streaming potential and the zeta potential is given [60] by the well known Helmholtz-Smoluchowski equation

$$\xi = \frac{E_S}{\triangle P} \cdot \frac{\eta}{\varepsilon\varepsilon_0} \cdot \frac{L}{A} \cdot \frac{1}{L} \tag{2.56}$$

where ξ is the zeta potential, E_S is the induced streaming potential, $\triangle P$ is the applied hydraulic pressure, η is the liquid viscosity, ε is the liquid permittivity, ε_0 is the permittivity in vacuum, R is the electrical resistance across the medium, and L and A are the length and cross-sectional area of the channel, respectively [69].

The ion concentration and pH value of electrolyte solutions can influence the streaming potential. Due to the materials differences in the membrane and the difference in the production process, the streaming potential will be different one from another. For example, in different electrolyte solution, the sodium surface flow membrane potential decreases as the absolute value of solution concentration increases.

The absolute value of the Zeta potential and Nanofiltration membrane surface streaming potential decrease with the increase in concentration of the solution (i.e., increased conductivity). There are two reasons for this phenomenon [70]: the first reason for this is because as the increasing of salt concentration of the solution, the Donnan potential difference becomes smaller. That is because the concentration of the far away from the membrane surface of the counter-ions in

the bulk solution and the concentration of adsorption ion concentration on membrane surface are getting close. The second reason is that as the salt solution concentration increases, the resistance to movement of ions in solution also increases, so that counter-ion resistance to movement of the adsorption surface of the membrane increases, causing the membrane surface flow and Zeta potential decreases.

ESNA2 nanofiltration membrane is used at different applied pressures to measure Zeta potential of the membrane surface. As can be seen, with the applied pressure increases, charged membrane absolute value of Zeta potential decreases. The lower the concentration of the solution is,the more dramatically decreases of the Zeta potential. As Zeta potential is calculated by formula (2.20), Zeta potential and streaming potential have similar variation. With other companies of the membrane to do the test, similar conclusion is obtained [70]. From streaming potential measurements, we can see that there is less direction influence without significant differences in magnitude of the Zeta potential (ξ) for both UF (ultrafiltration) and MF (microfiltration) membranes.

Sedimentation potential is the electric field created by the motion of charged particle relative to a stationary liquid [64]. In other words, when the electrolyte solution is placed in an accelerating field, an electrical signal is detected due to the movement of the cation and anion. The lower the viscosity of a liquid drop is, the larger the sedimentation potential is. In electroosmosis and streaming potential phenomenon, there is a thin liquid layer on the particle surface which does not move with the particle. While in the sedimentation potential and electrophoresis phenomenon, there is a thin liquid layer on the particle surface which moves with the particles.

2.5.2 Pressure driven flows

Most transport fluids in microchannel and nanochannel separation applications are driven by electrokinetic mechanisms that result in a uniform velocity profile and low dispersion [71]. This is because with applying a pressure difference across a fluidic channel, a pressure gradient generates a parabolic flow profile that leads to hydrodynamic dispersion, with a maximal velocity in the channel center and zero on the wall and a flow speed that depends strongly on the channel size [72]. These perceived disadvantages have made pressure-driven flow less popular than electrokinetic mechanisms in microfluidic and nanofluidic applications. A pressure-driven flow through a fluidic channel induces the flow of net charge in the double layer at the channel walls, which generates an electric current (Figure

2.12).

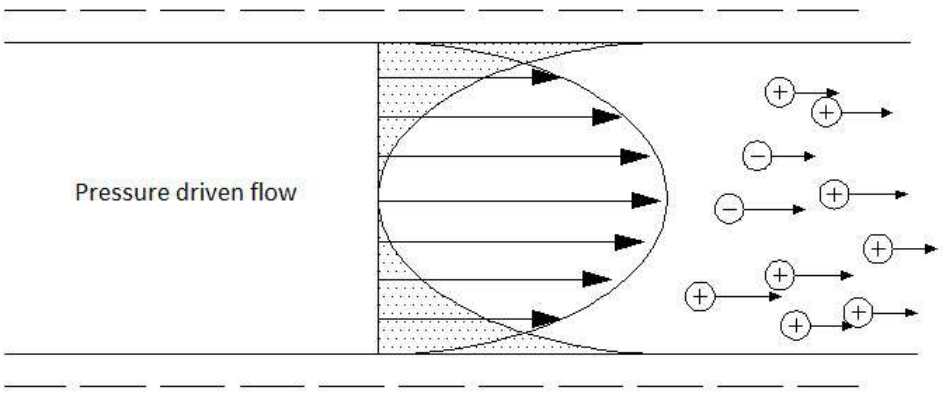

Figure 2.12: A pressure driving flow carries the net ionic charge within the double layer, drawn after Ming and Zhou [63].

The notion of generating electrical power in this way is not new, but has received renewed attention in the context of microfluidic and nanofluidic devices [73]. In [74], Frank and coworkers reported the efficiency of electrical power generation in individual rectangular nanochannels by streaming currents, the pressure driven transport of counterions in the electrical double layer. From their work, the highest efficiency occurs when double layers overlap, which means the nanoscale fluidic channels filled with aqueous solutions of low ionic strength.

Although pressure-driven flows is easy to be implemented and is ubiquitous in conventional chemical analysis techniques such as high-pressure liquid chromatography, many useful properties of the flows remain unexplored. Our understanding of an object's fundamental transport properties in parabolic flows, mobility and dispersion, is at present based mainly on models for rigid particles [75] that explains several important effects such as the following:(i) the velocity of large particles is faster than small particles because large particles are more strongly confined to the center of a channel, where the flow speeds are highest, and(ii)Taylor dispersion, the mechanism by which analyte molecules are hydrodynamically dispersed as they explore different velocity streamlines by diffusion, is an effect that has discouraged the use of pressure-driven flows in microfluidic separation technology. In [76], Derek studied the pressure-driven transport of individual DNA molecules in 175-nm to 3.8-μm high silica channels by fluorescence microscopy.

In [39], the electric double layer (EDL) on the solid-liquid interface and electric field effect are introduced to the traditional momentum equation. By solving the rectangle channel fully developed microfluidic pressure-driven flow governing

equations, electric field effect on the micro-flow channel fluid flow was investigated.

Wall slip at the nanoscale rheology, microfluidics, thin mold lubrication and micro-electromechanical systems (MEMS) and other areas has drawn increasing attention. Many studies have focused on the initial limiting shear stress on the surface of the thin wall slip mold lubrication and fluid dynamics effects. In the presence of the slip, the smaller the proportion of the ultimate shear stress always produce a smaller friction coefficient.

2.5.3 Time period electroosmotic flows

Wall thermal boundary conditions periodically change transient natural convection widespread in circuits of electronic equipment exothermic, biological engineering, electronic engineering, chemical engineering, and construction and solar applications, and many other engineering applications. Given this importance of natural convection heat transfer phenomena and nano enhanced heat transfer fluid, in this section, we review the alternating current (AC) electric field, alternating current (AC) magnetic, direct Current (DC) electromagnetic field and direct Current [77].

An AC electric fields is produced by the presence of electricity. It uses voltage to determine its strength, i.e. the field strength increases with the voltage. An AC electric field is produced by live electrical wires and generally travel 2m - 3m from the source, but in some cases it can travel further. An electric field will exist even when a device is not in use, for instance, when the device is turn off. That means the source produces a continual emission. An AC electric field has a natural attraction to the human body and ground. It has low frequency electromagnetic radiation (5 Hz C 400,000 Hz).

An alternating current electromagnetic field (EM field) is a physical field generated by mobile electrically charged objects. EM field continually changes polarity from positive to negative. It affects the behavior of charged objects in the vicinity of the field. The EM field can be considered as the combination of an alternating current magnetic field and an alternating current electric field.

AC magnetic fields are living spaces which contain many electronic devices and electrical appliances. When this device is turned on, there will be a flow of electrical current. They can be measured with a tesla meter in nanoTesa (nT) or with a gauss meter in milliGauss mG.

A Direct Current (DC) electromagnetic field refers to a constant or static DC electric or DC magnetic field emission which has a frequency of 0 Hz. DC electric

fields can be referred to as an electrostatic charge present on an object which can be created by rubbing two poorly conducting materials rub against each other.

Time period electroosmosis has received considerable attention and effort from engineers and chemists due to the emergence of microfluidic devices. We call the time period electroosmosis as AC electroosmosis, which is driven by an alternative field.

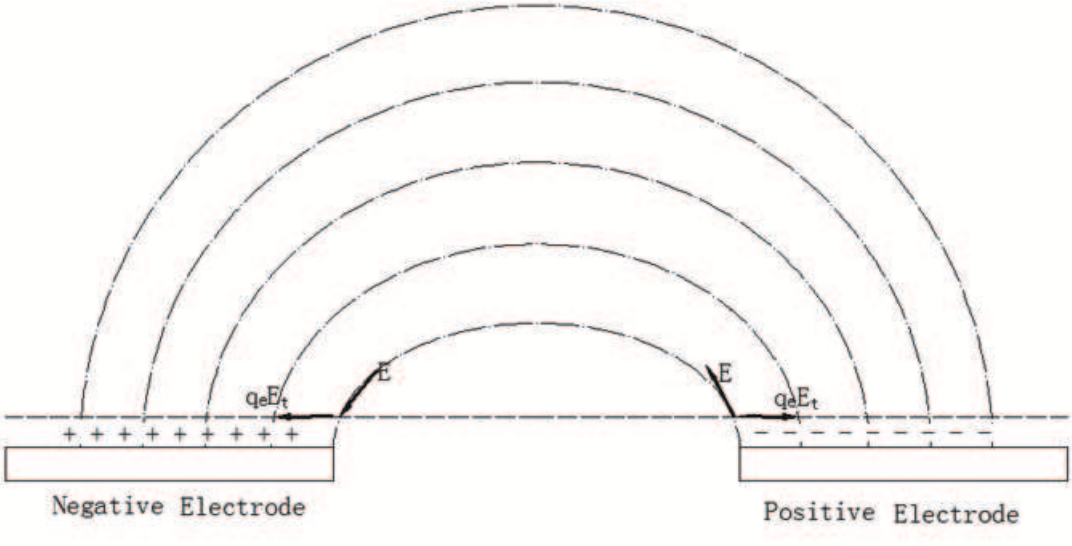

Figure 2.13: Schematic diagram for time period electroosmosis. The tangential electric field(E_t) close to the electrodes interacts with induced charges on the electrodes and generates electroosmotic force and the horizontal direction velocity. $q_e E_t$ is the velocity in the horizontal direction, drawn after Morgan and Green [78].

Time period (AC) electroosmosis can be observed when an AC electric field is applied on two electrodes which placed next to each other. From figure 2.13, we can see the electric field lines close to the electrodes surface display tangential components. The induced charges which can be seen on the two electrodes with + and - signs and the tangential electric field effect on each other. This will result the time period electroosmosis and fluid flow. Here we note that changing the electrode polarity does not alter the flow direction [78].

Time periodic electroosmosis (EO) has some advantageous features, such as low-voltage operation and stationary implementation, which make the time period electroosmosis (EO) suitable for integrating with micro devices. And we can apply these features on particle control, which will reinforce the sensitivity as a result of decreasing the transport time.

Wu and Ben [79] studied asymmetric-polarization time period (AC) electroos-

motic trapping for reducing the bacteria culturing time. The traditional method of bacteria detection which needs bacterial culturing consumes a lot of time, while AC electroosmosis is an efficient method.

Exact and numerical solutions to various flow problems of Newtonian fluidic under the no-slip assumption have been obtained. Dose and Guiochon published numerical results for impulsive started electroosmotic flow [49], and Soderman and Jonsson reported an analytical work on starting problems of electroosmotic flows for a number of geometries including the flow over a flat plate and two-dimensional microchannel and microtube flows [80]. However, very few exact solutions in time period with the slip case have been obtained.

Green and Ramos investigated AC electroosmosis on planner microelectrodues using steady and unsteady electric field [81]. Microscale combustion and power generation applications require development of reliable micromixers. Time period electroosmotic flows can be combined with steady electroosmotic or pressure-driven flows to induce temporal and spatial flow modifications.

In microtubules with various different geometries, various studies have been carried out to investigate the fully developed micro electroosmotic flow (EOF) of Newtonian fluid and heat transfer in relevant experiments [82–84]. However, this kind of phenomenon of constant electroosmotic flow (EOF) requires high voltage and strong field, which brings many difficulties for experiments. Recently, time depending electroosmotic flow as a driving mechanism of micro fluid mechanics has attracted more and more attentions from the research community.

Dutta and Beskok [85] are the first to use analytic method to explore cycle between two parallel plates electroosmotic flow. They stated the similarities and differences between the electroosmotic flow (EOF) between two parallel plates and Stokes' second problem. They found that the analytical solutions of time periodic electroosmotic fluid in two-dimensional straight tubes are effected by the electric double-layer (EDL) thickness, frequency of the externally applied electric field and kinematic viscosity. By using the green's function method, Kang and coworks [86] analysed the instantaneous velocity of the flow through microchannels under a time dependent electric field.

Jian [87] studied the time periodic electroosmotic flow through circular microchannels. They investigated two different kinds of situations, including the electroosmotic flow through parallel plates and circular tubes, and obtained various conclusions : (i) The analytical solution of electroosmotic flow is effected by the period length, the radial distance, the zeta potential ratio and Reynolds number. (ii) Electroosmotic flow (EOF) is affected by the zeta potential ratio

because the electroosmotic flow (EOF) is caused by the applied electric field and the EDL. (iii) As the Reynolds number decreases, the EDL thickness decreases and the electroosmotic velocity shows a square plug shape profile. While as the Reynolds number increases, the driving effect of the electric force decreases immediately away from the two cylindrical walls.

2.6 Concluding remarks

Over the last few decades, many micro devices and systems have been developed and applied to many areas in engineering, science, biomedicine and etc. Most of these devices and systems involve flow of fluids in microchannels or microtubes at some stage of the application. It is essential to understand the flow behaviour under different model parameters and externally controllable conditions in order to design or control the systems precisely for optimal performance. Over the last couple of decades, a great deal of work has been conducted to study the flows of fluids through microchannels with various different geometries driven by electrical force and pressure gradient, and a lot of analytical and numerical results have been obtained. However, some issues and problems still need to be investigated. This project will focus on investigating two problems, namely constructing models taking into account of boundary slip at microscale, and investigating the combined effect of electric driving and pressure gradient driving mechanisms under the boundary slip condition.

CHAPTER 3

Solution of time periodic electroosmosis flow with slip boundary

3.1 General

One of the major focuses in scientific research during the past decades has been the study of material behaviour at micro and nano-scale. The subject of micro and nanofluidics concerns mass and momentum transfer in micro on nano-scale systems or around micro or nano-sized objects. The study of microflows is attracting more and more attention from the science and engineering communities in order to derive a better understanding of the mechanism of microflows and develop better models. Traditionally the so called no-slip boundary condition is used, namely the fluid velocity relative to the solid is zero on the fluid-solid interface. However the no-slip condition is a hypothesis rather than a condition deduced from any principle. Evidence of slip of a fluid on the solid surface were reported by many researchers [36, 37].

In recent years, time period electroosmosis has received considerable attention from engineers and chemists due to the emergence of microfluidic devices. Time period electroosmosis is known as AC electroosmosis, which is driven by an alternative electric field. Dose and Guiochon published numerical results for impulsive started electroosmotic flow [49], and Soderman and Jonsson reported an analytical work on electroosmotic flows for a number of geometries including the flow over a flat plate and two-dimensional microchannel and microtube flows [80]. Green and Ramos investigated A/C electroosmosis on planner microelectrodues using steady and unsteady electric field [81].

Although exact and numerical solutions to various flow problems of Newtonian fluids under the no-slip assumption have been obtained, very few exact solutions for time dependent problems have been obtained for the slip case. Hence, in this

chapter, we study the time period electroosmotic flows in a straight microchannel under the slip assumption. The rest of the chapter is organized as follows. In section 3.2, the mathematical equations for the channel flow are presented, which include the partial differential equations and the boundary conditions based on the slip assumption. In section 3.3, the general solution for the velocity of the fluid in the channel is derived with some arbitrary constants. Then the slip boundary condition and symmetric condition are used to determine the arbitrary constants. Numerical investigations are then given in section 3.4, followed by a concluding remark in section 3.5.

3.2 Problem description and mathematical formation

The problem considered is the electric driven flow of a fluid through a channel with height 2h. The geometry of the channels and the coordinates (x,y,z) used are shown in Figure 3.1.

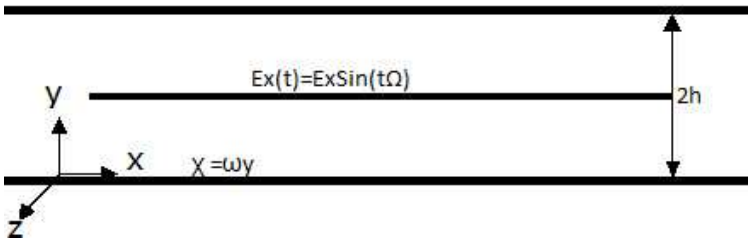

Figure 3.1: Schematic view of time periodic electroosmotic flow in a two-dimensional straight channel and the coordinates used. Here Ω is the frequency of the external electric field and ω is the Debye-Huckle parameter.

Based on the principle of continuous mechanics, the motion of ionized, incompressible fluids with electroosmotic body forces are governed by the incompressible Navier-Stokes equations:

$$\rho_f(\frac{\partial \overrightarrow{V}}{\partial t} + (\overrightarrow{V} \cdot \nabla)\overrightarrow{V}) = -\nabla P + \mu \nabla^2 \overrightarrow{V} + \rho_e \overrightarrow{E}, \tag{3.1}$$

where P is the pressure, $\rho_f$and ρ_e are respectively the fluid density and the electric charge density, and $\overrightarrow{V} = (u, v, w)$ is a divergence free velocity field, μ is the dynamic viscosity. The last term on the right side denotes the electroosmotic body forces, and $\overrightarrow{E}$ is the externally applied electric field.

We assume fully developed symmetric channel flow, and thus the swirling flow and the velocity components in y and z directions can be neglected. This allows us to use the superposition principle because the resulted unsteady Navier-Stokes equations for this case are linear in velocity. This means that we can solve exactly the pressure and electroosmotically driven flows separately and combine the solution for mixed electroosmotic /pressure-driven flows under a undirectional electric field. In general, the electroosmotic body force can be expressed in various form according to the externally applied electric field. In this chapter, we consider sinusoidally driven time period electroosmotic flows in the absence of pressure gradients.

Taking into account the above assumptions, equation (3.1) reduces to

$$\rho_f \frac{\partial u}{\partial t} = \mu \frac{\partial^2 u}{\partial y^2} + \rho_e E_x \sin(\Omega t), \tag{3.2}$$

where E_x and Ω are respectively the magnitude and the frequency of the unsteady external electric field $\overrightarrow{E}$. Equation (3.2) can then be used to determine the streamwise velocity component due to the time-periodic electric field.

Based on the theory of electric field [85], the ρ_e in equation (3.2) can be expressed by

$$\rho_e = -2n_0 ez \sinh(\frac{ez\psi}{k_B T}), \tag{3.3}$$

where n_0 denotes the average number of positive or negative ions in the buffer, e is the electron charge, z is the valance, k_B is the Boltzmann constant, and T is the absolute temperature. Let $\psi^* = \frac{\psi}{\xi}$ be the normalized electroosmotic potential in which ξ is the zeta potential, and $\alpha = \frac{ez\xi}{k_B} T$ be a parameter, then we have

$$\rho_e = -2n_0 ez \sinh(\alpha \psi^*).$$

Based on the work in [85], the electroosmotic potential ψ is governed by the Poisson-Boltamann equation

$$\nabla^2 \psi = -\rho_e / \epsilon$$

in which ϵ is the permittivity. We assume that ψ is not affected by the time fluctuations of the external electric field, which can be justified by analysis of the ion conservation equation in two-dimensional channels [81].

In general, it is difficult to obtain a closed form analytical solution for the Poisson-Boltzmann equation in a channel in terms of a first-kind elliptic integral for finite electric double-layer(EDL) thickness. In this chapter, the effective EDL thickness (δ_{99}) is a function of the ionic energy parameter α. For example, for

$\alpha = 5$, the effective EDL thickness is $\delta_{99} = 4.217\lambda$, where λ is an estimate of the electric double layer thickness based on the Debye-Huckel parameter obtained by

$$\omega = 1/\lambda = \sqrt{\frac{8\pi n_0 e^2 z^2}{D k_B T}}.$$

The top and bottom walls do not interact with each other when the channel half-height h is larger than 10λ because of the exponential decay of the electroosmotic potential away from the wall. In most microfluidic applications, λ is in the order of 10-100nm, which is much smaller than a typical microchannel height. Under these conditions, the electroosmotic potential reaches zero in the channel center, and the electroosmotic potential distribution can be written as a function of the distance from the wall($\chi = y/\lambda$) as [27, 85]

$$\psi^* = \frac{4}{\alpha} \tanh^{-1}[\tanh(\frac{\alpha}{4}) \exp(-\chi)]. \tag{3.4}$$

By using the definition of the Debye-huckel parameter ω, we can rewrite the electroosmotic body force on the fluid in the following form:

$$-2n_0 e z E_x \sin \Omega t = \frac{\omega^2 \mu u_{HS}}{\alpha} \sin \Omega t. \tag{3.5}$$

where $u_{HS} = -\epsilon\zeta E_x/\mu$ is the Helmholtz-Smoluchowski velocity. Then, equation (3.2) can be written as

$$\rho_f \frac{\partial u}{\partial t} = \mu \frac{\partial^2 u}{\partial y^2} + \frac{\omega^2 \mu u_{HS}}{\alpha} \sinh(\alpha\psi^*) \sin(\Omega t), \tag{3.6}$$

To completely determine the fluid flow in the channel, the differential equation (3.2) must be supplemented by a set of boundary and initial conditions. To describe the slip characteristics of fluid on the solid surface, the Navier slip condition is used, namely the velocity of fluid, relative to the solid surface, is assumed to be proportional to the sheer stress on the fluid-solid surface, that is

$$u(0,t) + l\frac{\partial u}{\partial y}(0,t) = 0, \tag{3.7}$$

where l is the so called slip length. It should be addressed here that for $l = 0$, condition (3.7) reduces to the no slip boundary condition.

In addition, due to the symmetry of velocity about the symmetric plane $y = h$,

we have

$$\frac{\partial u}{\partial y}(h,t) = 0, \tag{3.8}$$

Now the partial differential equation (3.6) together with the boundary condition (3.7) and the symmetric condition (3.8) constitute a complete boundary value problem for the fluid flow in the channel.

3.3 Solution of the boundary value problem

Introducing characteristic time$(1/\Omega)$ and characteristic length (λ), equation (3.6) can be expressed in normalized form

$$\rho_f u_{HS}\Omega\frac{\partial U}{\partial \theta} = \mu u_{HS}\omega^2[\frac{\partial^2 U}{\partial^2 \chi} + \frac{\sin(\theta)}{\alpha}\sinh(\alpha\psi^*)], \tag{3.9}$$

where $\theta = \Omega t$ is the nondimentional time, $\chi = y/\lambda$ is the nondimensional distance, and $U = u/u_{HS}$ is the nondimensional velocity. From (3.9), we have

$$\frac{\partial U}{\partial \theta} = \frac{1}{\kappa^2}[\frac{\partial^2 U}{\partial^2 \chi} + \frac{\sin(\theta)}{\alpha}\sinh(\alpha\psi^*)], \tag{3.10}$$

where $\kappa = (\Omega\lambda^2\rho_f/\mu)^{1/2}$ is a normalized parameter that is a function of the Debye length (λ), the electric field excitation frequency (Ω) and the kinematic viscosity (μ). The parameter κ can be interpreted as the ratio of the Debye length to a diffusion length scale(I_D), based on the kinematic viscosity and the excitation frequency. The diffusion length scale can be estimated from the unsteady Stokes equation using dimensional analysis as $I_D \simeq (\upsilon/\Omega)^{1/2}$. Therefore, the diffusion length scale is related to the Debye length and κ in the following form:

$$I_D = \lambda/\kappa.$$

Let $\widetilde{U}$ be the solution of the following equation

$$\frac{\partial \widetilde{U}}{\partial \theta} = \frac{1}{\kappa^2}[\frac{\partial^2 \widetilde{U}}{\partial^2 \chi} + \frac{\exp(i\theta)}{\alpha}\sinh(\alpha\psi^*)], \tag{3.11}$$

then from the linearity and the superposition principle, the solution of equation (3.10) will be $U = Im(\widetilde{U})$. It is noted that (3.11) admits solution of the form $\widetilde{U} = \exp(i\theta)F(\chi)$, where $\sin(\theta)$ is written as the imaginary part of $\exp(i\theta)$, and thus we proceed to solve (3.11) first.

The time derivative of $U(\chi,\theta)$ can then be expressed as

$$\frac{\partial \widetilde{U}}{\partial \theta} = i \exp(i\theta) F(\chi)$$

and the second spatial derivatives as

$$\frac{\partial^2 \widetilde{U}}{\partial^2 \chi} = \exp(i\theta) \frac{d^2 F}{d\chi^2}$$

Therefore equation (3.11) becomes

$$i \exp(i\theta) F(\chi) = \frac{\exp(i\theta)}{\kappa^2} [\frac{d^2 F}{d\chi^2} + \frac{\sinh(\alpha\psi^*)}{\alpha}]. \tag{3.12}$$

For the above to be true for all θ values, we require

$$\frac{d^2 F(\chi)}{d\chi^2} - i\kappa^2 F(\chi) = -\frac{\sinh(\alpha\psi^*)}{\alpha} \tag{3.13}$$

The complimentary solution of the above differential equation is

$$F_c = A \exp(\sqrt{i}\kappa\chi) + B \exp(-\sqrt{i}\kappa\chi), \tag{3.14}$$

where A and B are coefficients to be determined to meet the boundary conditions. The particular solution of equation (3.13) can be obtained as

$$\begin{aligned} F_p = & \frac{1}{2\kappa\alpha\sqrt{i}} \exp(-\sqrt{i}\kappa\chi) \int_0^\chi (\exp(\sqrt{i}\kappa\chi) \sinh(\alpha\psi^*) d\chi \\ & - \frac{1}{2\kappa\alpha\sqrt{i}} \exp(\sqrt{i}\kappa\chi) \int_0^\chi (\exp(-\sqrt{i}\kappa\chi) \sinh(\alpha\psi^*) d\chi \end{aligned} . \tag{3.15}$$

Therefore, we have

$$\begin{aligned} F(\chi) = & A \exp(\kappa\chi\sqrt{i}) + B \exp(-\kappa\chi\sqrt{i}) \\ & + \frac{1}{2\kappa\alpha\sqrt{i}} [\exp(-\kappa\chi\sqrt{i}) \int_0^\chi (\exp(\kappa\chi\sqrt{i}) \sinh(\alpha\psi^*) d\chi] \\ & - \frac{1}{2\kappa\alpha\sqrt{i}} [\exp(\kappa\chi\sqrt{i}) \int_0^\chi (\exp(-\kappa\chi\sqrt{i}) \sinh(\alpha\psi^*) d\chi \end{aligned} \tag{3.16}$$

and consequently we have

$$\begin{aligned}\widetilde{U}(\chi,\theta) =& A\exp(i\theta)\exp(\kappa\chi\sqrt{i}) + B\exp(i\theta)\exp(-\kappa\chi\sqrt{i}) \\ &+ \frac{\exp(i\theta)}{2\kappa\alpha\sqrt{i}}[\exp(-\kappa\chi\sqrt{i})\int_0^{\chi}\exp(\kappa\chi\sqrt{i})\sinh(\alpha\psi^*)d\chi] \\ &- \frac{\exp(i\theta)}{2\kappa\alpha\sqrt{i}}[\exp(\kappa\chi\sqrt{i})\int_0^{\chi}\exp(-\kappa\chi\sqrt{i})\sinh(\alpha\psi^*)d\chi]\end{aligned} \tag{3.17}$$

Now we proceed to determine the arbitrary constants in (3.17). In terms of the nondimensional time θ, the nondimensional distance χ, and the nondimensional velocity U, the boundary conditions (3.7) and (3.8) become

$$\begin{cases} U(0,\theta) + \dfrac{l}{\lambda}\dfrac{\partial U}{\partial\chi}(0,\theta) = 0 \\ \dfrac{\partial U}{\partial\chi}(\dfrac{h}{\lambda},\theta) = 0 \end{cases} \tag{3.18}$$

As $U(\chi,\theta) = Im(\widetilde{U}(\chi,\theta))$, (3.18) will be satisfied if $\widetilde{U}$ satisfies the following boundary conditions,

$$\begin{cases} \widetilde{U}(0,\theta) + \dfrac{l}{\lambda}\dfrac{\partial \widetilde{U}}{\partial\chi}(0,\theta) = 0 \\ \dfrac{\partial \widetilde{U}}{\partial\chi}(\dfrac{h}{\lambda},\theta) = 0 \end{cases} \tag{3.19}$$

Noticing that $\widetilde{U} = \exp(i\theta)F(\chi)$, the above boundary conditions becomes

$$\begin{cases} F(0) + \dfrac{l}{\lambda}F'(0) = 0 \\ F'(\dfrac{h}{\lambda}) = 0 \end{cases} \tag{3.20}$$

To apply the boundary condition (3.20), we first need to calculate the spatial derivative of $F(\chi)$. From equation (3.4) and (3.16), we have

$$\begin{aligned}F'(\chi) =& A(\kappa\sqrt{i})\exp(\kappa\chi\sqrt{i}) + B(-\kappa\sqrt{i})\exp(-\kappa\chi\sqrt{i}) \\ &- \frac{1}{2\alpha}[\exp(-\kappa\chi\sqrt{i})\int_0^{\chi}(\exp(\kappa\chi\sqrt{i})\sinh(\alpha\psi^*)d\chi] \\ &- \frac{1}{2\alpha}[\exp(\kappa\chi\sqrt{i})\int_0^{\chi}(\exp(-\kappa\chi\sqrt{i})\sinh(\alpha\psi^*)d\chi]\end{aligned} \tag{3.21}$$

At the central of the channel, $\chi = \frac{h}{\lambda}$, $\frac{dF}{d\chi} = 0$, and so from (3.20) and (3.21)

Table 3.1: A and B values for different set of model parameters.

κ	α	A	B
0.1	1	-1.5583-1.6348i	-4.6373+2.0952i
	3	-18.0859-2.6534i	-23.1309+3.2856i
	5	-23.6809-3.3261i	-30.0499+4.0098i
0.01	1	23.9849-37.1567i	-34.8651+38.3333i
	3	38.9742-59.1730i	-57.6358+60.8270i
	5	10.9090-537.4980i	-104.6609+610.5019i
0.001	1	372.8097-389.5891i	-385.0603+389.7408i
	3	593.6919-619.3798i	-611.3080+619.6202i
	5	732.7149-764.5012i	-754.4851+764.7988i

we have

$$\begin{aligned} F'(\frac{h}{\lambda}) =& A(\kappa\sqrt{i})\exp(\kappa\frac{h}{\lambda}\sqrt{i}) + B(-\kappa\sqrt{i})\exp(-\kappa\frac{h}{\lambda}\sqrt{i}) \\ &- \frac{1}{2\alpha}\exp(-\kappa\frac{h}{\lambda}\sqrt{i})\int_0^{\frac{h}{\lambda}}(\exp(\kappa\chi\sqrt{i})\sinh(\alpha\psi^*)d\chi \\ &- \frac{1}{2\alpha}\exp(\kappa\frac{h}{\lambda}\sqrt{i})\int_0^{\frac{h}{\lambda}}(\exp(-\kappa\chi\sqrt{i})\sinh(\alpha\psi^*)d\chi = 0 \end{aligned} \tag{3.22}$$

From (3.20) and (3.21), we get

$$(1+\frac{l}{\lambda}\kappa\sqrt{i})A + (1-\frac{l}{\lambda}\kappa\sqrt{i})B = 0 \tag{3.23}$$

Hence

$$B = -(1-\frac{l}{\lambda}\kappa\sqrt{i})^{-1}(1+\frac{l}{\lambda}\kappa\sqrt{i})A. \tag{3.24}$$

Substituting (3.24) into (3.22) yields

$$\begin{aligned} A =& \Big\{\exp(\kappa\frac{h}{\lambda}\sqrt{i}) + (1-\frac{l}{\lambda}\kappa\sqrt{i})^{-1}(1+\frac{l}{\lambda}\kappa\sqrt{i})\exp(-\kappa\frac{h}{\lambda}\sqrt{i})\Big\}^{-1} \\ &\times\Big\{\frac{1}{2\alpha\kappa\sqrt{i}}\exp(-\kappa\frac{h}{\lambda}\sqrt{i})\int_0^{\frac{h}{\lambda}}(\exp(\kappa\chi\sqrt{i})\sinh(\alpha\psi^*)d\chi \\ &+\frac{1}{2\alpha\kappa\sqrt{i}}\exp(\kappa\frac{h}{\lambda}\sqrt{i})\int_0^{\frac{h}{\lambda}}(\exp(-\kappa\chi\sqrt{i})\sinh(\alpha\psi^*)d\chi\Big\} \end{aligned} \tag{3.25}$$

3.4 Numerical investigation

In this section, we investigate the characteristic of the electric driven flow. In particular, we will investigate the influence of various model parameters on the flow behaviour, including the κ value, the energy parameter α, the channel height h and the slip parameter l. From Matlab, Table 3.1 shows the solutions of A and B for various sets of the model parameters.

In the first example of investigation, we set the channel height $2h$ to be 200λ where the λ typically has value of hundreds of nanometre. Other parameters are chosen as $\alpha = 1$ and $\lambda = 1$. Figures 3.2 and 3.3 show the distribution of velocity along the channel height obtained from the model with various l and κ values at $\theta = \pi/2$, as functions of χ for different values of the parameters κ and l. Figure 3.4 presents the velocity distribution $U(\chi, \kappa)$ and $U(\chi, l)$, at $\theta = \pi/2$ for $\alpha = 1$ and $h = 100\lambda$. The results show that as κ increases, the thickness of the layer with significant electrically driven flow decreases; and essentially the velocity at the centre of the channel is zero for $\kappa \geq 0.07$ as shown in Figure 3.3(d) and 3.4(a). It is also found that the slip parameter has significant influence on the flow behaviour. At $\kappa = 0.001$, as l increases from 0 to 0.5, the flow increases from 1 to about 1.685 as shown in Figure 3.2(a).

To investigate the effect of the energy parameter α on the flow behaviour, we choose four values of α including 1, 3, 5, and 7. Figure 3.5 shows the influence of α on the velocity distribution for $\theta = \pi/2$, $h = 100\lambda$, $l = 0.05$ and two different κ values of 0.001 and 0.03. For a fixed channel dimension and a given buffer solution, the value of κ depends directly on the frequency of the external electric field. Hence, in practice, it is possible to obtain the desired velocity field by controlling the frequency by electric switch [6]. We found that as α increases, the flow velocity increases. At $\kappa = 0.001$, as α increases from 1 to 7, the flow at the centre increases from 1 to 1.4 as shown in Figure 3.5. At $\kappa = 0.03$, as α increases from 1 to 7, the flow at the centre approaches zero.

At the typical values of $\alpha = 1$, $\kappa = 0.03$, $l = 0.05$, the distributions of velocity along the height of the channel at various instants of time in an oscillation cycle of electric field are shown in Figure 3.6. The magnitude of the velocity varies with time, which is because of the fluctuation of the external electric field in time.

Figure 3.7 shows the influence of channel height on the magnitude of velocity. We choose four values of h including $25\lambda, 50\lambda, 75\lambda, 1000\lambda$.It can be noted that the magnitude of velocity is influenced by the channel height h, while the pattern of velocity profile along the channel is the same. In other word, the velocity

maximum is at $\chi = 10$. Figure 3.8 shows that the influence of κ on the first derivative of the velocity.

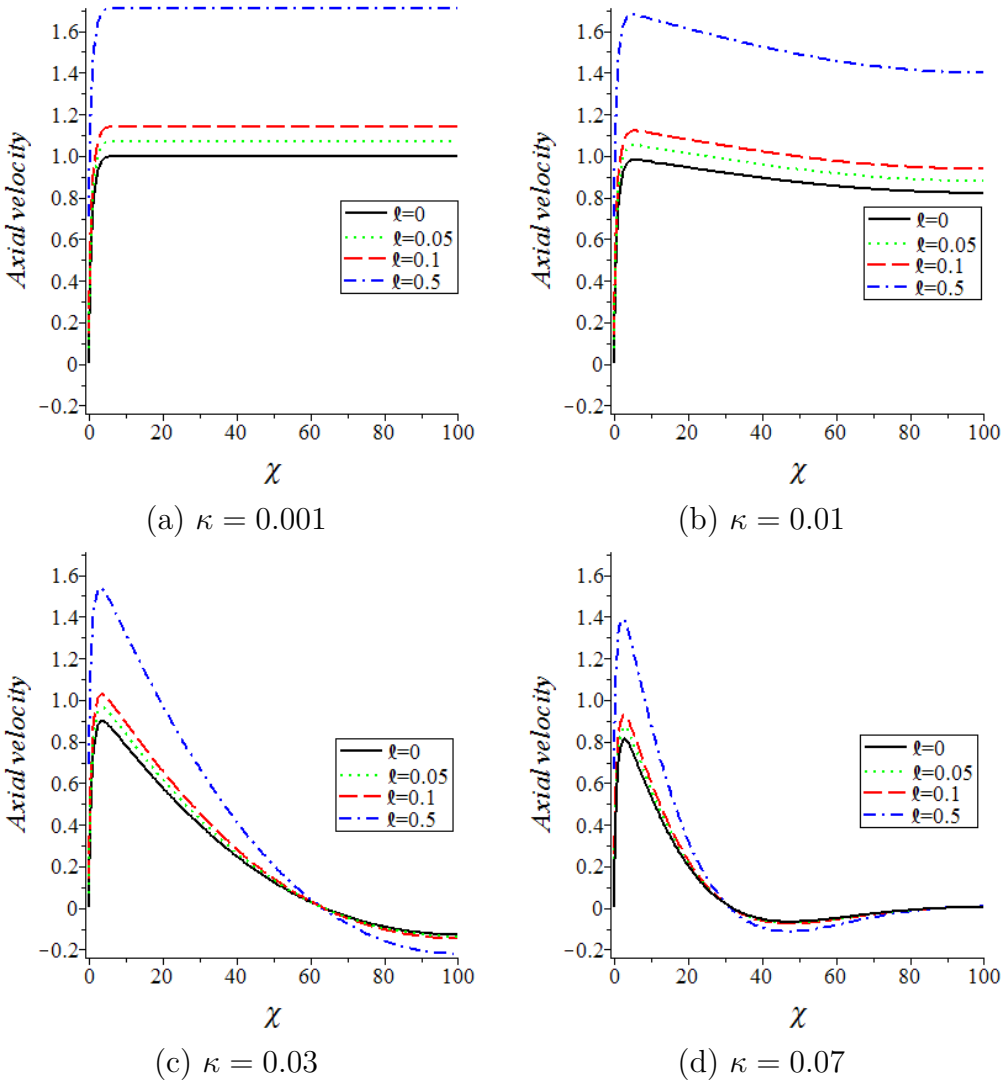

(a) $\kappa = 0.001$ (b) $\kappa = 0.01$

(c) $\kappa = 0.03$ (d) $\kappa = 0.07$

Figure 3.2: Effect of slip length on velocity profile obtained from the model with $\theta = \pi/2$, $\alpha = 1$ and $h = 100\lambda$ for various κ values: (a) $\kappa = 0.001$; (b) $\kappa = 0.01$; (c) $\kappa = 0.03$; (d) $\kappa = 0.07$.

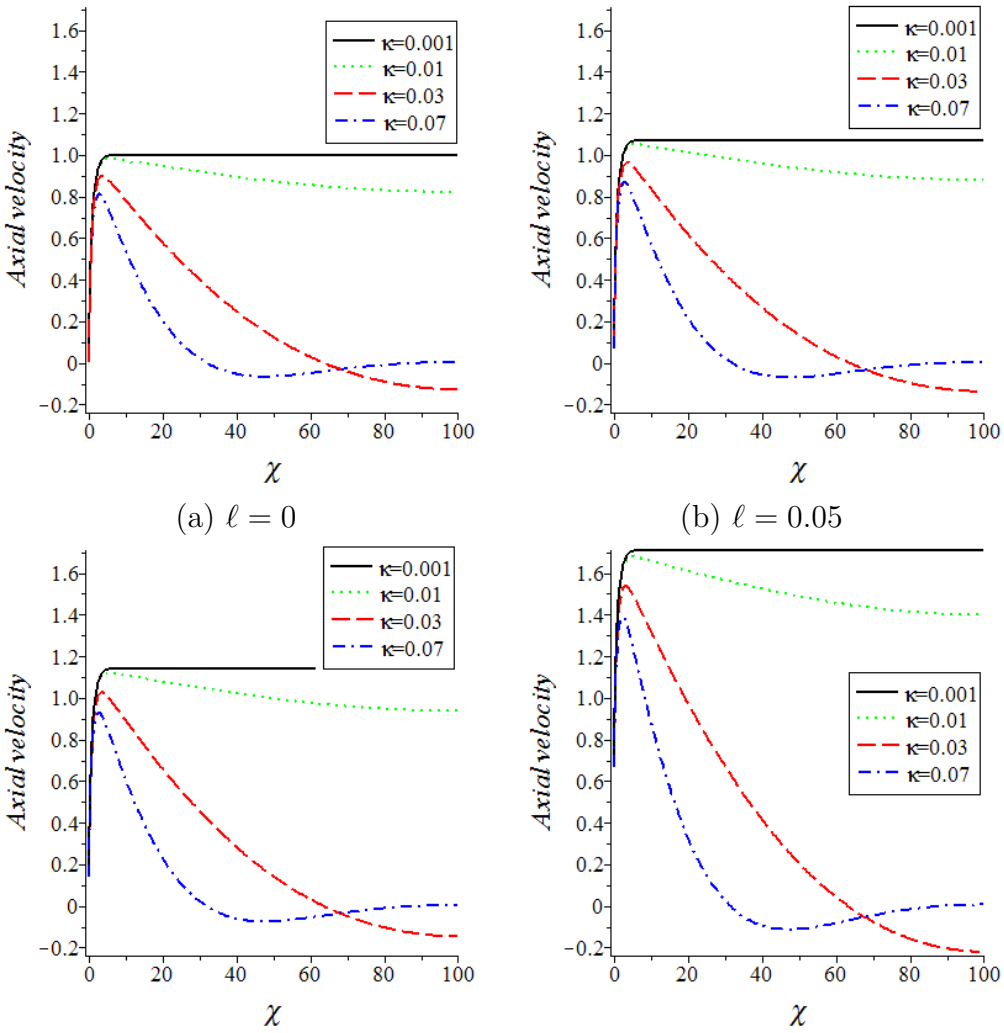

(a) $\ell = 0$ (b) $\ell = 0.05$

(c) $\ell = 0.1$ (d) $\ell = 0.5$

Figure 3.3: Effect of κ on velocity profile obtained from the model with $\theta = \pi/2$, $\alpha = 1$ and $h = 100\lambda$ for various slip length: (a) $\ell = 0$; (b) $\ell = 0.05$; (c) $\ell = 0.1$; (d) $\ell = 0.5$.

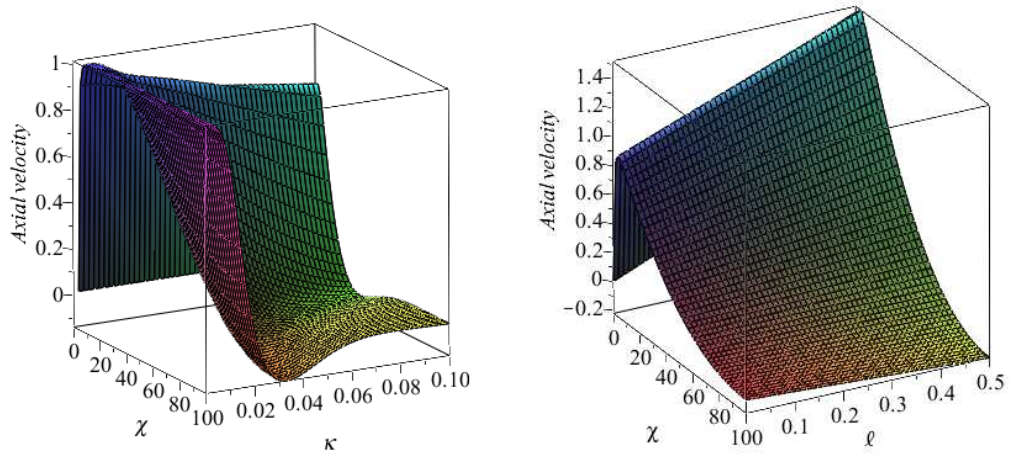

(a) $U(\chi, \kappa)$ when $\ell = 0.05$ (b) $U(\chi, l)$ when $\kappa = 0.03$

Figure 3.4: 3D plot of $U(\chi, \kappa)$ and $U(\chi, l)$ obtained from the model with $\theta = \pi/2$, $\alpha = 1$ and $h = 100\lambda$.

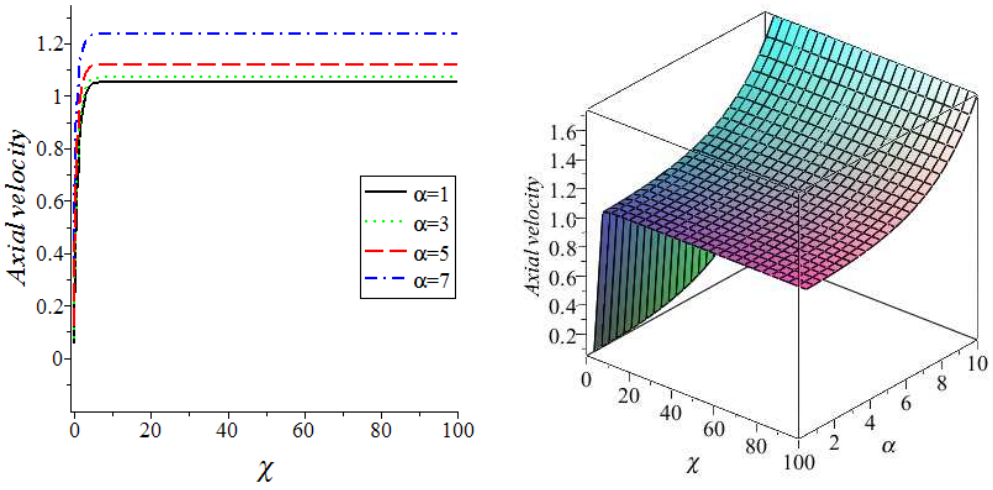

(a) $\kappa = 0.001$

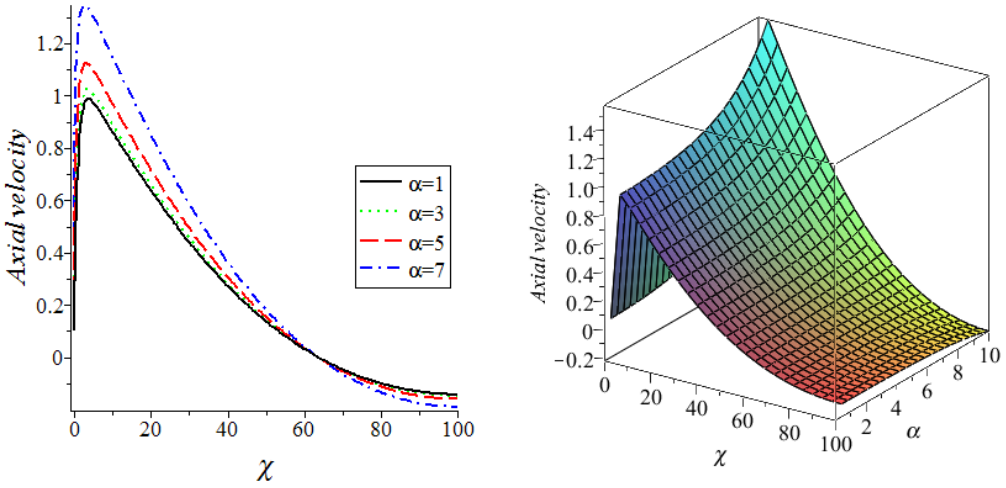

(b) $\kappa = 0.03$

Figure 3.5: Effect of the energy parameter α on the velocity profile obtained from the model with $\theta = \pi/2$, $h = 100\lambda$ and $l = 0.05$ for two different κ values: (a) $\kappa = 0.001$ (b)$\kappa = 0.03$.

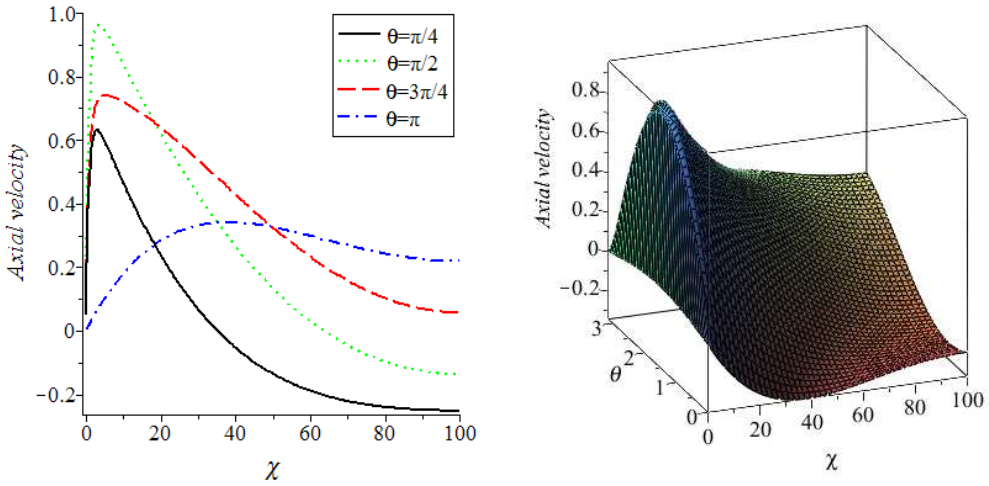

Figure 3.6: 2D and 3D plots of velocity profile at various instants of time obtained from the model with $\alpha = 1$, $\kappa = 0.03, \ell = 0.05$ and $h = 100\lambda$.

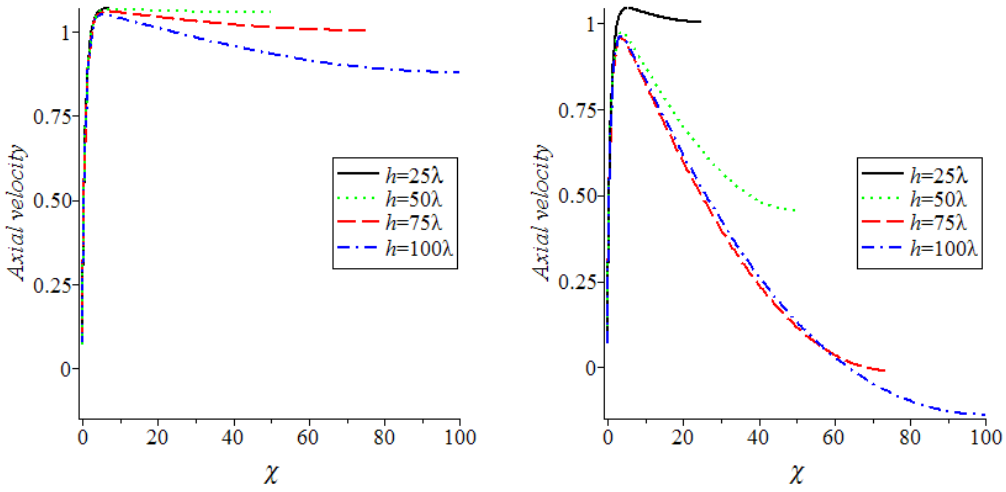

(a) $\kappa = 0.001$ (b) $\kappa = 0.03$

Figure 3.7: Effect of the channel half-height h on the velocity profile obtained from the model with $\theta = \pi/2$, $\alpha = 1$ and $\ell = 0.05$ for two different κ values: (a) $\kappa = 0.001$; (b) $\kappa = 0.03$.

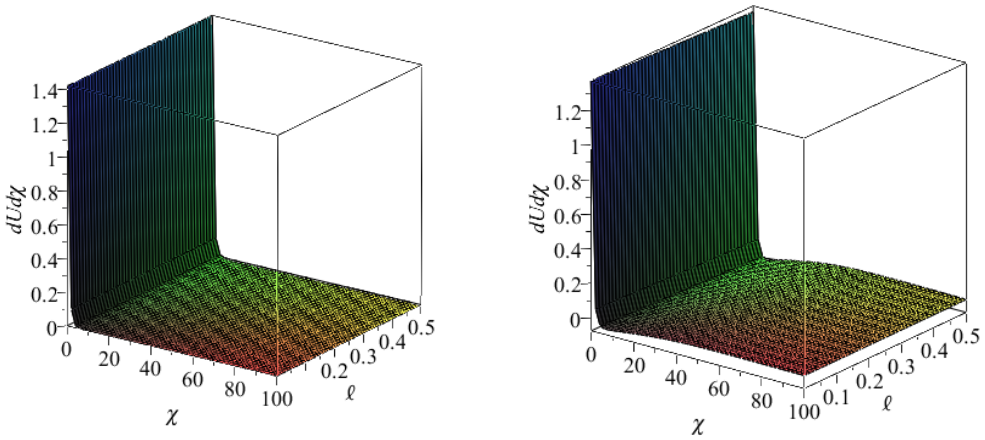

(a) $\frac{DU}{D\chi}(\chi, l)$ for $\kappa = 0.001$ (b) $\frac{DU}{D\chi}(\chi, l)$ for $\kappa = 0.03$

Figure 3.8: 3D plot of $\frac{DU}{D\chi}(\chi, l)$ for two κ values: (a) $\kappa = 0.001$; (b) $\kappa = 0.03$.

3.5 Concluding Remarks

We obtained an analytical solution for time-periodic electroosmotic flows in two-dimensional straight microchannels with slip boundary condition by assuming a constant ζ potential, constants buffer concentration, and Newtonian fluid.

Our results show that the flow behaviour depend on the parameters κ and α as well as the slip parameter l and channel height. The parameter κ represents the ratio of the electric double layer thickness to a characteristic diffusion length scale I_D while α is an energy parameter.

We found that depending on the value of the parameter κ, the flow pattern may change from oscillatory plug flow to uniform flat flow. Generally, as κ increases, the velocity at the centre drops to zero dramatically. We also found that the slip parameter has significant influence on the flow behaviour. As l increases, the flow rate increases.

CHAPTER 4

Solution of Newtonian fluid flows through circular microchannels with slip boundary and electrokinetic phenomena

4.1 General

Over the past few decades, advances in nano-science and nano- technology have led to the development of many microelectro-mechanical systems and devices such as heat exchanger [88], micropump [89], lab-on-a-chip diagnostic devises [59], drug delivery systems [5], energy conversion and biological sensing devices [6]. Most of these systems and devices involve fluid flows in microtubes and microchannels. To control the microfluidics in microchannels so as to achieve optional system performance, it is essential to study the fundamental mechanics of microflows and derive better models and understanding of the flow mechanism and flow behaviour. Flows of microfluidics may be driven by pressure gradient or by electrical forces. For electric-driven flows, the solid surface of the microchannel is electrically charged to generate a region in the fluid with a distribution of electrical charges near the channel surface. This region is called the electric double layer(EDL). The EDL, on one hand, has the effect of retarding liquid flow driven by external pressure gradient to form a streaming potential; whereas on the other hand, it can induce fluid flow by applying an external electric field. In the chapter, we will study the flow of microfluidics in microchannels driven by the combination of pressure gradient and externally applied electric field.

The equations governing the flow of microfluics in microchannels include the Navier-Stokes equations, the incompressible continuity equation, and boundary conditions. Traditionally, the no slip boundary condition is used [90]. However, recent molecular dynamic simulations and experiments in micrometer scale show

that the flow of fluids in micrometer scale is granular and slip occurs between the fluid and the solid surface [91–95]. Therefore, the no slip condition does not work for fluid flow in microchannels. In this work, the Navier slip boundary condition will be used, namely the tangential fluid velocity relative to the solid surface is proportional to the shear stress on the solid-fluid interface. The validity of the Navier slip boundary condition is supported by many experimental results [9, 12, 13].

For many fluid flow problems, under the non-slip assumption, exact and numerical solutions have been obtained and can be found in literature [7, 15, 90, 96]. Steady state solutions under slip conditions have also been established for flows of Newtonian fluids through pipes, channels and annulus [14, 97]. More recently, various analytical solutions for pressure-driven time dependant slip flows of Newtonian fluids through microtubes and microannulus were derived [7, 9, 96]. Various attempts have also been made to study the electrically driven fluid flows. Rice and Whitehead [98] investigated the steady- state liquid flow due to an electric field in circular capillaries. Levine et al [99] analysed the electrokinetic steady flow in a narrow parallel-plate microchannel. Yang et al [100] studied the flow in rectangular microchannels and Mala et al [101, 102] in parallel-plate microchannels.

Motivated by previous work, this chapter aims to generalize the result in [10] for the pressure-driven slip flow to the case with the combined effect of pressure-driving forces and electrically driving forces. The rest of the chapter is organized as follows. In section 4.2, we present the mathematical model for the problem, consisting of the governing field equations and boundary conditions. In section 4.3, we derive the exact solutions for the velocity field through use of Bessel functions in space and Fourier Series expansion in time. Based on the velocity solutions, we then establish the analytical solutions for the stress tensor and flow rate. In section 4.5, we investigate the influence of the electric field and the surface slippage on the flow behaviour. Then a conclusion is given in section 4.6.

4.2 Mathematical model and formulation

In this chapter, we consider the flow of microfludic through a circular microchannel driven by both pressure gradient and external electric field. The cylindrical polar coordinate (r, θ, z), with the z-axis being in the axial direction, is used

in the formulation. The governing field equations for the problem include the Navier-Stokes equations and the continuity equation. Let $\underline{v} = (v_r, v_\theta, u)$ be the velocity vector with v_r, v_θ and u being respectively the components of velocity in the radial direction, the transverse direction and axial direction. Then the continuity equation and the Navier-Stokes equation in the z-direction are

$$\frac{\partial^2 v_r}{\partial r^2} + \frac{v_r}{r} + \frac{\partial v_\theta}{r\partial\theta} + \frac{\partial u}{\partial z} = 0, \tag{4.1}$$

$$\frac{\partial u}{\partial t} + v_r\frac{\partial u}{\partial r} + \frac{v_\theta}{r}\frac{\partial u}{\partial \theta} + u\frac{\partial u}{\partial \theta} = g_z - \frac{1}{\rho_f}\frac{\partial p}{\partial z} + \frac{\mu}{\rho}(\frac{\partial^2 u}{\partial r^2} + \frac{\partial u}{r\partial r} + \frac{1}{r^2}\frac{\partial^2 u}{\partial \theta^2} + \frac{\partial^2 u}{\partial z^2}) + \frac{\rho_e}{\rho_f}E_z', \tag{4.2}$$

where p is the pressure, μ is the dynamic viscosity, E_z' is the externally applied electric field, ρ_f and ρ_e are respectively the fluid density and the electric charge density.

Assuming that the flow is axially symmetric, and the radial and transverse velocity components are negligible, then equations (4.1) and (4.2) admit solution of the form

$$v_r = 0, \tag{4.3}$$

$$v_\theta = 0, \tag{4.4}$$

$$u = u(r, t) \tag{4.5}$$

with $u(r, t)$ determined by

$$\frac{\partial u}{\partial t} - \frac{\mu}{\rho_f}(\frac{\partial^2 u}{\partial r^2} + \frac{1}{r}\frac{\partial u}{\partial r}) = -\frac{1}{\rho_f}\frac{\partial p}{\partial z} - \frac{\rho_e}{\rho_f}E_z'. \tag{4.6}$$

In this work, we study the flow driven by both pressure gradient $\frac{\partial p}{\partial z}$ and an externally applied electric field E_z. Without lost of generality, we express the pressure gradient by Fourier series, namely

$$\frac{\partial p}{\partial z} = \overline{q}(t) = a_0 + \sum_{n=1}^{\infty}[a_n \cos(n\omega t) + b_n \sin(n\omega t)]. \tag{4.7}$$

Remark 4.2.1 As a wide range of functions can be expressed in terms of Fourier series,the assumption of the form of pressure gradient (4.7) will not lose generaity.It should be addressed here that our work is limited to the cases where the pressure gradient varies with time only.

Remark 4.2.2 Flow of fluids driven by non-constant pressed gradient occurs in many natural and industrial progress. A typical example is the pulsatile blood flow through arteries in which the pressure gradient driving the flow of blood is in pulsatile form [15]. It should be addressed here that various methods can be used to generate pulsatile flows, such as those by using reciprocating piston,servo valves or air pulsation [103, 104].

For convenience in deriving analytical solutions of the field equations, we use complex variables to express (4.7) by exponential functions, namely

$$\frac{dp}{dz} = Re\sum_{n=0}^{\infty} c_n e^{in\omega t} \tag{4.8}$$

where

$$c_n = a_n - b_n i, \tag{4.9}$$

$$e^{in\omega t} = \cos(n\omega t) + i\sin(n\omega t). \tag{4.10}$$

For the electric field, the total potential U at location (r, z) at the given time t is taken to be

$$U = U(r, z, t) = \psi(r) + [U_0 - zE_z'(t)], \tag{4.11}$$

where $\psi(r)$ is the potential due to the double layer at the equilibrium state(i.e.,no liquid motion with no applied external field); U_0 is the potential at $z = 0$, (i.e.,$U_0 = U(r, 0, t)$). The total potential U in equation (4.11) is asymmetric, and when $E_z'(t)$ is time-independent, equation (4.11) is identical to equation (6.1) of Masliyah [105]. The time-dependent flow to be studied here is assumed to be sufficiently slow such that the radial charge distribution is relaxed at its steady state. Further, it is assumed that any induced magnetic fields are sufficiently small and negligible such that the total electric field may still be defines as $-\nabla U$ [106]. This definition can then be used to obtain the Poisson equation

$$\nabla U^2 = -\frac{\rho_e}{\epsilon}. \tag{4.12}$$

where ϵ is the permittivity of the medium.

We focus on a symmetric, binary electrolyte with univalent charges. The cations and anions are identified as species 1 and 2 respectively. On the basis of the assumption of thermodynamic equilibrium,the Boltzmann equation provides

a local charges density ρ_i of the ith specy. Thus

$$\rho_i = z_i e n_\infty \exp(-\frac{z_i e\psi}{kT}) \qquad (i = 1, 2), \tag{4.13}$$

where z_i is the valence of the ith specy;e is the elementary charge; n_∞ is the ionic concentration in an equilibrium electrochemical solution at the neutral state where $\psi = 0$, k is the Boltzmann constant; and T is the absolute temperature. Invoking the Debye-huckel approximation for low surface potentials ($z_i e\psi/kT << 1$),we have $\sinh(z_i e\psi/kT) \approx z_i e\psi/kT$ and the total charge density is

$$\rho_e = \sum \rho_i = -\frac{2n_\infty z_0^2 e^2 \psi}{kT}, (i = 1, 2) \tag{4.14}$$

where we have used $z_1 = -z_2 = z_0$. Finally, the definition of the reciprocal of the double layer thickness for a $(z_0 : z_0)$ electrolyte is given as [51]

$$\kappa = \sqrt{\frac{2n_\infty z_0^2 e^2}{\epsilon kT}}. \tag{4.15}$$

Combining equations (4.11), (4.12),(4.14) and (4.15), we have

$$\frac{d^2\psi}{dr^2} + \frac{1}{r}\frac{d\psi}{dr} = \kappa^2\psi. \tag{4.16}$$

The boundary conditions for ψ are

$$\psi(R) = \psi_s \tag{4.17}$$

$$\psi(0) \quad \text{is finite}, \tag{4.18}$$

where ψ_s is the surface potential at the wall $r = R$.

Once ψ is determined, ρ_e is also determined and by substituting ρ_e in terms of ψ into (4.6), we have

$$\frac{\partial u}{\partial t} - \frac{\mu}{\rho_f}(\frac{\partial^2 u}{\partial r^2} + \frac{1}{r}\frac{\partial u}{\partial r}) = -\frac{1}{\rho_f}\frac{\partial p}{\partial z} - \frac{\kappa^2\psi}{\rho_f}E_z'. \tag{4.19}$$

To completely define the velocity field, the field equations must be supplemented by the boundary condition. To describe the slip characteristics of fluid on the solid surface, Navier introduced a more general boundary condition. That is, on the solid-fluid interface $r = R$, the axial fluid velocity,relative to the solid

surface,is proportional to the shear stress on the interface.Assume that the rigid microtube moves with an axial velocity $v_t(t)$, then the Navier slip condition can be written as

$$u(R,t) - v_t(t) = -l\frac{\sigma_{rz}(R,t)}{\mu}, \tag{4.20}$$

where μ is the fluid viscosity and l is the so-called slip length,the negative sign on the right-hand side of the above equation is to reflect that shear stress on the interface is always in the opposite direction of the axial fluid velocity as any tangential movement of a fluid particle relative to the solid surface will always be restricted by a resistance force acting on the opposite directing on the relative movement, $\sigma_{rz}(R,t)$ is the shear stress on the interface between the fluid and the wall of the microtube. It should be addressed here that for $l = 0$, condition (4.20) reduces to the no-slip boundary condition; while, for $l \to \infty$, equation (4.20) gives a surface traction for a perfectly smooth surface, i.e.,$\sigma_{rz}(R,t) = 0$. For the problem under consideration here, we assume that the microtube is fixed spatially, i.e.,$v_t(t) = 0$. Thus by noting that $\sigma_{rz}(r,t) = \mu\frac{du}{dr}$, we have from equation (4.20) that

$$u(R,t) = -l\frac{du}{dr}(R,t). \tag{4.21}$$

Further, due to the axial symmetricity, we have

$$\frac{\partial u}{\partial r}(0,t) = 0, \tag{4.22}$$

Hence the problem is to solve the boundary value problem (4.16)-(4.18) for ψ, and then the partial differential equation (4.19) subject to boundary conditions (4.21)-(4.22) for u, which will be done in section 4.3.

4.3 Exact solution for the transient velocity field

First we solve equation (4.16) subject to boundary condition (4.17)-(4.18). Let $\kappa r = \overline{r}$, then equation (4.16) becomes

$$\overline{r}^2\frac{d^2\psi}{d\overline{r}^2} + \overline{r}\frac{d\psi}{d\overline{r}} - \overline{r}^2\psi = 0, \tag{4.23}$$

from which we obtain

$$\psi = AJ_0(\kappa r) + BY_0(\kappa r), \tag{4.24}$$

where A and B are integration constants constants, J_0 and Y_0 denote the zero-order Bessel functions of the first and second kind respectively. As ψ must be infinite at $r = 0$, we requires that $B = 0$. Substituting (4.24) into boundary condition (4.17) yields

$$A = \frac{\psi_s}{J_0(\kappa R)} \tag{4.25}$$

Hence, we obtain

$$\psi = \frac{\psi_s}{J_0(\kappa R)} J_0(\kappa r). \tag{4.26}$$

Thus equation (4.19) becomes

$$\frac{\partial u}{\partial t} - \frac{\mu}{\rho_f}(\frac{\partial^2 u}{\partial r^2} + \frac{1}{r}\frac{\partial u}{\partial r}) = -\frac{1}{\rho_f} Re \sum_{n=0}^{\infty} c_n e^{in\omega t} + \frac{1}{\rho_f}\frac{\kappa^2 \psi_s}{J_0(\kappa R)} J_0(\kappa r) E'_z \tag{4.27}$$

which admits solution of the form

$$u(r,t) = u_p(r,t) + u_e(r,t) \tag{4.28}$$

where u_p is the solution corresponding to the first term on the right hand side, and u_e is the solution contributed from the second term of the right hand side. From the superposition principle, if u_n is the solution of (4.27) for $\frac{dp}{dz} = c_n e^{in\omega t}$, then the complete solution of (4.27) for $\frac{dp}{dz} = Re(\sum_{n=0}^{\infty} c_n e^{inwt})$ is $u = \sum_{n=0}^{\infty} Re(u_n)$. To determine u_n, we solve

$$\frac{\mu}{\rho_f}(\frac{d^2 u_n}{dr^2} + \frac{1}{r}\frac{du_n}{dr}) - \frac{du_n}{dt} = \frac{c_n}{\rho_f} e^{in\omega t} \tag{4.29}$$

which admits solution of the form

$$u_n = f_n(r) e^{in\omega t}. \tag{4.30}$$

Substituting the above equation into (4.29) yields

$$\frac{\mu}{\rho_f}(\frac{d^2 f_n}{dr^2} + \frac{1}{r}\frac{df_n}{dr})e^{in\omega t} - in\omega f_n e^{in\omega t} = \frac{c_n}{\rho_f}e^{in\omega t}. \tag{4.31}$$

For $n = 0$, equation (4.31) becomes

$$r^2\frac{d^2 f_0}{dr^2} + r\frac{df_0}{dr} = \frac{c_0}{4\mu}r^2 \tag{4.32}$$

which has the general solution

$$f_0(r) = (C + Dlnr) + \frac{c_0}{4\mu}r^2. \tag{4.33}$$

As the solution $f(r)$ must be bounded at $r = 0$, we require $D = 0$ and hence, we obtain

$$u_0 = f_0(r) = C + \frac{c_0}{4\mu}r^2. \tag{4.34}$$

For $n \geq 1$, equation (4.31) gives

$$\frac{1}{\beta_n^2}\frac{d^2 f_n}{dr^2} + \frac{1}{\beta_n^2 r}\frac{df_n}{dr} + f_n = \frac{c_n}{\beta_n^2\mu}, \tag{4.35}$$

where $\beta_n^2 = n\beta^2$ in which $\beta^2 = -\frac{\rho_f\omega}{\mu}i$. Let $\overline{r} = \beta_n r$, then equation (4.35) becomes

$$\overline{r}^2\frac{d^2 f_n}{d\overline{r}^2} + \overline{r}^2\frac{df_n}{d\overline{r}} + \overline{r}^2 f_n = \frac{c_n}{\beta_n^2\mu}\overline{r}^2, \tag{4.36}$$

The associated homogeneous equation of the above equation is the zero-order Bessel equation and thus has the following solution

$$f_{nc} = d_n J_0(\overline{r}) + e_n Y_0(\overline{r}) = d_n J_0(\beta_n r) + e_n Y_0(\beta_n r), \tag{4.37}$$

where d_n and e_n are integration constants,J_0 and Y_0 denote the zero-order Bessel function of the first kind and the second kind respectively. As f_{nc} must be bounded in the computation domain but $Y(\beta_n r)$ has singularity at $r = 0$, we require that $e_n = 0$. To find the particular solution corresponding to the driving force, we let $f_{nc} = C$, and then by substituting it into equation (4.35), we have $C = \frac{c_n i}{\rho n\omega}$.

Hence, the general solution of (3.35) is

$$f_n = f_{nc} + f_{np} = d_n J_0(\beta_n r) + \frac{c_n i}{\rho n \omega}, \tag{4.38}$$

From (4.34), (4.38) and the superposition principle, we have

$$u_p = Re(C + \frac{c_0}{4\mu} r^2) + \sum_{n=0}^{\infty} Re\{(d_n J_0(\beta_n r) + \frac{c_n i}{\rho n \omega}) e^{in\omega t}\}.$$

As $c_0 = a_0 - ib_0$, we have from the above equation that

$$u_p = C + \frac{a_0}{4\mu} r^2 + \sum_{n=0}^{\infty} Re\{(d_n J_0(\beta_n r) + \frac{c_n i}{\rho n \omega}) e^{in\omega t}\}. \tag{4.39}$$

Now, we proceed to find the solution contributed from the second term on the right hand side of (4.28). Let $u_e(r) = C_0(r)t + C_1(r)$ and substitute it into equation (4.27), then we have

$$-\frac{\mu}{\rho_f}[C_0''(r) + \frac{1}{r}C_0'(r)]t + C_0(r) - \frac{\mu}{\rho_f}[C_1''(r) + \frac{1}{r}C_1'(r)] = \frac{1}{\rho_f}\frac{\kappa^2 \psi_s}{J_0(\kappa R)} E_z' J_0(\kappa r).$$

For the above equation to hold for any instant of time t, we require

$$C_0''(r) + \frac{1}{r}C_0'(r) = 0,$$

$$C_0(r) - \frac{\mu}{\rho_f}[C_1''(r) + \frac{1}{r}C_1'(r)] = \frac{1}{\rho_f}\frac{\kappa^2 \psi_s}{J_0(\kappa R)} E_z' J_0(\kappa r). \tag{4.40}$$

Thus

$$C_0 = D_1 \ln r + D_2$$

As C_0 must be bounded at $r = 0$ but $\ln r$ has singularity at $r = 0$, we require that $D_1 = 0$. From equation (4.40), we have

$$C_1 = \frac{1}{\mu}\frac{\psi_s E_z'}{J_0(\kappa R)} J_0(\kappa r) + \frac{\rho_f}{\mu}\frac{D_2}{4} r^2,$$

and then by substituting C_0 and C_1 into $u_e(r,t)$, we have

$$u_e(r,t) = D_2 t + \frac{1}{\mu}\frac{\psi_s E'_z}{J_0(\kappa R)} J_0(\kappa r) + \frac{\rho_f}{\mu}\frac{D_2}{4} r^2, \tag{4.41}$$

Hence, by substituting (4.39) and (4.41) to (4.28), we obtain

$$\begin{aligned} u(r,t) =& C + \frac{a_0}{4\mu} r^2 + \sum_{n=1}^{\infty} Re\{(d_n J_0(\beta_n r) + \frac{c_n i}{\rho_f n\omega}) e^{in\omega t}\} + \\ & D_2 t + \frac{1}{\mu}\frac{\psi_s E'_z}{J_0(\kappa R)} J_0(\kappa r) + \frac{\rho_f}{\mu}\frac{D_2}{4} r^2. \end{aligned} \tag{4.42}$$

Substituting (4.42) into boundary conditions (4.20) and (4.21) yields

$$\begin{aligned} & C + \frac{a_0}{4\mu} R^2 + l\frac{a_0}{2\mu} R + \frac{1}{\mu}\psi_s E'_z - l\frac{\kappa \psi_s E'_z}{\mu J_0(\kappa R)} J_1(\kappa R) + D_2 t + \frac{\rho_f D_2 R^2}{4\mu} + l\frac{\rho_f D_2 R}{2\mu} \\ & + \sum_{n=0}^{\infty} Re[(d_n J_0(\beta R) + \frac{c_n i}{\rho_f n\omega} - l\beta_n d_n J_1(\beta_n R)) e^{in\omega t}] = 0. \end{aligned}$$

For the above equation to hold for any instant of time t, we require $D_2 = 0$ and

$$C + \frac{a_0}{4\mu} R^2 + l\frac{a_0}{2\mu} R + \frac{1}{\mu}\psi_s E'_z - l\frac{\kappa}{\mu}\frac{\psi_s E'_z}{J_0(\kappa R)} J_1(\kappa R) = 0$$

$$d_n J_0(\beta R) + \frac{c_n i}{\rho_f n\omega} - l\beta_n d_n J_1(\beta_n R) = 0,$$

which give

$$C = -\frac{a_0 R^2}{4\mu}(1 + \frac{2l}{R}) - \frac{1}{\mu}\psi_s E'_z + l\frac{\kappa}{\mu}\frac{\psi_s E'_z}{J_0(\kappa R)} J_1(\kappa R) \tag{4.43}$$

$$d_n = \frac{-c_n i}{\rho_f n\omega[J_0(\beta R) - l\beta_n J_1(\beta_n R)]} \tag{4.44}$$

Hence, by substituting (4.43) and (4.44) into (4.42), we obtain

$$u = -\frac{a_0 R^2}{4\mu}(1 + \frac{2l}{R} - \frac{r^2}{R^2}) - \frac{1}{\mu}\psi_s E'_z + l\frac{\kappa}{\mu}\frac{\psi_s E'_z}{J_0(\kappa R)}J_1(\kappa R)$$
$$- \sum_{n=0}^{\infty} Re\{\frac{c_n i}{\rho_f n\omega}(\frac{J_0(\beta_n r)}{J_0(\beta_n R) - l\beta_n J_1(\beta_n R)} - 1)e^{in\omega t}\} + \frac{1}{\mu}\frac{\psi_s E'_z}{J_0(\kappa R)}J_0(\kappa r). \tag{4.45}$$

We should remark that if $l = 0$, solution (4.45) reduces to the no slip solution

$$u = -\frac{a_0 R^2}{4\mu}(1 - \frac{r^2}{R^2}) - \frac{1}{\mu}\psi_s E'_z - \sum_{n=0}^{\infty} Re\{\frac{c_n i}{\rho_f n\omega}(\frac{J_0(\beta_n r)}{J_0(\beta_n R)} - 1)e^{in\omega t}\}$$
$$+\frac{1}{\mu}\frac{\psi_s E'_z}{J_0(\kappa R)}J_0(\kappa r). \tag{4.46}$$

If $l \gg R$ and is sufficiently large, solution (4.45) can be approximated by

$$u \approx -\frac{a_0 lR}{2\mu} + \frac{\rho_e \rho_f}{\mu\kappa^2}\psi_s + \sum_{n=0}^{\infty} Re\frac{c_n i}{\rho_f n\omega}(\frac{J_0(\beta_n r)}{l\beta_n J_1(\beta_n R)} - 1)e^{in\omega t}$$
$$- l\frac{\rho_e \rho_f}{\mu\kappa}\frac{\psi_s}{J_0(\kappa R)}J_1(\kappa R), \tag{4.47}$$

which corresponds to the case in which the fluids-solid interface is very smooth. Obviously, the velocity profile across the cross-section of the tube tends to be uniform in this case.

4.4 Solutions for the flow rate and stresses

From the velocity solution (4.45), we get the flow rate as follows

$$\begin{aligned} Q(t) &= \int_0^R 2\pi r u dr \\ &= -\frac{a_0\pi R^3}{2\mu}(l+\frac{R}{4}) + l\frac{\pi R^2\kappa}{\mu}\frac{\psi_s E_z'}{J_0(\kappa R)}J_1(\kappa R) + \int_0^R \frac{1}{\mu}\frac{\psi_s E_z'}{J_0(\kappa R)}J_0(\kappa r) r dr \\ &\quad - \frac{2\pi}{\rho_f\omega}Re\Big[\sum_{n=0}^{\infty}\frac{c_n i e^{in\omega t}}{n}\int_0^R (\frac{J_0(\beta_n r)}{J_0(\beta_n R) - lJ_1(\beta_n R)} - 1) r dr\Big] - \frac{\pi R^2}{\mu}\psi_s E_z' \end{aligned} \tag{4.48}$$

From the identity

$$\frac{d}{dx}[x^n J_n(x)] = x^n J_{n-1}(x),$$

we have

$$\frac{d}{dr}[r J_1(\beta_n r)] = \beta_n r J_0(\beta_n r)$$

and hence

$$\int_0^R r J_0(\beta_n r) dr = \frac{1}{\beta_n}[r J_1(\beta_n r)]_0^R = \frac{1}{\beta_n} R J_1(\beta_n R)$$

Therefore from (4.48) and the above formula, we get

$$\begin{aligned} Q(t) = &-\frac{a_0\pi R^3}{2\mu}(l+\frac{R}{4}) + l\frac{\pi R^2\kappa}{\mu}\frac{\psi_s E_z'}{J_0(\kappa R)}J_1(\kappa R) + \frac{R}{\mu\kappa}\frac{\psi_s E_z'}{J_0(\kappa R)}J_1(\kappa R) \\ &- \frac{2\pi}{\rho_f\omega}Re\Big[\sum_{n=0}^{\infty}\frac{c_n i e^{in\omega t}}{n}(\frac{R J_1(\beta_n R)}{\beta_n[J_0(\beta_n R) - l\beta_n J_1(\beta_n R)]} - \frac{R^2}{2})\Big] - \frac{\pi R^2}{\mu}\psi_s E_z' \end{aligned} \tag{4.49}$$

The total amount of fluid, flowing through the tube during the period [0,T], can then be determined as follows

$$\begin{aligned} Q_T &= \int_0^T Q(t)dt \\ &= -\frac{a_0\pi R^3 T}{2\mu}(l+\frac{R}{4}) + l\frac{\pi R^2\kappa}{\mu}\frac{\psi_s E_z' T}{J_0(\kappa R)}J_1(\kappa R) + \frac{\pi R}{\mu\kappa}\frac{\psi_s E_z' T}{J_0(\kappa R)}J_1(\kappa R) \\ &\quad - \frac{2\pi}{\rho_f\omega^2}Re\Big[\sum_{n=0}^{\infty}\frac{c_n(e^{in\omega T}-1)}{n^2}\Big(\frac{RJ_1(\beta_n R)}{\beta_n[J_0(\beta_n R)-l\beta_n J_1(\beta_n R)]}-\frac{R^2}{2}\Big)\Big] - \frac{\pi R^2}{\mu}\psi_s E_z' T. \end{aligned} \tag{4.50}$$

Remark 4.4.1. For the constant component (a_0) of the pressure gradient,the flow rate increases linearly as the slip length l increases. However, for the harmonic component ($c_n e^{in\omega t}$)of the pressure gradient,the relation between the flow rate and slip length l is not immediately clear from the above solution form as it involves a complex parameter and Bessel functions with complex arguments, and so we will further investigate this in section 4.5.

In what follows, we determine the stresses in the fluid. The stress field in the fluid is related to the velocity field by the following constitutive equation

$$\sigma = -pI + 2\mu\mathbf{d} \tag{4.51}$$

while the rate of deformation tensor is related to the velocity vector by

$$\mathbf{d} = \frac{1}{2}(\nabla\overrightarrow{V} + (\nabla\overrightarrow{V})^T), \tag{4.52}$$

where $\sigma = (\sigma_{ij})$ and $\mathbf{d} = (d_{ij})$ denote respectively the second-order stress tensor and the rate of deformation tensor, and I is an identity matrix. In cylindrical polar coordinate (r,θ,z), $\overrightarrow{V} = \mathbf{e}_r v_r + \mathbf{e}_\theta v_\theta + \mathbf{e}_z u$ and the gradient operator is

$$\nabla = \mathbf{e}_r\frac{\partial}{r\partial r} + \mathbf{e}_\theta\frac{\partial}{r\partial r} + \mathbf{e}_z\frac{\partial}{\partial z} \tag{4.53}$$

where $\mathbf{e}_r, \mathbf{e}_\theta$ and $\mathbf{e}_z$ are respectively the radial unit vector and the axial unit vector.

Now in the problem under investigating $\mathbf{v} = e_r 0 + e_\theta 0 + e_z u(r)$, and so we get

$$\nabla v = \begin{pmatrix} 0 & 0 & \frac{\partial u}{\partial r} \\ 0 & 0 & 0 \\ \frac{\partial u}{\partial r} & 0 & 0 \end{pmatrix}$$

From the above formulae and (4.45), we obtain

$$d_{r\theta} = d_{\theta z} = d_{rr} = d_{\theta\theta} = d_{zz}$$

$$d_{rz} = \frac{a_0 r}{2\mu} + \sum_{n=0}^{\infty} Re\Big[\frac{c_n i}{\rho_f n\omega}\Big(\frac{\beta_n J_1(\beta_n r)}{J_0(\beta_n R) - l\beta_n J_1(\beta_n R)}\Big)e^{in\omega t}\Big] - \frac{\kappa}{\mu}\frac{\psi_s E_z'}{J_0(\kappa R)} J_1(\kappa r). \tag{4.54}$$

Thus from the constitutive equations for Newtonian fluid, we get

$$\sigma_{rr} = \sigma_{\theta\theta} = \sigma_{zz} = -p = \overline{q}(t)x + p_0(t),$$

$$\sigma_{r\theta} = \sigma_{\theta z} = 0$$

$$\sigma_{rz} = a_0 r + 2\mu \sum_{n=0}^{\infty} Re\Big[\frac{c_n i}{\rho_f n\omega}\Big(\frac{\beta_n J_1(\beta_n r)}{J_0(\beta_n R) - l\beta_n J_1(\beta_n R)}\Big)e^{in\omega t}\Big] - 2\mu\kappa\frac{\psi_s E_z'}{J_0(\kappa R)} J_1(\kappa r). \tag{4.55}$$

where $p_0(t)$ is an arbitrary constant which may be chosen to meet certain pressure conditions.

Remark 4.4.2. For the constant component (a_0) of the pressure gradient ,the shear stress in the fluid is independent of the slip length l, while for the harmonic component $c_n e^{in\omega t}$ of the pressure gradient,the shear stress is influenced by the slip length.

4.5 Numerical investigation

In this section, we use the solutions obtained in previous sections to study the influence of the combined effect of electrical field and pressure gradient on the velocity profile and flow rate. As the pressure gradient can be expressed as a Fourier series, without loss of generality, we consider here only two cases of pres-

sure gradient, including the constant pressure gradient and a cosine wave form pressure gradient.

Case 1: $dp/dz = a_0$

In this case, we have $c_n = 0$ for all $n \geq 1$ and thus, from (4.45) and (4.50), we get the normalized velocity and flow rate as follows

$$\begin{aligned} u^* =& -\frac{4\mu}{a_0 R^2} u \\ =&(1 + \frac{2l}{R} - \frac{r^2}{R^2}) - \frac{4\mu}{a_0 R^2}\Big[l\frac{\kappa}{\mu}\frac{J_1(\kappa R)}{J_0(\kappa R)} + \frac{1}{\mu}\frac{J_0(\kappa r)}{J_0(\kappa R)} - \frac{1}{\mu}\Big]\psi_s E_z' \end{aligned} \tag{4.56}$$

$$\begin{aligned} Q^*(t) =& -\frac{2\mu}{a_0 \pi R^3} Q(t) \\ =&(l + \frac{R}{4}) - \frac{2\mu}{a_0 \pi R^2}\Big[l\frac{\pi\kappa R}{\mu}\frac{J_1(\kappa R)}{J_0(\kappa R)} + \frac{1}{\mu\kappa}\frac{J_1(\kappa R)}{J_0(\kappa R)} - \frac{\pi R}{\mu}\Big]\psi_s E_z'. \end{aligned} \tag{4.57}$$

We should address here that the velocity and flow rate are linearly propositional to the slip length l.

Remark 4.5.1 The flow rate is linearly propositional to the slip length l. The flow rate-slip length relation (4.57) can be used to design simple experiments to determine the slip length by measuring the flow rate for a given set of value of μ, R and a_0.

Case 2: $dp/dz = a_1 \cos(\omega t)$

In this case, we have $a_0 = 0, c_1 = a_1 \in R, c_n = 0$ for all $n \geq 2$. For simplification,

we normalize the variables as follows

$$\beta^* = \beta R, \tag{4.58}$$

$$r^* = \frac{r}{R} \in [0,1], \tag{4.59}$$

$$l^* = \frac{l}{R}, \tag{4.60}$$

$$t^* = \frac{\omega t}{2\pi}, \tag{4.61}$$

$$u^* = -\frac{\rho_f \omega}{a_1} u \tag{4.62}$$

$$K = \kappa R. \tag{4.63}$$

Then from (4.45), we get

$$\begin{aligned} u^* =& Re\Big((\frac{J_0(\beta^* r^*)}{J_0(\beta^*) - l^* \beta^* J_1(\beta^*)} - 1) i e^{2\pi i t^*} \Big) \\ & - \frac{\rho_f \omega}{a_1} \Big[\frac{1}{\mu} \frac{J_0(K r^*)}{J_0(K)} + \frac{\kappa R l^*}{\mu} \frac{J_1(K)}{J_0(K)} - \frac{1}{\mu} \Big] \psi_s E_z'. \end{aligned} \tag{4.64}$$

Let

$$M = M(r^*) = Re\Big(\frac{J_0(\beta^* r^*)}{J_0(\beta^*) - l^* \beta^* J_1(\beta^*)} \Big), \tag{4.65}$$

$$N = N(r^*) = Im\Big(\frac{J_0(\beta^* r^*)}{J_0(\beta^*) - l^* \beta^* J_1(\beta^*)} \Big), \tag{4.66}$$

$$A_1 = -\frac{\rho_f \omega}{\mu J_0(K)}, \tag{4.67}$$

$$A_2 = \frac{\rho_f \omega K}{\mu J_0(K)} J_1(K) R, \tag{4.68}$$

$$A_3 = \frac{\rho_f \omega}{\mu}, \tag{4.69}$$

then

$$u^* = A(r^*) \cos(2\pi t^* - \theta) + (A_1 J_0(K r^*) + A_2 l^* + A_3) \frac{\psi_s E_z'}{a_1}, \tag{4.70}$$

where

$$A = \sqrt{N^2 + (1-M)^2}, \tag{4.71}$$

$$\theta = \arctan(\frac{M-1}{N}). \tag{4.72}$$

As the M and N in the above solution form are expressed in terms of the complex parameter β^* and the Bessel function with complex arguments, it is not immediately clear from this solution form whether the velocity is linearly proportional to l^* of inversely linearly proportional to l^* or is related to l^* nonlinearly. Thus, we first proceed below to derive a more explicit formulae relating u^* and l in the real domain. As $\beta^2 = -\frac{\rho\omega}{\mu}i = -\frac{\rho\omega}{\mu}e^{-\pi/2}$, we have

$$\beta = \sqrt{\frac{\rho\omega}{2\mu}}(1-i) = \frac{\overline{\beta}}{R}(1-i), \tag{4.73}$$

$$\frac{1}{\beta} = \frac{R}{2\overline{\beta}}(1+i), \tag{4.74}$$

$$\beta^* = \overline{\beta}(1-i), \tag{4.75}$$

where $\overline{\beta} = R\sqrt{\frac{\rho\omega}{2\mu}}$. Further,we let

$$J_0(\beta^*) = \gamma_0 + \lambda_0 i, \tag{4.76}$$

$$J_1(\beta^*) = \gamma_1 + \lambda_1 i, \tag{4.77}$$

$$J_0(\beta^* r^*) = \gamma_{0r} + \lambda_{0r} i, \tag{4.78}$$

then

$$\frac{J_0(\beta^* r^*)}{J_0(\beta^*) - l^*\beta^* J_1(\beta^*)} = [\gamma_{0r} + \lambda_{0r} i]\frac{[\gamma_0 - l^*\overline{\beta}(\gamma_1+\lambda_1)] - [\lambda_0 - l^*\overline{\beta}(\lambda_1-\gamma_1)]i}{[\gamma_0 - l^*\overline{\beta}(\gamma_1+\lambda_1)]^2 + [\lambda_0 - l^*\overline{\beta}(\lambda_1-\gamma_1)]^2} \tag{4.79}$$

$$M = \frac{\gamma_{0r}[\gamma_0 - l^*\overline{\beta}(\gamma_1+\lambda_1)] + \lambda_{0r}[\lambda_0 - l^*\overline{\beta}(\lambda_1-\gamma_1)]}{[\gamma_0 - l^*\overline{\beta}(\gamma_1+\lambda_1)]^2 + [\lambda_0 - l^*\overline{\beta}(\lambda_1-\gamma_1)]^2}, \tag{4.80}$$

$$N = \frac{\lambda_{0r}[\gamma_0 - l^*\overline{\beta}(\gamma_1+\lambda_1)] - \gamma_{0r}[\lambda_0 - l^*\overline{\beta}(\lambda_1-\gamma_1)]}{[\gamma_0 - l^*\overline{\beta}(\gamma_1+\lambda_1)]^2 + [\lambda_0 - l^*\overline{\beta}(\lambda_1-\gamma_1)]^2} \tag{4.81}$$

For $\|y\| \ll 1$, we have the following asymptotic formulae for approximating Bessel functions [95]

$$J_n(x+yi) \approx J_n(x) - \frac{iy}{2}[J_{n+1}(x) - J_{n-1}(x)], \tag{4.82}$$

$$J_n(y) \simeq \frac{1}{n!}(\frac{y}{2})^n \tag{4.83}$$

Thus, for $\overline{\beta} \ll 1$, we have

$$\begin{aligned}
&J_0(\beta^*) = J_0(\overline{\beta} - \overline{\beta}i) \approx J_0(\overline{\beta}) + i\overline{\beta}J_1(\overline{\beta}) \approx 1 + \frac{\overline{\beta}^2}{2}i \\
&J_1(\beta^*) = J_1(\overline{\beta} - \overline{\beta}i) \approx \frac{\overline{\beta}}{2} - \frac{\overline{\beta}}{2}\Big[1 - \frac{\overline{\beta}^2}{8}\Big]i \\
&J_0(\beta^* r^*) \approx 1 + \frac{\overline{\beta}^2 r^{*2}}{2}i, \\
&J_1(\beta^* r^*) = \frac{\overline{\beta} r^*}{2} - \frac{\overline{\beta} r^*}{2}\Big[1 - \frac{(\overline{\beta} r^*)^2}{8}\Big]i
\end{aligned} \tag{4.84}$$

Substituting the above into (4.80) and (4.81) yields

$$M \approx \frac{1 - \overline{\beta}^4 l^*(1 - 8r^{*2})/16}{1 + \overline{\beta}^4 l^*(\frac{7}{8} + l^*)}, \tag{4.85}$$

$$N \approx -\frac{\overline{\beta}^2(1 - r^{*2} + 2l^*)}{2[1 + \overline{\beta}^4 l^*(\frac{7}{8} + l^*)]}. \tag{4.86}$$

Hence we have

$$A = A(r^*) = \frac{\overline{\beta}^2}{2[1 + \overline{\beta}^4 l^*(\frac{7}{8} + l^*)]}\sqrt{(1 - r^{*2} + 2l^*)^2 + \frac{\overline{\beta}^4 l^{*2}}{64}(15 - 8r^2 + 16l^*)^2} \tag{4.87}$$

$$u^* = A(r^*)\cos(2\pi t^* - \theta) + [A_1 J_0(Kr^*) + A_2 l^* + A_3]\psi_s E_z'/a_1 \tag{4.88}$$

Thus, it can be concluded that the velocity consists of a time depending part in terms of a trigonometric function and a time independent part in terms of a Bessel function of the first kind of order zero. To demonstrate the velocity profile of the mixed pressure-driving and electrical-driving flow and the influence of the slip parameter and electric field on the flow, we carry out numerical investigation under various conditions. The typical value chosen for the model parameters R, ρ_f, ω, μ are $R = 20mm, \rho_f = 1000km/m^3, \omega = \frac{1}{2\pi}, \mu = 0.86Ns/m^2$. Based on

references [107–109], the K value varies from one electrolyte solution to another as shown in Table 4.1; and thus in this work we use a wide range of values to demonstrate the influence of K on the flow. The slip length l is related to the smoothness of the surface of the tubes and is controllable within certain range; and hence we also use a wide range of l values in the investigation to demonstrate the influence of l on the flow profile and flow rate. The $\psi_s E'_z$ is set to 0.05V in all experiments except for the experiment in which the influence of the intensity of electric field relative to the pressure-driving force is to be investigated.

Table 4.1.K values for typical electrolyte solutions used in the literature

Reference	Solution	Concentration(mM)	K
[107]	Na_2HPO_4	40	1316
[107]	KH_2PO_4	40	3290
[108]	$Na_2B_4O_7 \cdot 10H_2O$	10	6585
[108]	$NaHCO_3$	54	7645
[109]	KCI	10	3290

As the velocity profile consists of two parts due respectively to pressure gradient and electrical field, we first show the profile of these two velocity components in Figures 4.1 and 4.2 under different electric fields $\psi_s E'_z/a_1$ and K values. From the figure, it is clear that it is possible to control the velocity profile in an optimal manner based on the need of application for the mixed driving flow by finding proper combination of the pressure field and electrical field. Figures 4.3 and 4.4 show typical velocity profile for a mixed driving flow.

To demonstrate the influence of the slip length on the velocity, we vary the value of l^* from 0 to 100 while maintaining other parameter values unchanged. Figure 4.5 shows the effect of slip length on the velocity on the wall at a typical time step $t^* = \theta/2\pi$, obtained with $\psi_s E'_z/a_1 = 10^{-6}$, and K=3000 and K=2000. It is clear that the relationship between the slip parameter and the velocity is non-linear and there is an optimal value for which the slip velocity takes the maximum value.

As the K value changes across different electrolyte solutions, we investigate the influence of K on the velocity profile. Figure 4.6 shows the velocity profiles for different K values for $\psi_s E'_z/a_1 = 10^{-3}$ and under the same pressure gradient and slip length $l^* = 1$. It is clear from the result that the K value influences the velocity profile significantly. For lower K, the velocity profile is smooth; while under high K values, the velocity shows wave form profile, and the frequency of the waves increases as K increases. It is also noted that the amplitude of the waves increases as the $\psi_s E'_z/a_1$ value increases. The magnitude of the velocity

is also affected significantly by the $\psi_s E_z'/a_1$ value as shown in Figure 4.7. As $\psi_s E_z'/a_1$ increases, the magnitude of the velocity increases.

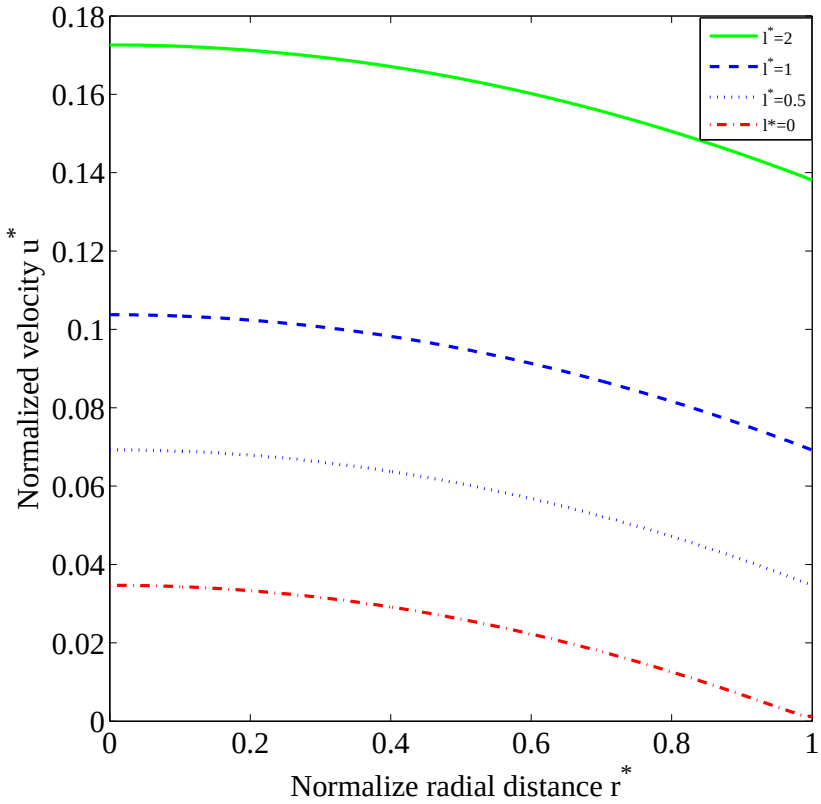

Figure 4.1: Typical profiles of the velocity component due to pressure gradient under different l^* values .

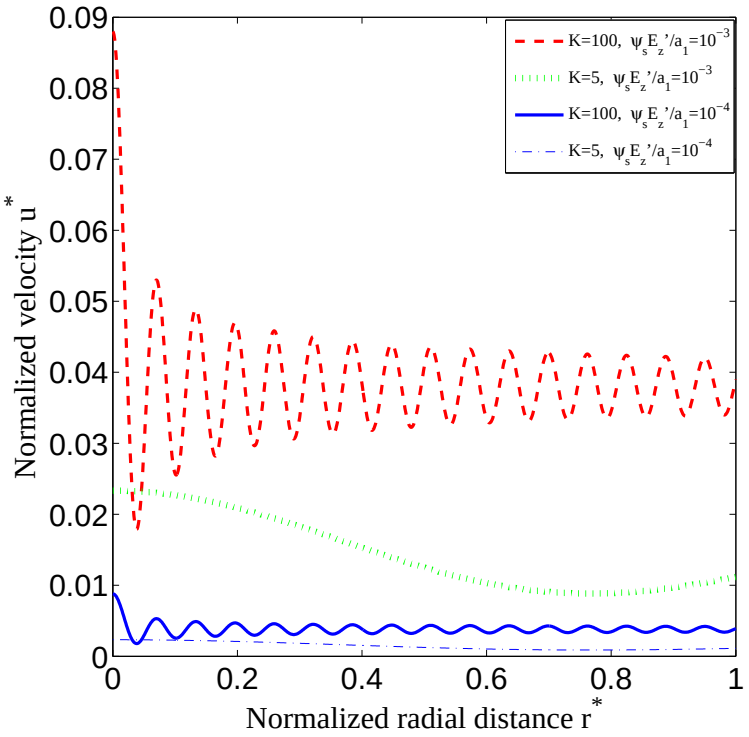

Figure 4.2: Typical profiles of the velocity component due to electric field for $l^* = 0.5$ under different $\psi_s E_z'/a_1$ and K values.

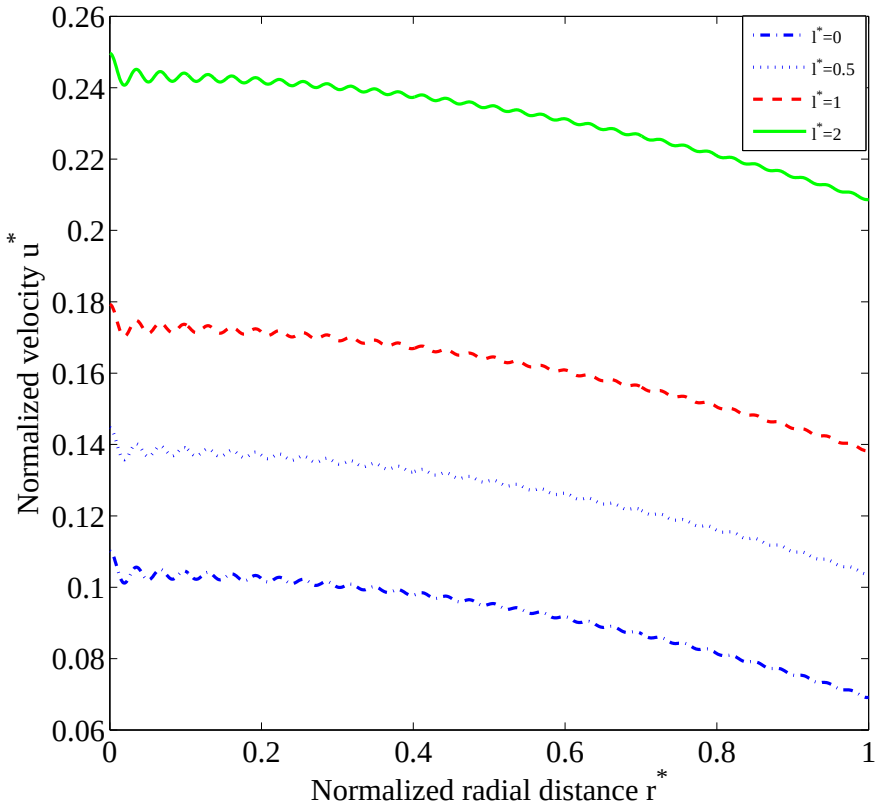

Figure 4.3: Typical velocity profile for various different values of slip length l^* at a typical time $t^* = \frac{\theta}{2\pi}$,obtained with $\psi_s E'_z/a_1 = 10^{-4}$, K=200.

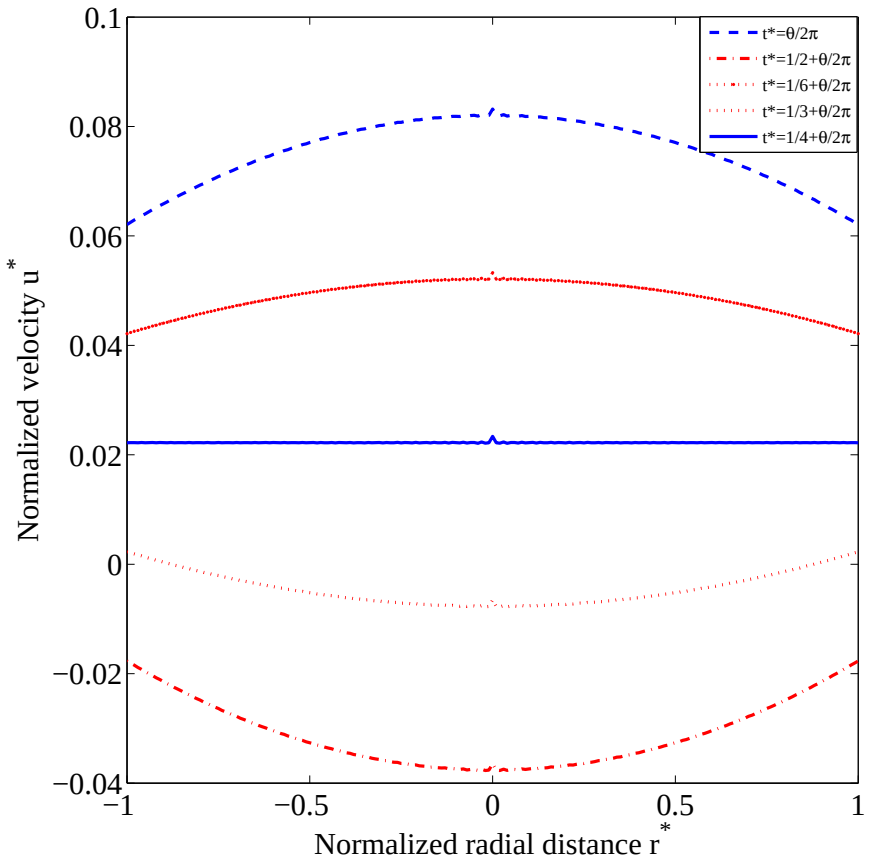

Figure 4.4: Typical velocity profile for the mixed pressure and electric driven flow at various instants of time t^*, obtained with slip length $l^* = 1$, $\psi_s E'_z/a_1 = 10^{-6}$ and K=1500.

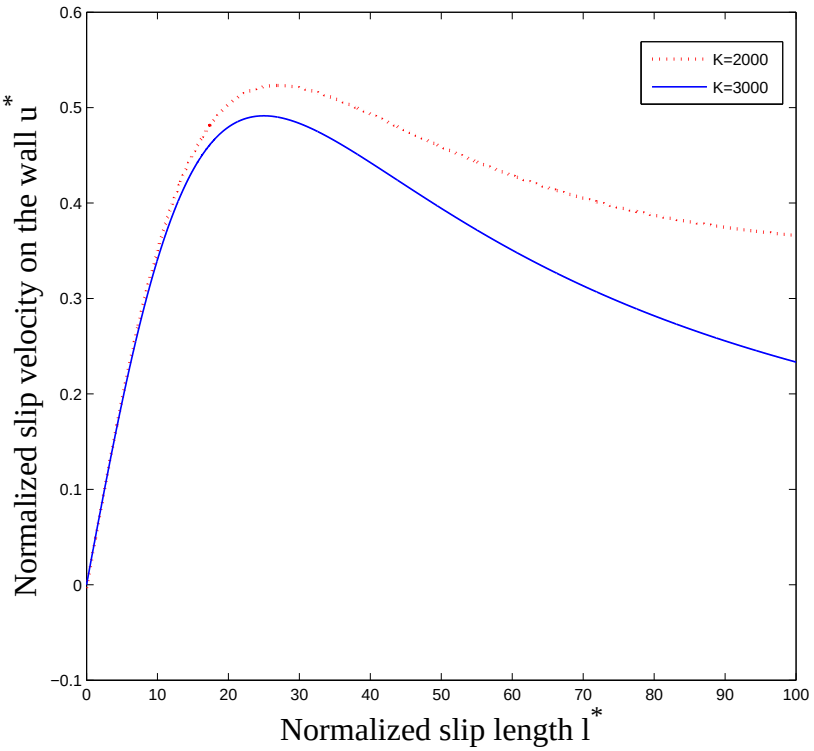

Figure 4.5: The influence of slip length on the slip velocity on the wall at a typical time $t^* = \theta/2\pi$, obtained with $\psi_s E'_z/a_1 = 10^{-3}$, $l^* = 1$.

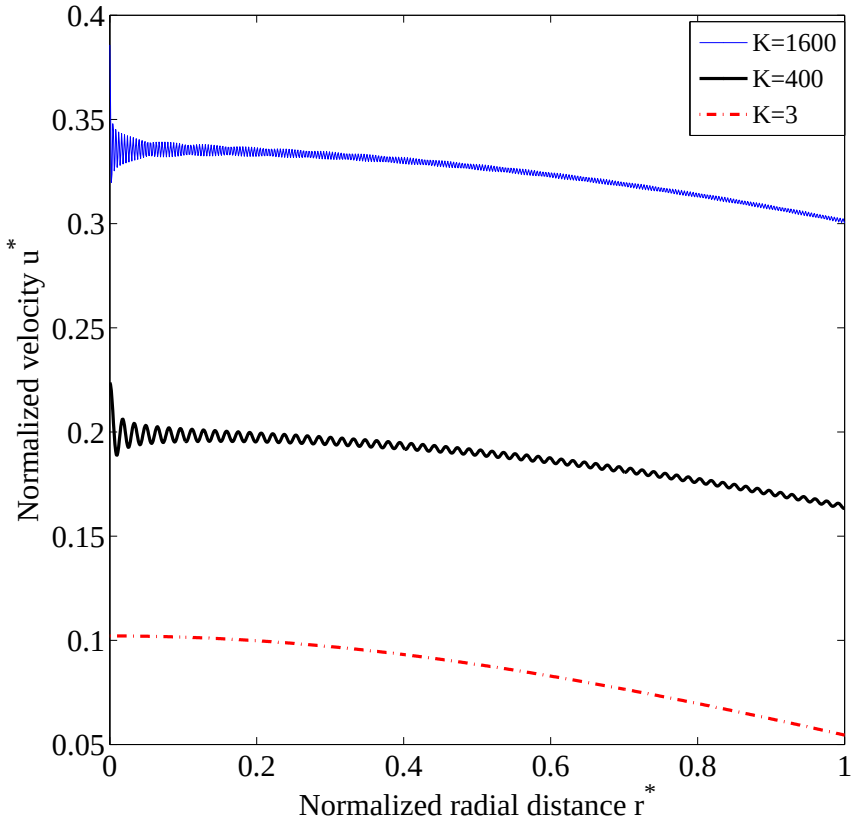

Figure 4.6: Influence of K value on the velocity profile at a typical time $t^* = \theta/2\pi$, obtained with $\psi_s E'_z/a_1 = 10^{-3}, l^* = 1$

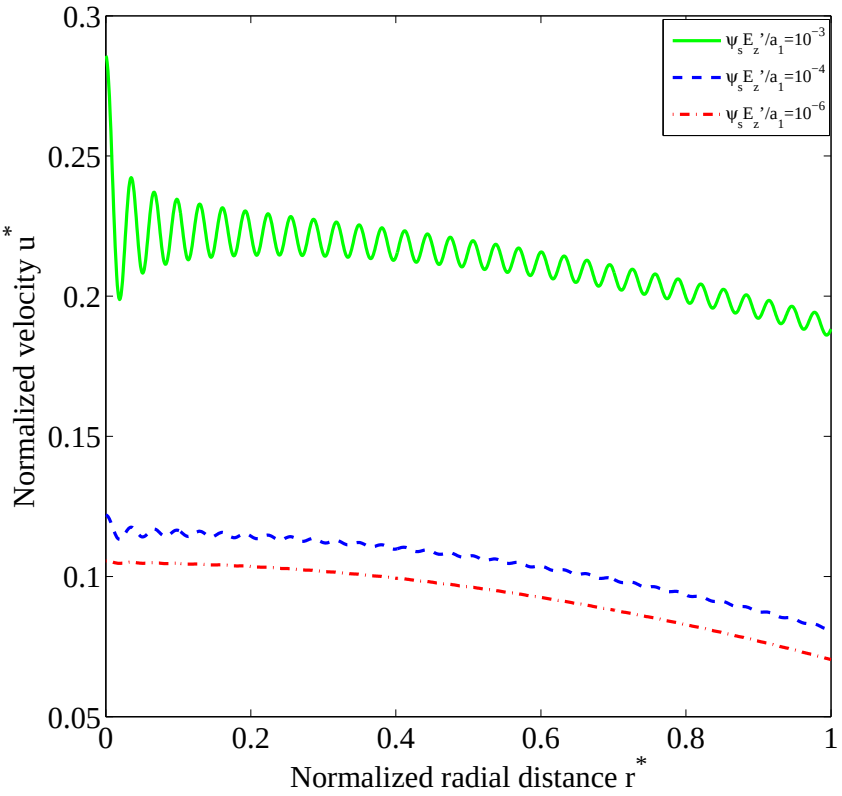

Figure 4.7: Influence of magnitude of electric field on the velocity profile at a typical time $t^* = \theta/2\pi$, obtained with $l^* = 0.5$, K=200.

4.6 Concluding Remarks

In this chapter, an exact solution for the transient flow of an incompressible Newtonian fluid in microtubes is derived taking into account the electrokinetic effect and the boundary slip. We have shown that both boundary slip and electrokinetic field have significant effect on the flow. The results are summarized as follows.

(i) Both the pressure-gradient driving force and electric driving force influence the velocity profile significantly, and it is possible to construct an optimal control problem to achieve the desired velocity profile based on the need of the application.

(ii) For the case of constant pressure gradient, the relationship between the slip parameter and the velocity is linear. However, for pressure gradient in wave form, the influence of the slip parameter on the velocity magnitude is non-linear and there exits a critical slip length where the magnitude and consequently the transient flow rate attain maximum values, which indicate that there exits an optimal slip length in terms of the magnitude of velocity and flow rate.

(iii) The K value of the electrolyte solution has significant influence on the velocity profile on the cross-section of the tube. At low K value, no wave form profile exists. However as K increases, the cross-section velocity exhibits wave from profile, and the frequency of the wave increases as K increases.

(iv) The magnitude of the intensity of electric field relative to the pressure gradient, measured by $\psi_s E_z'/a_1$, also has very significate influence on the velocity profile. As $\psi_s E_z'/a_1$ increases, the velocity component increases and also the amplitude of the wave in the wave-form velocity profile also increases.

CHAPTER 5

Summary and future research directions

5.1 Summary

In this thesis, we study two kinds of microflows taking into account of microslip on the boundary, including the time periodic electroosmotic flow between two parallel plates with boundary slip and the flow of a Newtonian fluid in microtube of circular cross-section under the combined effect of electric driving force and pressure driving force. Based on previous work in the field, we have derived some analytical and numerical results. The main results are summarized in two aspects as follows

(1) Results for time periodic electroosmosis flows with boundary slip

(i) The equations governing electroosmosis flows have been formulated and established based on the Navier-Stokes equations and the equation of continuity in rectangular coordinates. By assuming fully developed one-dimensional flow in the channel, the field equations for the velocity field reduce to a second order partial differential equation with a wave-form electrical driving force. The boundary conditions based on the Navier slip model have also been established.

(ii) The partial differential equation subject to the slip boundary condition has been solved to yield the exact solutions for the velocity field in the channel. Based on the model and the analytical expressions of the solutions obtained, a number of investigations have been carried out to study the influence of various parameters on the flow behaviour, and the following conclusions have been obtained.

(a)The normalized parameter κ has very significant influence on the velocity profile. As κ increases, the flow pattern may change from uniform flat flow to oscillatory plug flow, and the thickness of the layer with significant electric driven flow decreases and essentially the velocity becomes zero at the centre.

(b) The slip length has significant influence on the magnitude of the velocity. As l increases, the magnitude of the velocity near the wall increases while the flow

pattern basically remains the same. The shear deformation rate $\frac{du}{d\chi}$ is influenced by l for small value of l; but tend to constant when l is sufficiently large.

(c) Other parameters, the energy parameter α and the channel height $2h$, also have influence on the magnitude of the velocity.

(2) Results for microflows in circular tubes with boundary slip under the combined effect of electric driving force and pressure driving force.

(i) The equations governing the microflow and the electric potential have been formulated in cylindrical polar coordinates. The problem becomes to first determine the electric potential by solving the electric potential equation and then solve the velocity partial differential equation. Slip boundary conditions have also been established to supplement the field equations.

(ii) Exact solutions for the velocity field have been established for microflows through circular channels with boundary slip. The basic method used for the determination of the velocity field is through use of Bessel functions in space and Fourier series expansion in time. From the velocity solution, analytical solutions for the stress tensor and flow rate have also been established.

(iii) Based on the mathematical model and the analytical expressions derived for the velocity field and stress field, a number of investigations have been carried out to study the influence of model parameters and the combined effect of electrical field and pressure gradient on the velocity profile and flow behavior. Form the investigations, it can be concluded that

(a) By changing the model parameters κ and $\psi_s E_z/a_1$, the velocity profile many display different patterns varying form smooth curve to wave-form curve and from small velocity magnitude to large velocity magnitude as shown in Figure 4.2. This clearly demonstrate that it is possible to control the velocity profile in a desired manner based on the need of application for mixed driving flows by finding proper combination of the pressure field and electrical field.

(b) Microslip on boundary has significant influence on the flow pattern and velocity profile. For microflows driven by wave form pressure gradient, there exists a critical slip length l_c. When $l < l_c$, the fluid slip velocity on the wall increases as l increases; while for $l > l_c$, the slip velocity on the wall decreases as l increases. This demonstrates that there exists an optimal slip length in terms of maximizing the magnitude of velocity and flow rate for certain applications.

(c) The magnitude of the intensity of electric field relative to the pressure gradient, measured by $\psi_s E_z/a_1$, also has very significant influence on the velocity profile. As $\psi_s E_z/a_1$ increases, the velocity component increases and also the amplitude of the wave in the wave-form velocity profile increases.

5.2 Future research directions

Further work may include various areas. The first area is to extend the work to more complex cases such as curved microchannels and microchannel with different shapes of cross-section such as rectangular and elliptic microchannels. Another possible extension is to consider different types of boundary slip models including nonlinear models, and consider the non-Newtonian effect of fluids.

Another area of further work is the optimal control of microflows based on the pre-determined desired velocity profile. The basic idea is to construct the optimal control problem as a constrained optimization problem with the objective function measuring the distance between the model predictions and the pre-determined velocity profile, and the constraints being the governing boundary value problem as established in this thesis. Then the problem is to find the parameters and the controls required to minimize the objective function.

Bibliography

[1] B. Bourlon, J. Wong, C. Mik, L. Forr. A nanoscale probe for fluidic and ionic transport, nature nanotechnology. *Computer Methods in Applied Mechanics and Engineering*, 2(2):104–107, 2007.

[2] C. M. Ho and Y. C. Tai. Micro-electro-mechanical systems (mems) and fluid flows. *Annual Review of Fluid Mechanics*, 30:579–612, 1998.

[3] H. Herwig, O. Hausner. Critical view on new results in micro-fluid mechanics: an example. *International Journal of Heat and Mass Transfer*, 46(5):935–937, 2003.

[4] H. Huang, T. S. Lee, C. Shu. Lattice boltzmann method simulation gas slip flow in long microtubes. *International Journal of Heat and Mass Transfer*, 17(6):587–607, 2007.

[5] Y. C. Su and L. W. Lin. A water-power micro drug delivery system. *Journal of Microelectromechanical System*, 13(1):75–80, 2004.

[6] J. J. Nakane, M. Akeson and A. Marziali. Nanopores sensors for nucleic acid analysis,journal of physics condensed matter. *Journal of Rhelogy*, 15:R1363, 2005.

[7] B. Wiwatanapataphee, Y. H. Wu, J. Archapitak and P. F. Siew. A numerical study of the turbulent flow of molten steel in a domain with a phase-change boundary. *Journal of Computational and Applied Mathematics*, 166:307–312, 2004.

[8] R. B. Bird, W. E. Stewart and E. N. Lightfoot,. *Transport Phenomena*. John Wiley Sons, 2007.

[9] Y. Christophe, B. Catherine and C. B. Ccile . Joseph pierre,achieving large slip with superhydrophobic surfaces:scaling laws for generic geometries. *Physics of Fluids*, 19:123601, 2007.

[10] Y. H. Wu and B. Wiwatanapataphee. Pressure-driven transient flows of newtonian fluids through microtubes with slip boundary. *Electrophoresis*, 387:5979–5990, 2008.

[11] Z. Duan and Y. S. Muzychka. Slip flow in elliptic micro-channels. *Int. Journal of Thermal Sciences*, 46:1104–1111, 2007.

[12] P. Huang and K. S. Breuer. Direct measurement of slip length in electrolyte solutions,physics of fluids. 19:028104, 2007.

[13] R. Pit, H. Hervet and L. leger. Direct experimental evidence of slip in hexadecane:solid interfaces. *Physical Review Letter*, 85:980–985, 2000.

[14] M. T. Matthews and J. M. Hill. Newtonian flow with nonlinear navier boundary condition. *Acta Mechanica*, 191(3):195, 2007.

[15] B. Wiwatanapataphee, D. Poltem,Y. H. Wu and Y. Lenbuty. Simulation of pulsatile flow of blood in stenosed coronary artery bypass with graft. *Mathematical,Bioscience and Engineering*, 3(2):371–383.

[16] B. Wiwatanapataphee, Y. H. Wu, M. B. Hu and K. Chayantrakom . A study of transient flows of newtonian fluids through micro-annuals with a slip boundary. *J. Phys A: Math. Theor.*, 42(6):065206 (14pp), 2009.

[17] S. R. Deshmukh and D. G. Vlachos. Cfd simulations of coupled, countercurrent combustor/reformer microdevices for hydrogen production. *Ind. Eng. Chem. Res.,*, 44(14):4982–4992, 2005.

[18] Z. Duan and Y. S. Muzychka. Slip flow in non-circular micro-channes. *Int. Journal of Thermal Sciences*, 3:473–484, 2007.

[19] N. Maluf. An introduction to microelectromechanical system engineering. 2000.

[20] Z. J. Yang and W. Y. Chen. Lab-on-a-chip techniques and applications ii. *National Central University Institutional*, 2010.

[21] P. S. Dittrich, K. Tachikawa, A. Manz. Micro total analysis systems. latest advancements and trends. *Anal. Chem.*, (78):3887–3908, 2006.

[22] J. G. Wu, R. F. Yue and X. F. Zeng. The research on the lab-on-a-chip and discrete droplet control chip. *Chinese Journel of Analytical Chemistry*, 34(2):276–279, 2006.

[23] W. D. Volkmuth and R. H. Austin. Dna electrophoresis in microlithographic arrays. *Nature*, 13(358):600–302, 1992.

[24] S. W. Turner, A. M. Perez, A. Lopez, and H. G. Craighead. Monolithic nanofluid sieving structures for dna manipulation. *Journal of Vacuum Science and Technology B*, 16(20):3835–3840, 1998.

[25] M. A. Burns, B. N. Johnson, S. N. Brahmasandra, K. Handique and J. R. Webster. An integrated nanoliter dna analysis device. *Science Maganize*, 282(5388):484–487, 1998.

[26] N. Maluf. *An introduvtion to microelectromechanical system engineering.* Artech House,Inc., 2nd edition, 2000.

[27] R. J. Hunter. Zeta potential in colloid science:principle and applications. *Academic Press Inc*, 1981.

[28] D. J. Griffiths. *Introduction to Electrodynamics.* 3nd edition, 2007.

[29] I. S. Grant and W. R. Phillips. *Electromagnetism* . 2nd edition, 2008.

[30] J. N. Israelachvili. *Intermolecular And Surface Forces.* Marcel Dekker Inc, 2nd edition, 1994.

[31] R. P. Feynman and R. B. Leighton. Electrokinetics:the properties of the stagnant layer unraveled. *Langmuir*, 14(20):5659–5663, 1978.

[32] R. P. Feynman, R.B. Leighton and M. L. Sands . The faynman and lectures on physics: Mainly mechanics, radiation, and heat. *Massachusetts*, 1977.

[33] Z. Zheng, D. J. Hansford, and A. T. Conlisk. Effect of multivalent ions on electroosmotic flow in micro- and nanochannels. *Electrophoresis*, 24(7):3006–3017, 2003.

[34] G. Gouy. Characteristic of electric charge on electrolyte surface. *Physical A.*, 9(2):457–162.

[35] Z. Zhu, X. Cai, and J. Jian. An improved sqp algorithm for solving minimax problems. *Applied Mathematics Letters*, 22(4):464–469, 2009.

[36] G. Chauveteau. Rodlike polymer solution flow through fine pores: influence of pore size on rheological behavior. *Journal of Rhelogy*, 2(26):111, 1982.

[37] R. Pit, H. hervet and L. Leger. A sequential quadratic programming algorithm for nonconvex, nonsmooth constrained optimization. *Physics Review Letters*, 2(85):980, 2000.

[38] Y. Liu and D. K. Tan. streaming potential and wall-slip effects on pressure-driven microchannel flow. *CIESC*, 64(5):1173–1179, 2013.

[39] P. Zhang, C. C. Zuo and D. Y. Zhou. study on characterics of liquid flow through a rectangular microchannel with electrokinetic effects. *Optics and Precision Engineer*, 15(4):523–529, 2007.

[40] M. Whitby and N. Quirke. Fluid flow in carbon nanotubes and nanopipes. *Nat Nanotechnol*, 2(2):87–94, 2007.

[41] E. Lauga and H. A. Stone. Effective slip in pressure-driven stokes flow. *Fluid Meth*, 489(2):55, 2003.

[42] E. Lauga, M. P. Brenner and H. A. Stone. *Handbook of Experimental Fluid Dynamica*. Springer, Newyork,2005,Chapter 15, 1950.

[43] C. Cottin-Bizonne, C. Barentin and E. Charlaix. Dynamics of simple liquids at heterogeneous surfaces: molecular dynamics simulations and hydrodynamic description. *Eur.Phys*, 15(4):427–438, 2004.

[44] C. Cottin-Bizonne, B. Cross, A. Steinberger and E. Charlaix . Boundary slip on smooth hydrophobic surface:intrinsic effects and possible artifacts. *Phys.Lett*, 94:056102, 2005.

[45] H. B. Lee, I. W. Yeo and K. K. Lee. Water flow and slip on napl-wetted surfaces of a parallel-walled fracture. *Geophysical Research Letters*, 34(19):L14901, 2007.

[46] F. Saidi. Non-newtonian flow in a thin film with boundary conditions of coulomb's type. *Journal of Applied Mathematics and Mechanics*, 86(9):702–721, 2006.

[47] D. H. You and P. Moin . Effects of hydrophobic surfaces on the drag and lift of a circular cylinder. *Phys. Fluids*, 19(8):081701, 2007.

[48] K. Stewartson. On the impulsive motion of a flat plate in a viscous fluid. *Oxford Journel*, 4(2):182–198, 1950.

[49] E. V. Dose and G. J. Guiochon. Time scales of transient processes in capillary electrophoresis. *Chromatogr.*, 2(652):263–275, 1993.

[50] K. Zhang, L. J. Zhong and Z. H. Li. Diffusion in the micro channel flow driven by electroosmosis. *Applied Mathematics and Mechanics*, 27(5):512–518, 2006.

[51] J. Yang and D. Kwok. Time-dependent laminar electrokinetic slip flow in infinitely extended rectangular microchannels. *Journal of Chemical Physics*, 118(1):354–363, 2003.

[52] Ja. Nordstrma, M. H. Carpenterb. Boundary and interface conditions for high-order finite-difference methods applied to the euler and navierstokes equations. *Journal of Computational Physics*, 148(2):621–645, 1999.

[53] A. N. Brooks and T. J. R. Hughes. Streamline upwind/petrov-galerkin formulations for convection dominated flows with particular emphasis on the incompressible navier-stokes equations. *Computer Methods in Applied Mechanics and Engineering*, 32(1-3):199–259, 1982.

[54] R. Codina. Stabilized finite element approximation of transient incompressible flows using orthogonal subscales. *Computer Methods in Applied Mechanics and Engineering*, 191(39-40):4295–4321, 2002.

[55] R. Codinaa, J. Principea, O. Guaschb, S. Badiaa,. Time dependent subscales in the stabilized finite element approximation of incompressible flow problems. *Computer Methods in Applied Mechanics and Engineering*, 196(21-24):2413–2430, 2007.

[56] V. Gravemeier, W. A. Wall, E. Ramm . A three-level finite element method for the instationary incompressible navierstokes equations. *Computer Methods in Applied Mechanics and Engineering*, 193(15-16):1323–1366, 2004.

[57] E. Hachem, B. Rivaux, T. Kloczko, H. Digonnet, T. Coupez. Stabilized finite element method for incompressible flows with high reynolds number. *Journal of Computational Physics*, 229(2):8643–8665, 2010.

[58] S. Arulanandam and D. Q. Li. Liquid transport in rectangular microchannels by electroosmotic pumping. *Physicochem ica l a nd Engineer in g Aspects*, 161(1):89–102, 2000.

[59] D. J. Harrison, K. Fluri, K. Seiler, Z. H. Fan, C. S. Effenhauser, A. Manz. Micromachining a miniaturized capillary electrophoresis-based chemical analysis system on a chip. *Journal of Rhelogy*, 216:895–897, 1993.

[60] S. C. Jacobson, L.B. Koutny and R. Hergenroeder. Microchip capillary electrophoresis with an integrated postcolumn reactor. *Analytical Chem istr y*, 66(20):3472–3476, 1999.

[61] R. Wang, J. Z. Lin and Z. H. Li. Analysis of electroosmotic flow characteristics at joint of capillaries with step change in f potential and dimension. *Interna tional For um on Biochip Techn ologies*, 10:21–25, 2004.

[62] S. George. On the effect of the internal friction of fluids on the motion of pendulums. *Transactions of the Cambridge Philosophical Society*, 9(4):8–106, 1985.

[63] N. D. Ming, L. J. Zhong and S. Xing. Numerical simulation and research on the electroosmotic flow in the curve channel. *Chinese Journal of Analytical Chemistry*, 32(8):988–992, 2004.

[64] Probstein,R.F. *Physiochemical hydrodynamics:An Introduction.* John Wiley Sons,Inc, 1994.

[65] T. Wehr, R. R. Diaz and M. Zhu . *Capillary Electrophoresis of Proteins.* Marcel Dekker Inc, 1998.

[66] Y. Xu. Tutorial: capillary electrophresis. *The Chem. Educ*, 1(2):1–14, 1996.

[67] F. van der Heyden, D. Stein and C. Dekker. Streaming currents in a single nanofluidic channel. *Phy s Rev Lett*, 95(11):116104, 2005.

[68] M. Ali, S. Carl and B. Subir. Transient streaming potential in a finite length microchannel. *J Colloid Interfa ce Sci*, 292(2):567–580, 2005.

[69] M. Elimelech, W. H, Chen and J. J. Waypa. Measuring the zeta (electrokinetic) potential of reverse osmosis membranes by a streaming potential analyzer. *J Colloid Interfa ce Sci*, 95(2):269–286, 1994.

[70] M. Xuan, D. Yun, W. Wei and W. Y. Liang. Researches on streming potential and zeta potential of nanofiltration membrane. *Technology of Water treatment*, 33(11):42–44, 2007.

[71] C. E. Hunt, C. A. Desmond and D. R. Ciarlo . Microfluidics: Fluid physics at the nanoliter scale. *Rev. Mod. Phys.*, 77(26):9771026, 2005.

[72] H. A. Stone, A.D. Stroock and A. Ajdari. engineer flows in small devices: Microfluidics toward a lab-on-a-chip. *Annu. Rev. Fluid Mech.*, 36:381–411, 2004.

[73] M. S. Chun, T. S. Lee and N. W. Choi. Microfluidic analysis of electrokinetic streaming potential induced by microflows of monovalent electrolyte solution. *Journal of Micromechanics and Microengineering*, 15(4):710, 2005.

[74] F. H. J. van der Heyden, D. J. Bonthuis, D. Stein and C. Meyer. Power generation by pressure-driven transport of ions in nanofluidic channels. *Nano Letters*, 7(4):1022–1025, 2007.

[75] E. A. DiMarzio , C. M. Guttman. Separation by flow. *Marcromolecules*, 3(2):131–146, 1970.

[76] D. Stein and F.H.J. van der Heyden. Pressure-driven transport of confined dna polymers in fluidic channels. *Biophysics*, 103(43):15853–15858, 2006.

[77] N. C. Blumenthal1, J. Ricci, L. Breger, A. Zychlinsky, H. Solomon1 . Effects of low-intensity ac and/or dc electromagnetic fields on cell attachment and induction of apoptosis. *Bioelectromagnetics*, 18(3):264–272, 1997.

[78] H. Morgan and N. G. Green. *AC electrokinetics: colloids and nanoparticles.* Research Studies Press, Philadelphia, 2003.

[79] J. Wu, Y. X. Ben, H. C. Chang . Particle detection by electrical impedance spectroscopy with asymmetric-polarization AC electroosmotic trapping . *Microfluidics and Nanofluidics*, 1(2):161–167, 2005.

[80] O. Soderman and B. Jonsson . Electro-osmosis: Velocity profiles in different geometries with both temporal and spatial resolution. *J. Chem. Phys*, 105(23):10300, 1996.

[81] N. G. Green, A. Ramos, A. Gonzlez, H. Morgan and A. Castellanos . Fluid flow induced by nonuniform ac electric fields in electrolytes on microelectrodes. iii. observation of streamlines and numerical simulation. *Phys. Rev. E*, 66(2):026305, 2002.

[82] D. Burgreen and F. R. Nakache . Electrokinetic flow in ultrafine capillary slits. *The Journal of Physical Chemistry*, 68(5):1084–1091, 1964.

[83] J. Su , Y. J. Jian and L. Chang . Thermally fully developed electroosmotic flow through a rectangular microchannel. *International Journal of Heat and Mass Transfer*, 55(21-22):6285–6290, 2012.

[84] Y. J. Kang, C. Yang and X. Y. Huang. Electroosmotic flow in a capillary annulus with high zeta potentials. *International Journal of Heat and Mass Transfer*, 253(2):285–294, 2002.

[85] P. Dutta and A. Beskok . Analytical solution of time periodic electroosmotic flows: Analogies to stokes' second problem. *Anal. Chem.*, 73(21):50975102, 2001.

[86] Y. J. Kang, C. Yang, X. Y. Huang . Dynamic aspects of electroosmotic flow in a cylindrical microcapillary. *International Journal of Engineering Science*, 40(20):2203–2221, 2002.

[87] Y. J. Jian, L. G. Yang and Q. S. Liu. Time periodic electro-osmotic flow through a microannulus. *Physics of Fluids*, 22(4):042001, 2010.

[88] C. E. Hunt, C. A. Desmond, D. R. Ciarlo, and W. J. Benett . Direct bounding of micromachined silicon wafers for laser diode heat exchanger applications. *Journal of Rhelogy*, 1(26):152–156, 1991.

[89] Y. J. Song and T. S. Zhao. Modelling and testing of a thermally-driven phase-change nonmechanical micropump. *J.Micromech. Microeng*, 11:713–719, 2001.

[90] J. C. Slattery. Advanced transport phenomena. *Cambridge University Press*, 1999.

[91] B. Y. Cao, M. Chen, Z. Y. Goo. Velocity slip of liquid flow in nanochannels. *International Journal of Control*, 55(10):5305, 2006.

[92] B. Y. Cao, M. Chen and Z.Guo. Liquid flow in surface-nanostructured channels studied by molecular dynamics simulation-art. *Physical Review*, 6(6):6311–6317, 2006.

[93] L. Szalmas. Slip-flow boundary condition for straight walls in the lattice boltzmann model-art. *Physical Review*, 6:6710–6718, 2006.

[94] J. L. Xu and Y. X. Li. Boundary conditions at the solid-liquid surface over the multiscale channel size from nanometer to micron. *International Journal of Heat and Mass Transfer*, 50(13):2571–2581, 2007.

[95] Y. X. Zhu and S.Granich. Rate-dependent slip of newtonian liquid at smooth surfaces-art. *Physical Review Letters*, 9:6105–6113, 2001.

[96] Y. H. Wu and B. Wiwatanapataphee. Modeling of turbulent flow and multiphase heat transfer under electromagnetic force. *Discrete and Continuous Dynamical Systems-Series B*, 8(3):695, 2007.

[97] S. P. Yong and K. Q. Zhu. Analytical solutions for squeeze flow of bingham fluid with navier slip condition,. *Journal of Non-Newtonian Fluid Mechanic*, 138(2-3):173, 2006.

[98] C. L. Rice and R. Whitehead. Electrokinetic flow in a narrow cylindrical capillary. *J.Phys.Chem.*, 69:4017–4024, 1965.

[99] S. Levine, J. R. Marriott and K. Robinson. Theory of electrokinetic flow in a narrow parallel-plate channel. *J.Chem.Soc.Faraday Trans.II*, 71:1–11, 1975.

[100] C. Yang, D. Li and J. H. Masliyah . Modeling forced liquid convection in rectangular microchannel with electrokinetic effect. *Heat Mass Transfer*, 41:4229–4249, 1998.

[101] Mala G. M.,Li D Q,Werner C,Jacobasch H-J and Ning Y.B. *Int.J.Heat Liquid Flow*. New Jersey: John Wiley & Sons, 1997.

[102] Mala G. M.,Li D Q and Dale J D . *Int.J.Heat Liquid Flow.* , 1997.

[103] S. Ray, B. Unsal, F.Durst, O. Ertunc,O. A. Bayoumi. Mass flow rate controlled fully developed laminar pulsating pipe flow. *Journal of fluids Engineering*, 127:405–411, 2005.

[104] M.Chauveteau,M.Gundogdu. A critical review on pulsatile pipe flow studies directing towards futures research topic. *Flow Measurement and instrumentation*, 12:163–170, 2001.

[105] C. Feller, T. A. Johansen, and S. Olaru. An improved algorithm for combinatorial multi-parametric quadratic programming. *Automatica*, 2012.

[106] Shadowitz,A. *The Electromagnetic Field*. Dover, 1975.

[107] P. C. H. Li and J. D. Harrison. Transport manipulation and reaction of biological cells on chip using electrokinetic effects. *Anal. Chem.*, 69:1564–1568, 1997.

[108] H. Fan, D. Jed Harrison. Micromachining of capillary electrophoresis injectors and separators on glass chips and evaluation of flow at capillary intersections. *Anal. Chem.*, 66(1):177–184, 1994.

[109] G. Ocvirk, M. Munroe, T. Tang, R. Oleschuk, K. Westra, D. Jed Harrison. Electrokinetic control of fluid flow in native poly(dimethylsiloxane) capillary electrophoresis devices. *Electrophoresis*, 21(1):107–115, 2000.